Analysis of Turbulent Transport Properties in a Swirling Flow of a Can-type Combustor

by

Kamorudeen Babatunde Abidogun

A Thesis Presented to the

FACULTY OF THE COLLEGE OF GRADUATE STUDIES

KING FAHD UNIVERSITY OF PETROLEUM & MINERALS

DHAHRAN, SAUDI ARABIA

In Partial Fulfillment of the
Requirements for the Degree of

MASTER OF SCIENCE

In

MECHANICAL ENGINEERING

January, 1996

Analysis of Turbulent Transport Properties in a Swirling Flow of a Can-type Combustor

BY

Kamorudeen Babatunde Abidogun

A Thesis Presented to the

FACULTY OF THE COLLEGE OF GRADUATE STUDIES

KING FAHD UNIVERSITY OF PETROLEUM & MINERALS

DHAHRAN, SAUDI ARABIA

In Partial Fulfillment of the
Requirements for the Degree of

MASTER OF SCIENCE

In

Mechanical Engineering

January, 1996.

Analysis of Turbulent Transport Properties in a Swirling Flow of a Can-type Combustor

MS Thesis

By

Kamorudeen Babatunde ABIDOGUN

January, 1996.

KING FAHD UNIVERSITY OF PETROLEUM AND MINERALS

DHAHRAN 31261, SAUDI ARABIA.

COLLEGE OF GRADUATE STUDIES

This thesis, written by ABIDOGUN Kamorudeen Babatunde under the direction of his Thesis Advisor and approved by his Thesis Committee, has been presented to and accepted by the Dean of the College of Graduate Studies, in partial fulfilment of the requirements for the degree of MASTER OF SCIENCE IN MECHANICAL ENGINEERING.

Thesis Commitee

Saad Ahmed

Thesis Advisor (Dr. Saad A. Ahmed)

Member (Dr. Bekir S. Yilbas)

Member (Dr. Ahmet Z. Sahin)

Department Chairman (Dr. Muhammad O. Budair)

Dean, College of Graduate Studies (Dr. Ala H. Rabeh)

28·1·96

Date

Dedicated to

my parents

&

my immediate family members

whose patience, forbearance, and courage are

instrumental to this accomplishment

Acknowledgment

In the name of Allah, the Beneficent, the Merciful. All praises are due to Allah, *subhanahu-wa-ta'ala*, the Almighty, for all His blessings on me and memebers of my family. I feel privileged to glorify His name in the sincerest way through this small accomplishment. I seek His mercy, favor, and forgiveness. And I ask Him to accept this little effort as an act of worship.

Acknowledgement is due to King Fahd University of Petroleum and Minerals (KFUPM) for giving me the opportunity to study here. I would also like to appreciate the contributions of faculty and staff of the department of mechanical engineering, KFUPM towards making my stay here memorable.

I would like to express my deep gratitude to my thesis committee chairman, Dr. Saad Ahmed for his assistance and support during the course of this thesis. I am also grateful to committee members Dr. Bekir Yilbas and Dr. Ahmet Sahin for their sincere help and advice during the course of this thesis.

I would also like to appreciate the patience, forbearance, and courage of members of my household, especially my immediate family members, mother, and father, during the period of my stay in KFUPM.

Finally, I pray to Allah to reward all those who contributed in one way or the other towards this accomplishmnet with an immense reward (amin).

Contents

List of Tables

List of Figures

Abstract

Name:	**Kamorudeen Babatunde ABIDOGUN**
Title:	**Analysis of Turbulent Transport Properties in a Swirling Flow of a Can-type Combustor**
Major Field:	**Mechanical Engineering**
Date of Degree:	**January, 1996.**

The data obtained from the measurements of the flow properties of flow in a confined, isothermal, swirling flowfield are analyzed for turbulent kinetic energy terms. The axisymmetric flow measurements were carried out with a two-component laser Doppler velocimeter (LDV). The main objective of this study is to analyze a detailed experimental database to help in the understanding of the behavior of swirled, axisymmetric, recirculating, turbulent flows. In addition, the data from this study will be available for upgrading advanced design codes. Furthermore, the influence of swirl number and swirl type on the flowfield characteristics (e.g., turbulent kinetic energy terms: convection, diffusion, dissipation, and production terms) are investigated. These terms were calculated directly from the experimental data using central differencing. The contributions of various components of the turbulent kinetic energy terms to the convection, diffusion, dissipation, and production of the turbulent kinetic energy are presented, as functions of radial and axial positions.

Master of Science Degree
Department of Mechanical Engineering
King Fahd University of Petroleum and Minerals
Dhahran, Saudi Arabia
January, 1996.

خلاصة الرسالة

الإسم : قمر الدين باباتنودي أبيدوغون

عنوان الرسالة : تحليل الخواص المنتقلة الدوامية لانسياب دوار بداخل غرفة إحتراق

التخصص : الهندسة الميكانيكية

تاريخ الشهادة : يناير ١٩٩٦م

في هذه الإطروحة ، أستخدمت نتائج القياسات لانسياب دوار داخل غرفة إحتراق وحللت باستخدام الطاقة الدوامية ولقد استخدم جهاز ليزر مركب من عنصرين لقياس الإنسياب المتماثل ٠

ولقد كان الهدف من هذه الدراسة ذو أهمية ثلاثية : -

أولا : لفهم وبحث وتسجيل تأثير الحركة الدوامية لإنسياب دوار

ثانيا : لتزويدنا بمعلومات دقيقة من أجل تطوير البرامج المتقدمة الخاصة بالحلول للحركات الدوامية ٠

ثالثا : تم دراسة معدل الدوران أو طريقة الدوران لإنسياب دوار على الطاقة الدورامية من حيث إنتشارها وانتقالها وتبديدها ٠

ولقد تم استخدام نتائج القياسات مباشرة في حساب هذه المعلومات وتم عرضها وشرحها في الإطروحة كدوال متغيرة تعتمد على مكان نقطة القياس ٠

درجة الماجستير

قسم الهندسة الميكانيكية

جامعة الملك فهد للبترول والمعادن

الظهران - المملكة العربية السعودية

يناير ١٩٩٦م

Chapter 1

INTRODUCTION

Turbulent swirled flows are of significant theoretical and practical importance, since they can cause a flow reversal. Despite the fact that such flows have been the subject of extensive analytical and experimental studies for decades, many issues are still unresolved. For example, because of the complexity of the flowfield and the associated difficulties with measurements, detailed information on reacting turbulent flows are very limited. As a result, development and evaluation of analytical models of the flowfield, especially for confined turbulent recirculating flow configurations, have been fettered by the lack of reliable and detailed experimental data. In order to develop these numerical codes such as the $k-\epsilon$ model to become general (i.e. applicable to more than a limited range of simple configurations), reliable and well-documented experimental data are a necessity.

Therefore the objective of the current study is to analyze a credible and detailed experimental database to help in the understanding of the behavior of swirled, axisymmetric, recirculating, incompressible turbulent flows. There are limited data available for geometries that parallel the current study. However, in one way or another, the data lack detail and accuracy (i.e., initial conditions or resolution) or do not represent a realistic geometry or combustor operating condition. Several researchers have reported data for geometries that may complement the current study. Flow characteristics of interest that were examined included the velocity field characteristics, and the length of the corner recirculation zone (CRZ). The most recent studies relevant to the present one are discussed in the following paragraphs.

As a result of the theoretical and practical importance of turbulent flows in a dump combustor, several studies have been carried out to determine the characteristic features of the associated complex flowfield accurately. These studies include the non-swirl flows, such as sudden expansion of flow in a dump combustor, and swirled flows where a swirler is employed to recirculate the in-flow.

The benefits of swirled flows have been reported by Ahmed et al.[1]. These include increased combustion efficiency, reduced emission of pollutants such as nitrogen oxides, soot, and unburnt hydrocarbons, reduced flame length which provides

the opportunity to use smaller combustors, improved stability, improved blow-off limits, and uniform pattern factor that enhances the increase of turbine life.

Generally, the strength or degree of swirl is the term employed to classify swirling flows. As shall be seen in the later part of this report, the method of generating the swirl, as well as the initial inlet swirl profile, also contributes greatly to the combustor flowfield.

Pitz and Daily[24] investigated reacting flow behind a step in a rectangular duct with a 2 :1 area ratio. They reported that the presence of reaction (equivalence ratio = 0.57) reduced the length of the CRZ by 20 - 30 percent. Turbulence parameters were not of prime interest and were not heavily discussed. The limited data that were plotted indicated combustion has an insignificant effect on turbulent kinetic energy (TKE).

ElBanhawy et al.[9] studied reacting flows with equivalence ratios ranging from 0.77 - 0.95 and expansion area ratios of 2.0 and 4.0 in a coaxial dump combustor. They observed a CRZ extending approximately three step heights. The reported value was less than half of the commonly observed value in nonreacting flows and 30 - 40 percent lower than the documented results of Pitz and Daily[24]. Therefore, it is important not only to state the strength of a swirler, but also the

Table 1.1: Summary of the Reported Swirl Generation Techniques

Author	Method	Measurement	S	CTRZ
Chigier[4]	Tangential ports	Impact probe	0.30-1.43	Yes
Keer[15]	Vanes	Impact probe	0-0.72	No
Chigier[5]	Tangential ports	Impact probe	0.13-0.66	Yes
Mathur[22]	Vanes	Impact probe	0-2.7	Yes
Maier[20]	Vanes	Impact probe	1.7-2.9	Yes
Craya[7]	Tangential ports	Hot-wire	0-1.58	Yes
Syred[32]	Tangential ports	Hot-wire	2.2	Yes
Pratte[26]	Rotational pipe	Hot-wire	0.3	No
Hosel[14]	Tangential ports	LDA	0-1.7	Yes
Fornoff[10]	Tangential ports	LDA	0.53	No
Riberio[27]	Tangential ports	Hot-wire	0.32	No

method of its generation and the initial inlet swirl profile. Table 1.1 shows some of the previously reported method of swirl generation.

Stevenson et al.[31] reviewed relevant results and made measurements in an axisymmetric sudden expansion combustor with an equivalence ratio of of 0.28, using non-premixed flow conditions. They found that the reaction shortened the CRZ by approximately 15 percent, increased the maximum backflow velocity and the axial TKE on the centerline while reducing TKE elsewhere. In agreement with prior investigators, they reported the significance of axial pressure gradient on CRZ length in nonreacting flows.They indicated that this parameter needed to be isolated and monitored closely before considering the effects of combustion on the behavior of the CRZ.

Chapter 2

EXPERIMENTAL SET-UP

It is highly imperative to present the model and condition by which the experimental database used for this analysis was obtained. The raw data were collected at Wright-Patterson Air Force Base and published by Ahmed et al.[1] and were obtained through special communications with Ahmed. The set-up of the experiment carried out previously by Ahmed is given under the following sub-headings.

2.1 Combustor Model

A modular can-type research combustor was designed and constructed for the experiment through which the database used for the purpose of this research was collected. Special care was taken to ensure that the fabricated model satisfied the axisymmetric nature of the flowfield. In addition, a superb provision was

provided on the model to facilitate the use of a two-component fiber-optic laser velocimeter. The model consist of three main sections.

2.1.1 Inlet Sections

The inlet section is made up of a 300 *mm* diameter settling chamber, a plexiglas inlet pipe, and a cylindrical teflon swirler housing. The plexiglas inlet pipe is 2850 *mm* long and 101.6 *mm* internal diameter while the teflon swirler housing has an inner and outer diameters of 104.5 *mm* and 152.4 *mm* respectively. A flat 38 *mm* x 38 *mm*, optical quality, quartz window was installed in the inlet pipe at a distance of 50.8 *mm* upstream of the swirler housing as shown in Figure 2.1a. This window enabled flow characteristics upstream of the swirler to be determined with the laser Doppler Velocimeter (LDV). The measurements are done by replacing the quartz window with a plug of the same radius of curvature as the inlet pipe. This is meant to remove the usual inlet flow disturbances. The swirler housing has the ability of being positioned relative to the measurement station in the combustion chamber. This was made possible by placing the entire inlet assembly on a traversing mechanism controlled by a stepping motor. Having assumed the flow across the pipe to be a simple plug one, an average inlet velocity of 16.0 ± 0.4 *m/s* (large enough to ensure turbulent flow in the combustor) was maintained. This value of the inlet average velocity was checked with a flowmeter, situated far upstream of the swirler housing, at a Reynolds number - based on

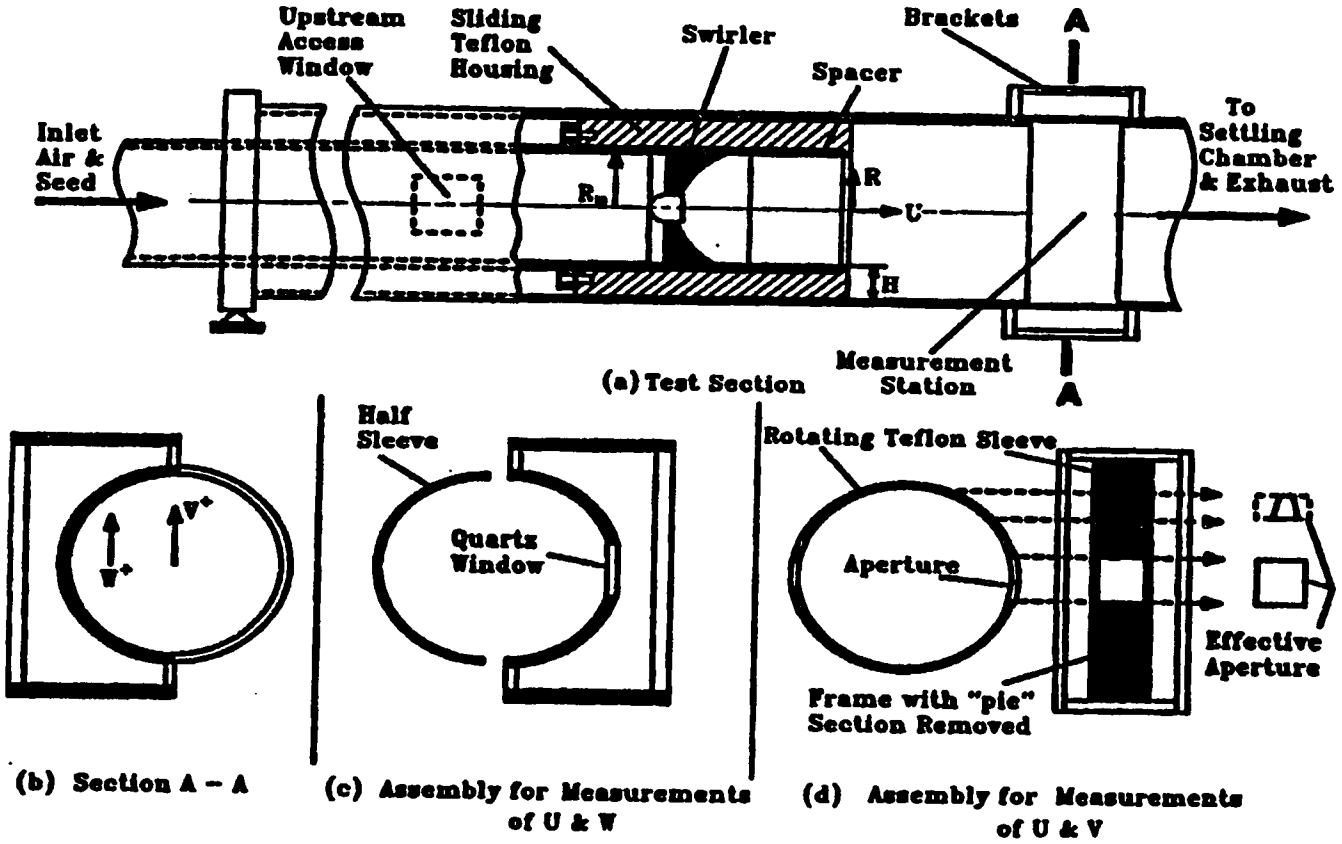

Figure 2.1: Schematic of the test section of the dump combustor model

the outer diameter of the swirler - of 1.5 x 10^5.

2.1.2 Combustion Chamber

The combustion chamber is made up of a plexiglas tube, measuring 152.4 *mm* in internal diameter and 1850 *mm* in length. This section terminates into an exhauster of a larger diameter. To enable the measurement of the three component velocity vectors with a two component LDV system, the measurement station was designed to accommodate two different window assemblies. The design of one of the windows is such that provision is made for the optical instrument to traverse in the vertical direction along the diameter of the pipe while the other window allows for the movement of the measuring instrument in the horizontal direction along the diameter of the pipe. Figure 2.1b shows the two different window assemblies that enabled the three component velocity vectors to be measured. The design of the test section also incorporates a plug assembly at the combustor exit that may be employed to increase the pressure of the chamber while the mass flow rate remain unchanged. A 40% contraction nozzle was situated at the combustor exit as part of the components of the test section necessary for this experiment.

2.1.3 Window Assemblies

Measurements in the horizontal plane

This window assembly is made up of a flat 38 *mm* x 38 *mm* optical quality quartz window which is installed in a frame made from 152.4 *mm* ID plexiglas. This frame, fixed to two brackets, is attached to the combustor section as illustrated in Figure 2.1a. To ensure a smooth flow passage, a 40 *mm* wide and 152.4 *mm* ID, teflon made, half sleeve is situated in the combustor wall recess. Non-leaking is ensured by sealing the whole assembly with a vacuum grease. Figure 2.1c illustrates the setup of the experiment for velocity measurements in the horizontal plane.

Measurements in the vertical plane

Similar to the setup for the horizontal plane measurements, the setup for the vertical plane measurement of velocities comprised of a frame made from 154.4 *mm* ID plexiglas, and a rotating teflon sleeve of 40 *mm* wide, 2 *mm*, and 152.4 *mm* ID. The frame has a pie-shaped section cut out from it. The assembly also consisted of a 30 *mm* x 20 *mm* centrally located rectangular aperture. The mounting of this assembly in the combustor section was as described for the assembly of the horizontal plane measurement. The combination of the sleeve and frame allowed the minimum optical access opening and, at the same time,

reduced flow disturbance to the minimum. This is achieved when the LDV was moved in the vertical plane.

2.2 Swirler Design

The design of the swirler is quite critical to the performance of the combustor. This assertion has been given attention by many authors such as Lefebvre[19]; Martin[21]; Fujii et al.[11]; *Kilik*^{a}[16]; and *Kilik*^{b}[17]. The angle, as well as the number and size of swirl vanes, dictate the amount of rotation imparted to the flow and the size of the recirculation zone. The swirl vanes notably assume either of the two shapes viz: flat or curved shapes. Flat-shaped swirl vanes are easy to manufacture but curved swirl vanes are usually preferred for their better aerodynamic properties such as smaller pressure loss.

Despite the fact that the design of the swirler for this experiment was based on the one reported by Wilhelmi[33], the required swirler vane curvature was calculated using a procedure reported by Buckley et al.[3]. The swirler consisted of 12 circular arc inlet guide vanes. These vanes were welded between between a 101.6 *mm* outer ring and a 19 *mm* central hub. Designed to be tangent to the incoming flow, the leading edge of each swirler blade is made to be perpendicular to the centerline of the combustor model. The swirl number was first introduced

by Chigier and Beér[4] on the ground that the axial flux of angular momentum are conserved along a path of a swirling jet.

The axial flux of linear momentum is given by:

$$G_x = 2\pi\overline{\rho}\int_0^\infty \overline{U}^2 r dr + 2\pi\int_0^\infty \overline{p} r dr, \tag{2.1}$$

while the axial flux of angular momentum is given by:

$$G_\theta = 2\pi\overline{\rho}\int_0^\infty \overline{U}\,\overline{W} r^2 dr \tag{2.2}$$

The swirl number S is generally referred to as the swirl strength. For unconfined flow, the swirl number is defined as the ratio of the angular momentum flux to the axial momentum flux multiplied by some characteristic length scale L (which is the OD of the swirler in this study). Mathematically, S can be defined as

$$S = \frac{G_\theta}{G_x L} \tag{2.3}$$

Gore and Ranz[12] suggested that the swirl number be only dependent on the swirler geometry . Thus, for an annular swirler with an inner hub diameter d_i and an outer hub diameter d_o with a constant swirl vane angle γ, the swirl number is defined as

$$S = \frac{2}{3}\left[\frac{1-\left(\frac{d_i}{d_o}\right)^3}{1-\left(\frac{d_i}{d_o}\right)^2}\right]\tan\gamma \tag{2.4}$$

Furthermore, strongly swirling flow can be either subcritical or supercritical. The main difference between these two category of the strongly swirling flow is that

initial influences are able to propagate upstream against the flow in the case of subcritical flows while this is not the case with supercritical flows. If a highly confined strongly swirling flow revert back to its supercritical state after vortex breakdown, the velocity in the axial direction regain its normal status as the flow develops downstream and the swirl disintegrates. Squire[30] has shown that flow tends to remain in a subcritical state after vortex breakdown if the maximum swirl velocity go beyond the average axial value.

2.3 Laser Velocimeter

The velocity measurements for this study were done using a TSI Inc. 9100-7 four beam, two color, back scatter LDV system. The LDV system has two TSI 9180-3A frequency shifters to provide directional sensitivity. The optical setup was mounted on a three axis traversing table with a resolution of 0.0025 *mm*. The features of the optical setup include:

- Setting the fringe inclinations at 45.7° and 135.17° to the combustor centerline.
- The approximate measurement volume dimensions were 390 μm in length and 60 μm diameter based on the $1/e^2$ intensity points.

The chemical seeder developed by Craig et al.[6] was used for the present study. This chemical seeder produces micron size Titanium dioxide particles. These

particles were passed into the upstream settling chamber in order to ensure the a uniformly seeded flow.

2.4 Data Acquisition and Analysis

Measurements done with the LDV involves different stages. The LDV signals from the photomultipliers were treated by two TSI burst counters - models 1990 B & C with low pass filters, set at 20 MHz, and high pass filters set at 100 MHz on each processor. Having comparison settings of 1% and fringe counts of 16, a typical validated data rates lie between 1,000/sec and 5,000/sec. The time between two doppler bursts is 20 μsec coincidence window. Having accomplished this time, the ensuing coincidence data transfer rate lie between 500/sec and 2,500/sec. In order to ensure the accuracy of the measurements taken, especially when calculating the higher order moments of turbulent fluctuations, 50,000 realizations per channel were collected at each measurement location. Having certified that 5000 realizations are enough for a minimal uncertainty in the calculation of statistical moments, the number of realizations per channel collected at each measurement location was reduced to 5000. The number of realizations could be further reduced to 2,000 or 1,000 for uncommon cases of very low data rates.

The data collected were transferred to the mini-vax computer system in DMA

mode. This was done at a maximum rate of one megabyte per second via a custom made interface. Calculation of statistical moments from standard formulae were done at each measurement location using double precision (48 bit). Worthnoting is the fact that the use of cut-off limits on the calculated velocity histograms was avoided since, in most cases, the data were sufficiently noise free.

The problem of velocity bias in LDV measurements was corrected in this study by the use of the time between individual realization as a weighing factor as reported by Nejad et al.[23]. The uncertainty of the measured mean velocities was determined using the method of Snyder et al.[29]. The uncertainty, ΔU, is expressed as:

$$\Delta\overline{U} = \pm 1.96\frac{\overline{\sigma_u}}{\sqrt{N}} \tag{2.5}$$

The constant 1.96 is used for 95% confidence level. While N represents the sample size, which is 5000 for this study, $\overline{\sigma_u}$ is the true standard deviation. The maximum uncertainties of the mean velocities $\overline{U}, \overline{V}$, and $\overline{W}$ due to random error were found to be 2.0, 1.8, and 1.1% of the upstream centerline velocity; respectively.

Chapter 3

CALCULATION PROCEDURES

3.1 Turbulent Kinetic Energy (TKE) Equation

The experimental data were analyzed for the turbulent kinetic energy terms viz:- production, diffusion, convection, and dissipation. Swirl number and swirl type were determined for these terms. Since axisymmetry was assumed for the flow (this was seen as a valid assumption from the experimental results), a two-dimensional cylindrical coordinate system was used. The modelled domain was from the swirler inlet to the last measurement plane, that is, $x/H = 0.0 - 18.0$ and a grid of 25 x 12 (radial x axial) was used. The turbulence energy equation in cylindrical coordinates (for steady, axisymmetric, and constant density flow),

employed in the determination of the turbulent kinetic energy terms in this analysis, could be written as (see Appendix A and B for the derivation of this equation):

$$\overline{U}\frac{\partial k}{\partial x}+\overline{V}\frac{\partial k}{\partial r}=\frac{1}{\overline{\rho}}\frac{\partial}{\partial x}\left[\mu\frac{\partial k}{\partial r}-\overline{\rho}\frac{\overline{u'v'^2}}{2}-\overline{\rho}\frac{\overline{u'w'^2}}{2}-\overline{\rho}\frac{\overline{u'^3}}{2}-\overline{u'p'}\right]+$$
$$\frac{1}{\overline{\rho}r}\frac{\partial}{\partial r}\left[\mu r\frac{\partial k}{\partial r}-\overline{\rho}r\frac{\overline{v'^3}}{2}-\overline{\rho}r\frac{\overline{v'w'^2}}{2}-\overline{\rho}r\frac{\overline{u'^2v'}}{2}-r\overline{v'p'}\right]-\left[\frac{\mu}{\overline{\rho}}\frac{\overline{v'^2}}{r^2}+\frac{\mu}{\overline{\rho}}\frac{\overline{w'^2}}{r^2}\right]-$$
$$\left[\overline{v'^2}\frac{\partial\overline{V}}{\partial r}+\overline{u'v'}\frac{\partial\overline{U}}{\partial r}+\overline{u'v'}\frac{\partial\overline{V}}{\partial x}+\overline{u'^2}\frac{\partial\overline{U}}{\partial x}+\overline{w'^2}\frac{\overline{V}}{r}+\overline{u'w'}\frac{\partial\overline{W}}{\partial x}+\overline{v'w'}\frac{\partial\overline{W}}{\partial r}+\overline{v'w'}\frac{\overline{W}}{r}\right]-$$
$$\frac{\mu}{\overline{\rho}}\left[\overline{\left(\frac{\partial v'}{\partial r}\right)^2}+\overline{\left(\frac{\partial w'}{\partial r}\right)^2}+\overline{\left(\frac{\partial u'}{\partial r}\right)^2}+\overline{\left(\frac{\partial v'}{\partial x}\right)^2}+\overline{\left(\frac{\partial w'}{\partial x}\right)^2}+\overline{\left(\frac{\partial u'}{\partial x}\right)^2}\right]$$

This form of the equation is essentially the same as the one given by Rouse and Humphreys[28]. The equation is composed of the following terms:

1. axial and radial convection of turbulent kinetic energy

$$\overline{U}\frac{\partial k}{\partial x}+\overline{V}\frac{\partial k}{\partial r}$$

2. axial diffusion of turbulent kinetic energy

$$\frac{1}{\overline{\rho}}\frac{\partial}{\partial x}\left[\mu\frac{\partial k}{\partial x}-\overline{\rho}\frac{\overline{u'v'^2}}{2}-\overline{\rho}\frac{\overline{u'w'^2}}{2}-\overline{\rho}\frac{\overline{u'^3}}{2}-\overline{u'p'}\right]$$

3. radial diffusion of turbulent kinetic energy

$$\frac{1}{\overline{\rho}r}\frac{\partial}{\partial r}\left[\mu r\frac{\partial k}{\partial r}-\overline{\rho}r\frac{\overline{v'^3}}{2}-\overline{\rho}r\frac{\overline{v'w'^2}}{2}-\overline{\rho}r\frac{\overline{u'^2v'}}{2}-r\overline{v'p'}\right]$$

4. additional terms which are usually very small relative to other terms

$$\left[\frac{\mu}{\overline{\rho}}\frac{\overline{v'^2}}{r^2}+\frac{\mu}{\overline{\rho}}\frac{\overline{w'^2}}{r^2}\right]$$

5. production of turbulent kinetic energy

$$\left[\overline{v'^2}\frac{\partial \overline{V}}{\partial r} + \overline{u'v'}\frac{\partial \overline{U}}{\partial r} + \overline{u'v'}\frac{\partial \overline{V}}{\partial x} + \overline{u'^2}\frac{\partial \overline{U}}{\partial x} + \overline{w'^2}\frac{\overline{V}}{r} + \overline{u'w'}\frac{\partial \overline{W}}{\partial x} + \overline{v'w'}\frac{\partial \overline{W}}{\partial r} + \overline{v'w'}\frac{\overline{W}}{r}\right]$$

6. viscous dissipation of turbulent kinetic energy

$$\frac{\mu}{\overline{\rho}}\left[\overline{\left(\frac{\partial v'}{\partial r}\right)^2} + \overline{\left(\frac{\partial w'}{\partial r}\right)^2} + \overline{\left(\frac{\partial u'}{\partial r}\right)^2} + \overline{\left(\frac{\partial v'}{\partial x}\right)^2} + \overline{\left(\frac{\partial w'}{\partial x}\right)^2} + \overline{\left(\frac{\partial u'}{\partial x}\right)^2}\right]$$

3.2 Calculation Procedure

All the terms of the turbulent kinetic energy are calculated from the experimental data except the viscous dissipation terms, which were obtained by algebraic energy balance of the turbulent kinetic energy equation.

To calculate each term in the turbulence energy equation using experimental data, first and second derivatives have to be evaluated. For example, central difference was used to calculate the first derivatives while the second derivatives were estimated using the method of undetermined coefficients as recorded by Lapidus and Pinder[18]. This method takes care of the non-uniformity in spacing along the x and r axes. The method is also valid for uniform spacing (e.g., when the method of undetermined coefficients is used for equal spacing of points, its result is the same as the conventional method). The descretized expression for the second derivatives of k with respect to a coordinate axis x at a location (i, j),

using the method of undetermined coefficient, is as follows:

$$\frac{\partial^2 k_{i,j}}{\partial x^2} = \alpha_{i+1,j} k_{i+1,j} + \alpha_{i,j} k_{i,j} + \alpha_{i-1,j} k_{i-1,j}$$

$$\textit{where} \qquad \alpha_{i,j} = \left(\frac{\Delta x_1^2}{2} + \frac{\Delta x_2 \Delta x_1}{2} \right)^{-1} ,$$

$$\alpha_{i+1,j} = \left(\frac{\Delta x_2 \Delta x_1}{2} + \frac{\Delta x_2^2}{2} \right)^{-1} , \quad \textit{and}$$

$$\alpha_{i-1,j} = -1.0 * (\alpha_{i,j} + \alpha_{i+1,j})$$

$$\textit{while,}\ \Delta x_1 = x_i - x_{i-1}\ ,\ \textit{and}\ \Delta x_2 = x_{i+1} - x_i$$

A computer program, written in fortran language, was developed to calculate the required TKE terms. The main program and its subroutines are provided in Appendix E. This program is written in a general format such that it can handle any data input, with little alteration in the array dimensions and proper variable specification in the read statement.

Chapter 4

RESULTS AND DISCUSSIONS

4.1 Results

The experimental database employed for this analysis was made non-dimensional appropriately with respect to the inlet upstream centerline mean velocity, $\overline{U_o}$. In the same vein, physical dimensions of the combustor and the measurement coordinates are made non-dimensional with respect to the dump step height, H. Since the flow is treated as being axisymmetric, the results presented here are for half of the lateral section of the combustor. The summary of the inlet flow conditions is tabulated in Table 4.1.

Table 4.1: Summary of Inlet Flow Conditions

S	Designed Swirl Profile	Purpose
0.0	Simple Dump	a) Study Effects of Inlet Profile
0.4	Forced Vortex	
0.4	Constant Angle	
0.4	Free Vortex	
0.0	Simple Dump	b) Study Effects of Swirl Strength
0.3	Constant Angle	
0.4	Constant Angle	
0.5	Constant Angle	

The results of this analysis are presented in two folds. The effects of inlet swirl strength on the turbulent kinetic energy terms are first presented. In a similar manner, the effects of inlet swirl profile on the combustor flowfield are then presented. The findings of this analysis are discussed in the later part of this thesis. Meanwhile, the discussion of a preliminary analysis of the turbulent flowfield follows.

4.2 Discussions

The mesh used for the purpose of this study is as shown in Figure 4.1. It shows non-uniform grid along the horizontal and vertical directions. The non-uniformity in the grid spacing resulted from the experimental data as measurements were not taken at some points due to some difficulty encountered coupled with the relative unimportance of measurement at those points. Figures 4.2a and 4.2b show the distribution of all relevant combustor inlet flow velocity components. From these figures, three distinct zones could be discerned from the axial velocity profiles. The first is a core zone, which could be as large as the combustor inlet area in the case of the simple dump flow, that is in the vicinity of the centerline of the combustor. The second, which is present in all flows, is a corner recirculation zone that has the same width as the step height. Between these two zones is located a third layer known as the mixing layer (i.e, shear layer). The relative

size of each of these zones varies from one case to the other, and also from one axial location to another. The mixing layer, for instance, is small in the case of simple dump flow, but significantly large in the case of free vortex flow where it occupied a substantial part of the combustor inlet area.

For swirling flows, the width of the vortex cores are categorically different. For free and forced vortex swirlers ($S = 0.4$), the core occupied about 16% of the combustor cross-sectional area while it occupied only about 1% of the area in the case of constant angle swirler ($S = 0.4$).

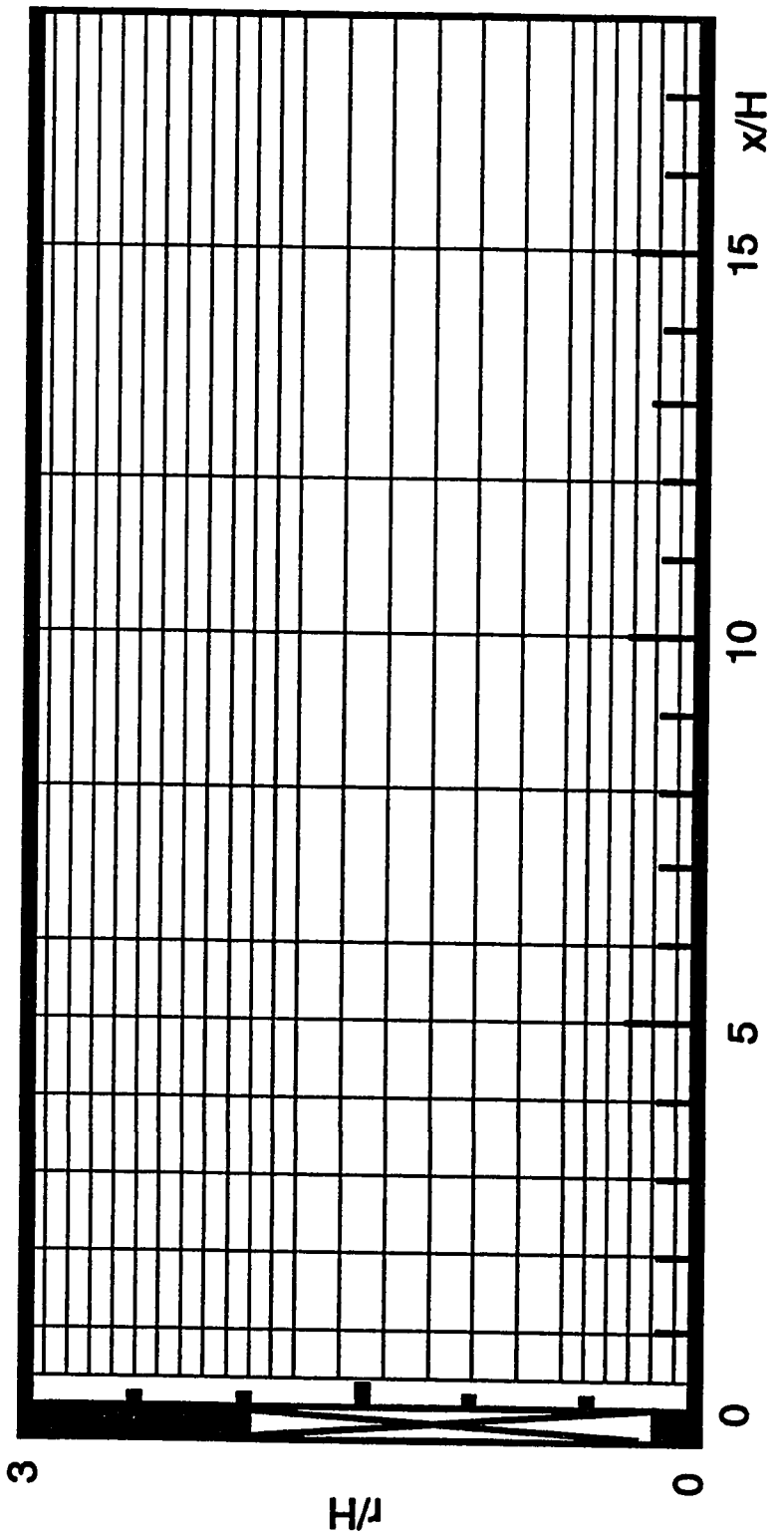

Figure 4.1: Computational Mesh

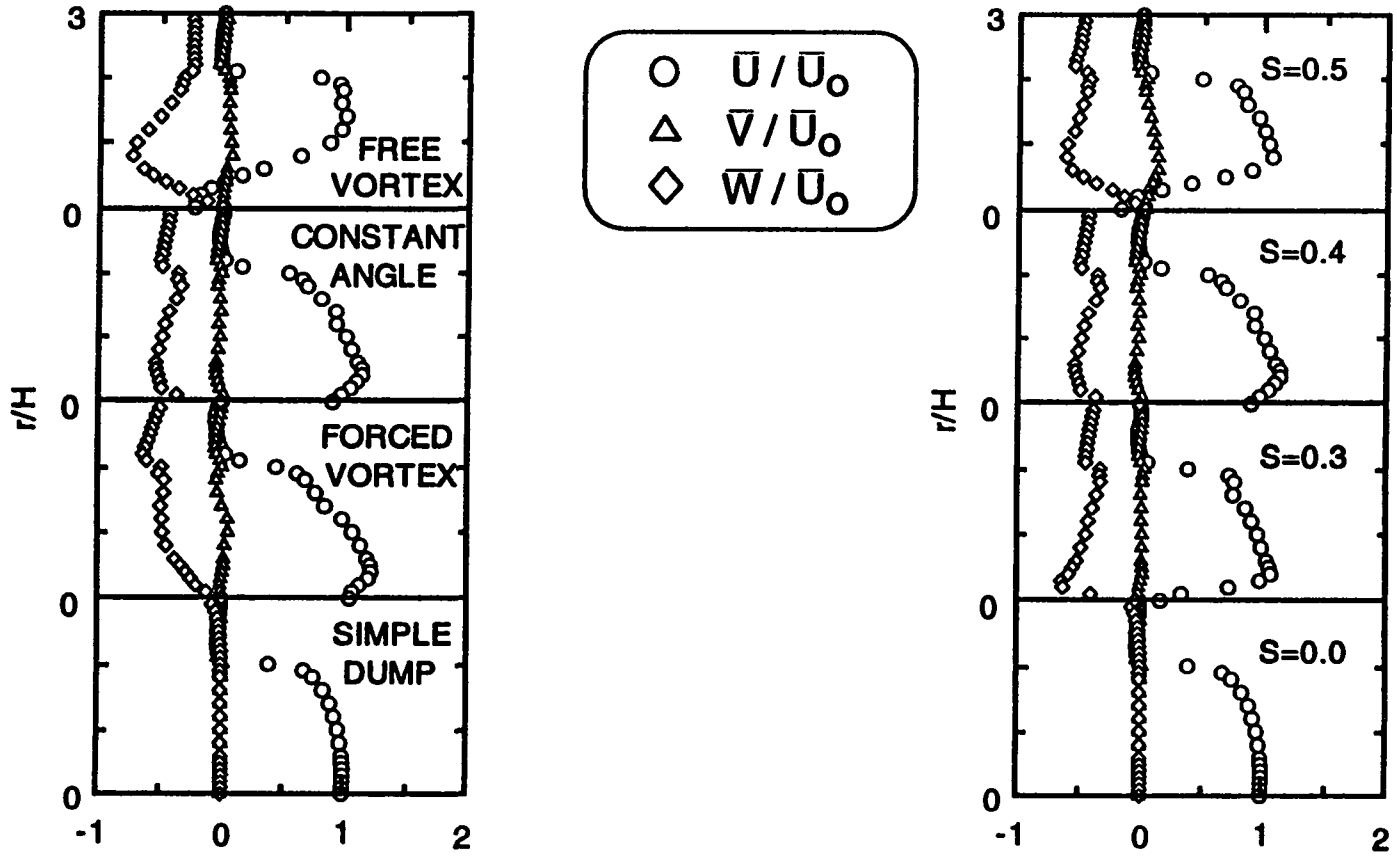

Figure 4.2: Distribution of Combustor Inlet Flow Variables at x/H=0.38

The normalized stream function, whose contours are shown in figures 4.3 and 4.4, is defined as follows:

$$\Psi(r) = \frac{\Psi(0) - \Psi(r)}{\Psi(r)} \qquad or$$

$$\Psi(r) = 1 - \left(\frac{\int_0^r \overline{U} r dr}{\int_0^{R_c} \overline{U} r dr} \right) \tag{4.1}$$

Zero values of Ψ depicts the Corner Recirculation Zone (CRZ) boundaries while $\Psi = 1$ values shows the Central Toroidal Recirculation Zone (CTRZ) boundaries. It is glaring from Figure 4.3 that CRZ reduces significantly with increase in the strength of swirl. Reverse flow regions, with different sizes, were generated in the cases of free vortex ($S = 0.4$) and $S = 0.5$ (constant angle). CTRZ for the $S = 0.5$ swirler extended up to about $x/H = 5.0$ with a maximum radius approximately equal the swirler hub radius. Although weaker in strength than the $S = 0.5$ swirler, the free vortex swirler ($S = 0.4$) generated a CTRZ that extended up to about $x/H = 8.0$ with a maximum diameter of $r/H = 1.2$ occurring at $x/H = 5.0$. The shortest CRZ was produced by the forced vortex ($L/L_0 = 0.34$). Table 4.2 shows a comparison of CTRZ and CRZ for the inlet swirl conditions. The CRZ and CTRZ are distinctly shown in the vector plots of the time mean axial velocity of Figures 4.5 and 4.6.

The effects of swirl on the flowfield, shown in Figures 4.3 and 4.4, conforms with the well-known ideas about swirl effects on axisymmetric confined swirling

flowfield. For instance, in the far field for $x/H > 15.0$, uniform spacing exist between the streamlines for swirling flows. This indicates complete flow recovery downstream of the CRZ in the combustor. Streamlines diverged over the entire length of the combustor for the flow without inlet swirl. This is an indication that the flow did not recover even far beyond the reattachment point.

Figures 4.7 and 4.8 show the turbulent kinetic energy contour plots in the combustor. Unlike the zero inlet swirl case, the swirled flows produced a significant increase in the turbulent kinetic energy over about half the length of the test section. The K-contours produced by the $S = 0.3$ and $S = 0.4$ constant angle swirlers have similar features. The strongest tested swirler, the $S = 0.5$ swirler, shows steeper radial and longitudinal gradients immediately after the dump. The free vortex case ($S = 0.4$) shows a very similar feature of the radial and longitudinal gradients when compared to the $S = 0.5$ (constant angle) case. The reason for this is the presence of the two recirculation regions, CRZ and CTRZ. The values of the turbulent kinetic energy are less in the forced vortex and simple dump inlet condition cases relative to the other inlet conditions.

Out of the three turbulent shear stress components, only two are reported here, the third component, $\overline{vw}$, being less important and can not be measured with a two component LDV system. Figures 4.9 and 4.10 show the contours of the shear

stress $\overline{u'v'}/\overline{U_o}^2$. In the case of the swirling flows, this shear stress (i.e., $\overline{u'v'}/\overline{U_o}^2$) has two peaks - one at the outer part of the CRZ and the other at the centerline. However, only one peak was observed with the simple dump flow and this occurred on the boundaries of the CRZ. Although all values of this shear stress are insignificant in the region $x/H > 10.0$, as such indicating full mixing and flow recovery (i.e, uniform flow) in this region, all swirlers produced higher turbulent shear stress relative to the zero-swirl flow in the region $x/H \leq 10.0$. The $S = 0.5$ (constant angle) swirler exhibit contour features similar to the free vortex ($S = 0.4$) swirler.

Represented in Figure 4.11 and 4.12 is the contour plots of $\overline{u'w'}/\overline{U_o}^2$. Generally, the peak values of the $\overline{u'w'}/\overline{U_o}^2$ are either observed near the centerline or the boundaries of the CTRZ for all the cases shown. However, no important values of this shear stress is seen in the CRZ for all the shown cases. Expectedly, the simple dump case showed relatively insignificant values everywhere in the combustor. Tangential stress values are lower in the far field region when compared to their corresponding values in the near field region.

Table 4.2: Comparison of Central Toroidal Recirculation Zones (CTRZ) and Corner Recirculation Zones (CRZ)

S	Designed Swirl Profile	CTRZ x/H	CRZ L/L_o
0.4	Forced Vortex	none	0.34
0.4	Constant Angle	none	0.43
0.4	Free Vortex	7.9	0.48
0.3	Constant Angle	none	0.52
0.5	Constant Angle	5.0	0.41

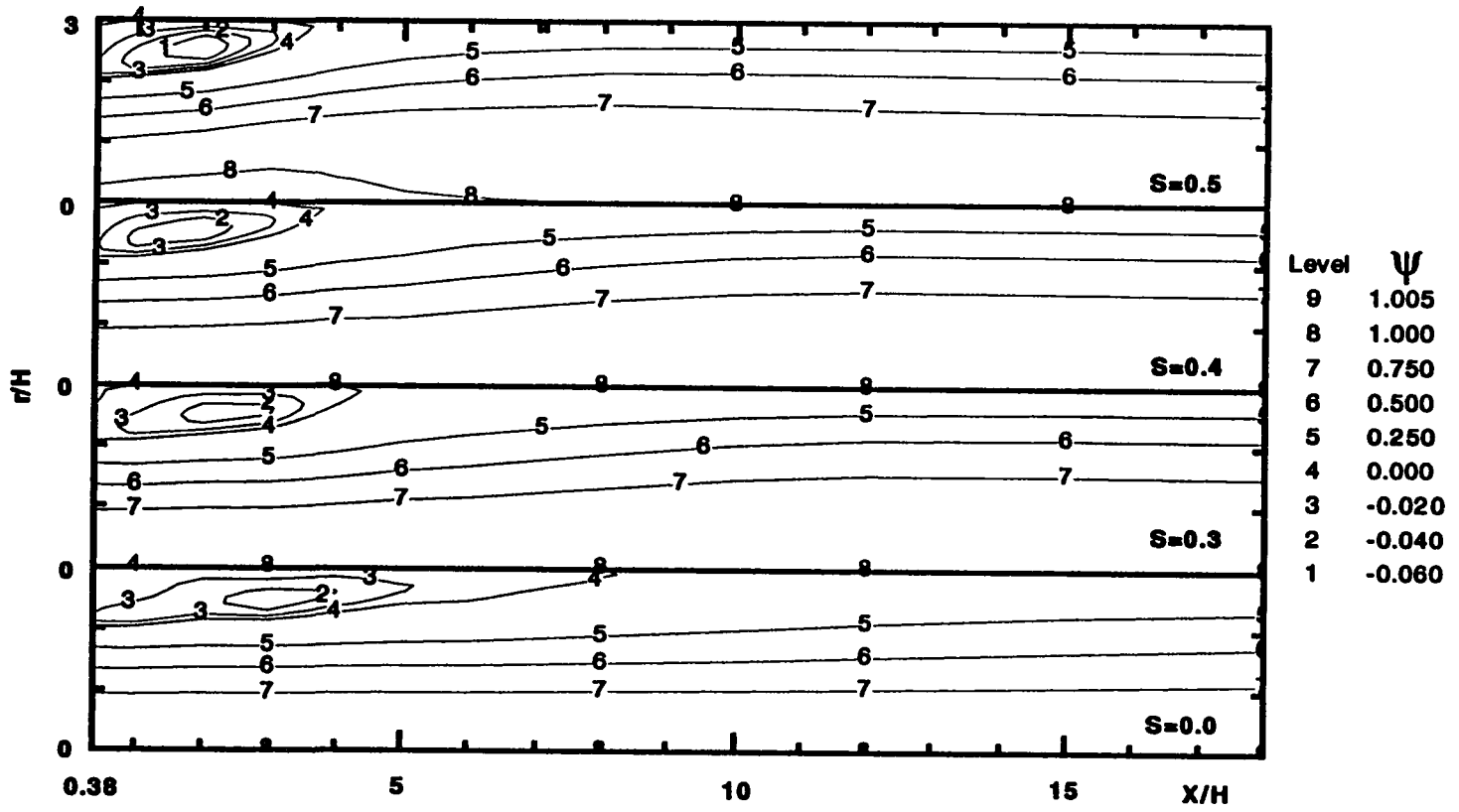

Figure 4.3: The Normalized Stream Function, Effects of Inlet Swirl Strength

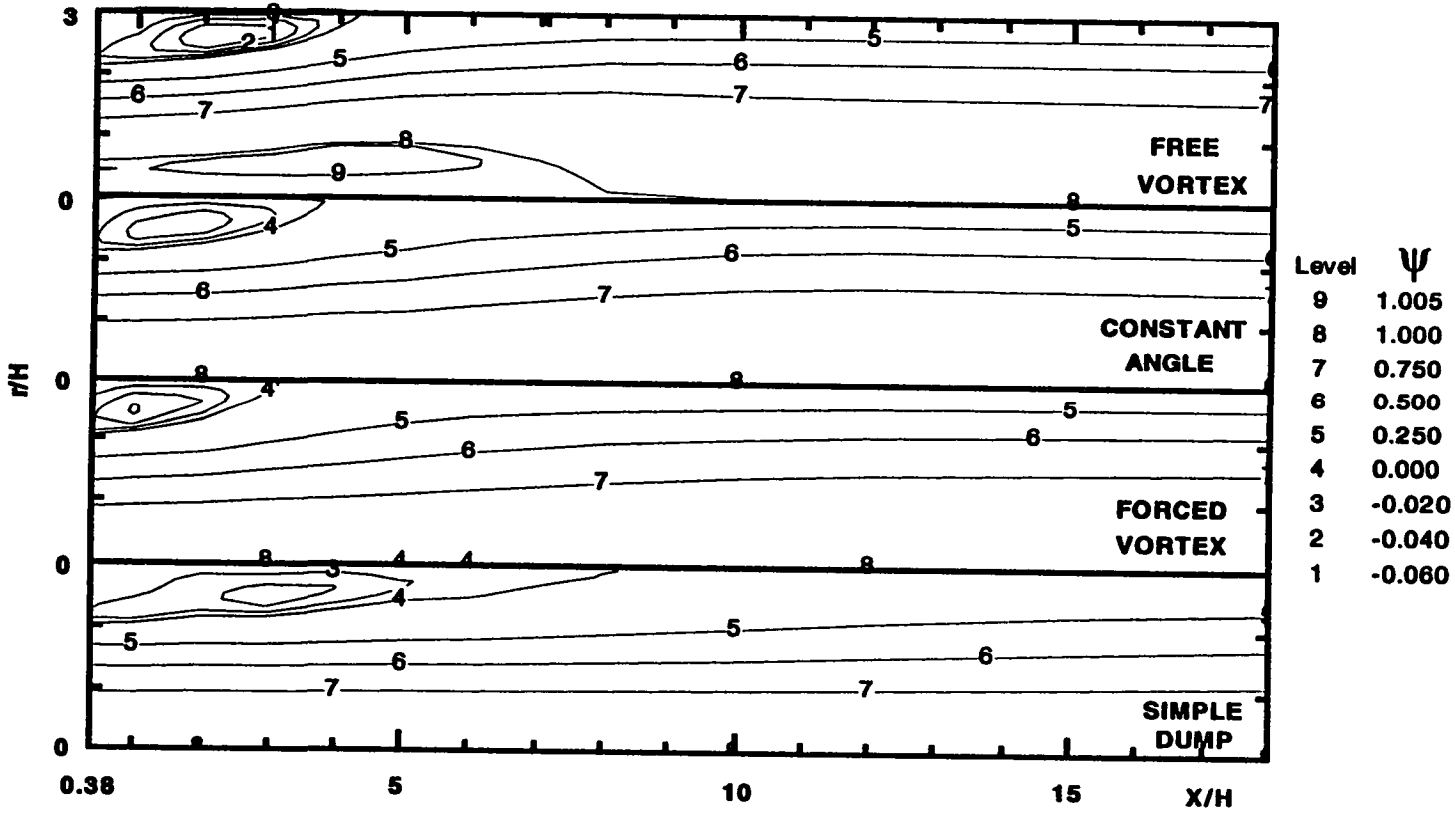

Figure 4.4: The Normalized Stream Function, Effects of Inlet Swirl Profile

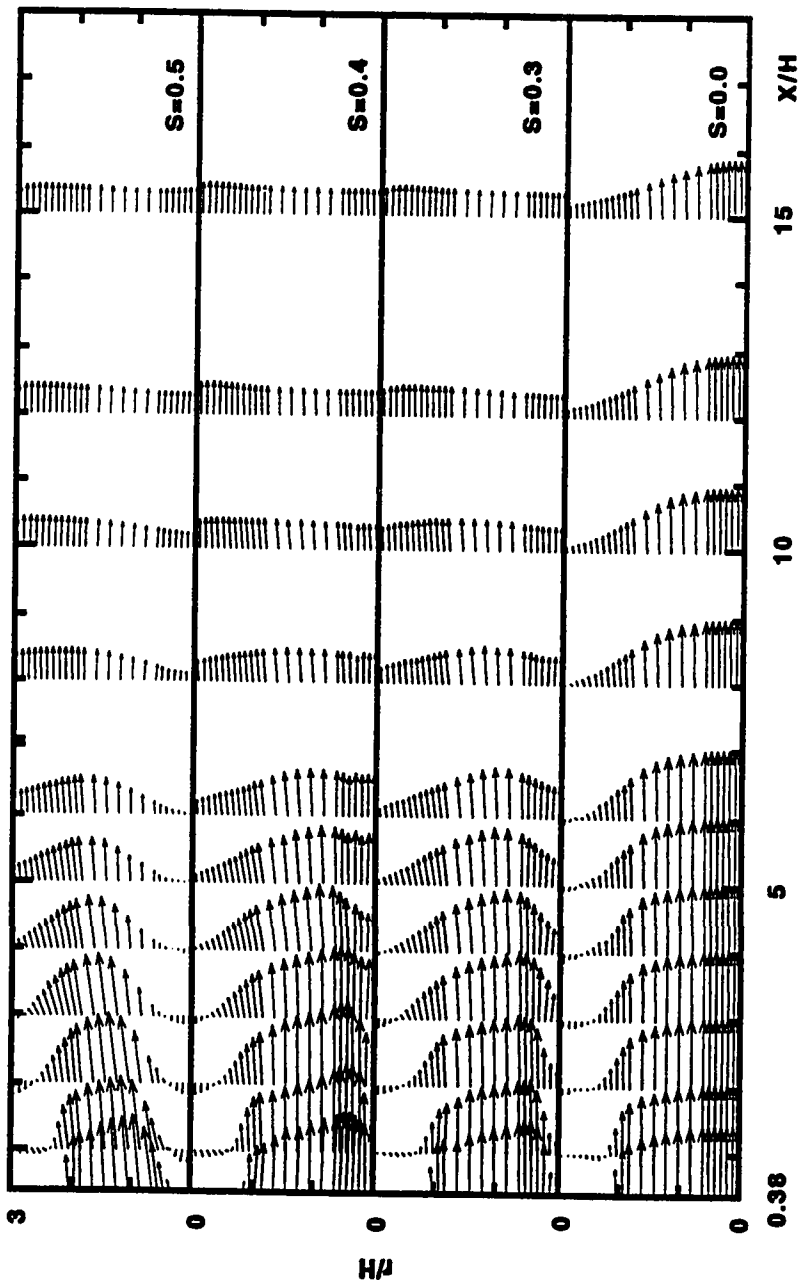

Figure 4.5: Vector Plots of the Time Mean Velocity in the $\bar{U}$-$\bar{V}$ Plane, Effects of Inlet Swirl Strength

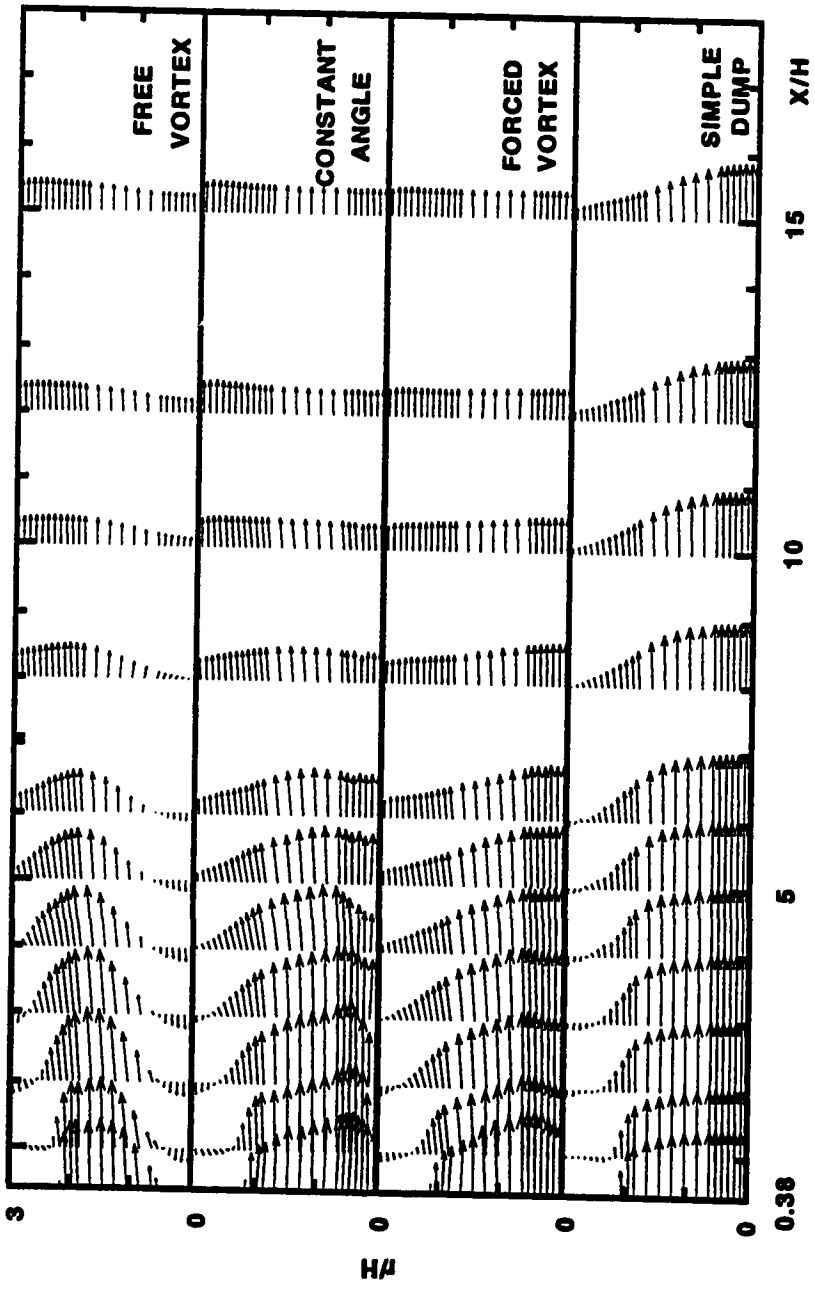

Figure 4.6: Vector Plots of the Time Mean Velocity in the $\bar{U}$-$\bar{V}$ Plane, Effects of Inlet Swirl Profile

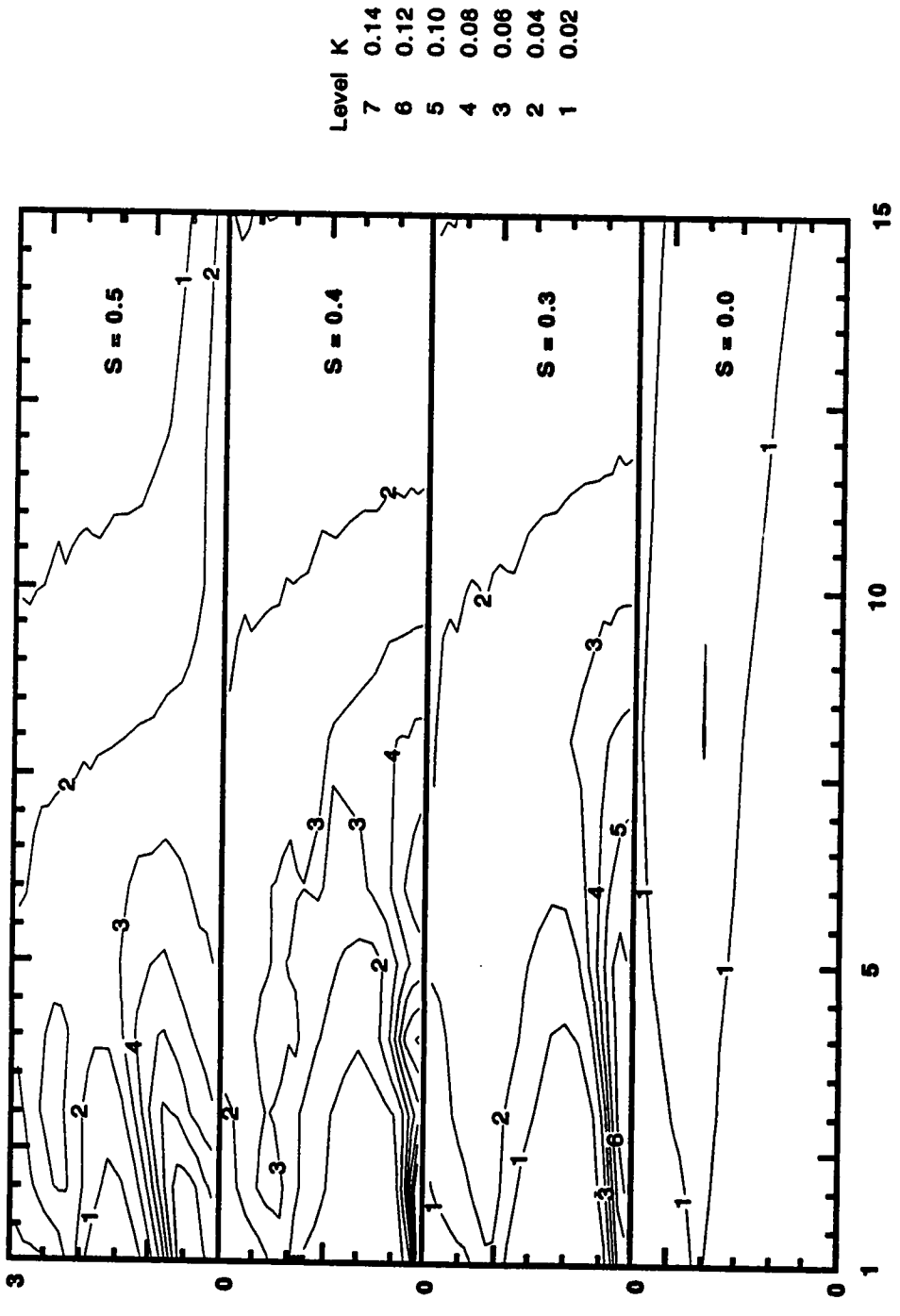

Figure 4.7: Turbulent Kinetic Energy Contour Plots, Effects of Inlet Swirl Strength

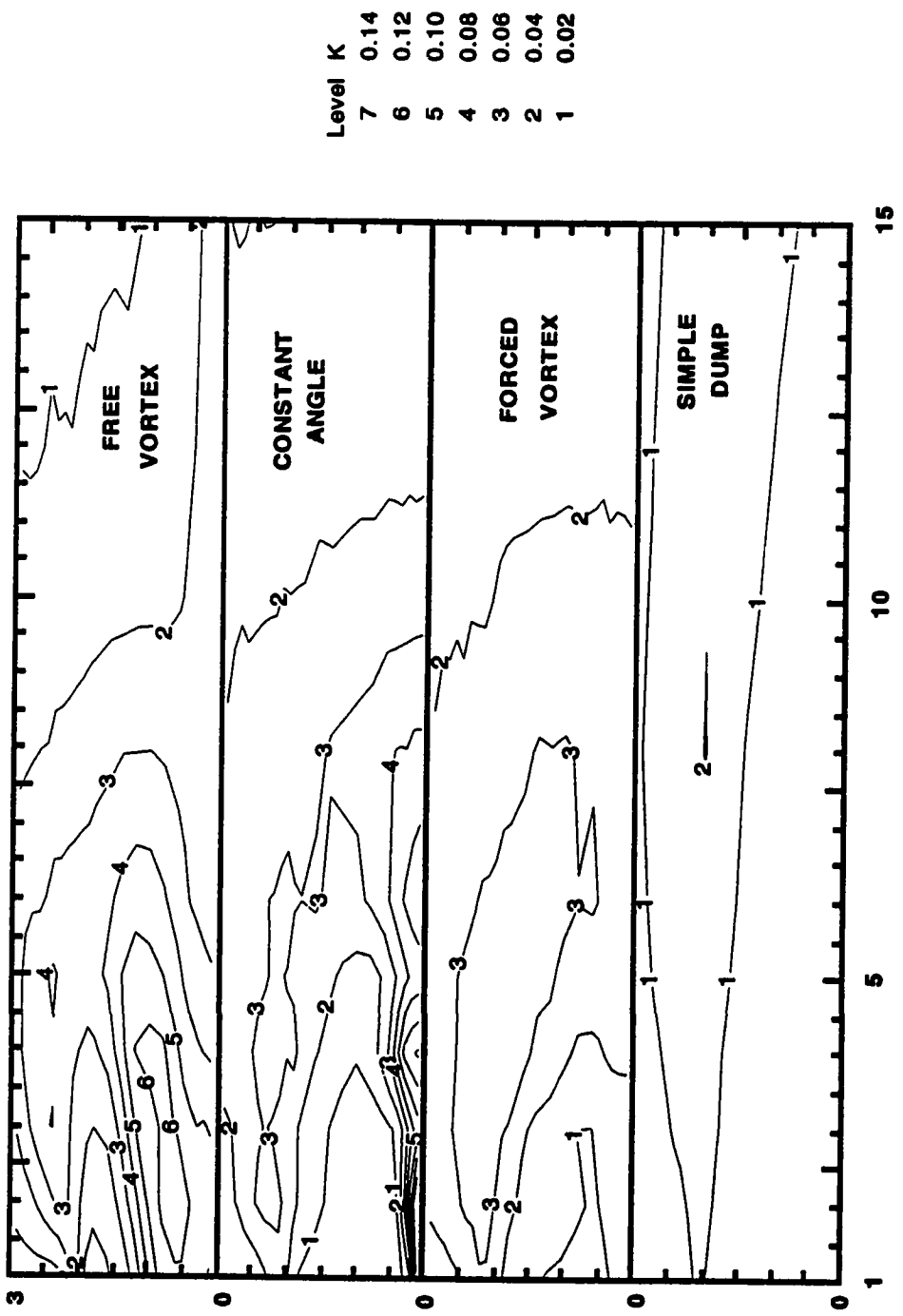

Figure 4.8: Turbulent Kinetic Energy Contour Plots, Effects of Inlet Swirl Profile

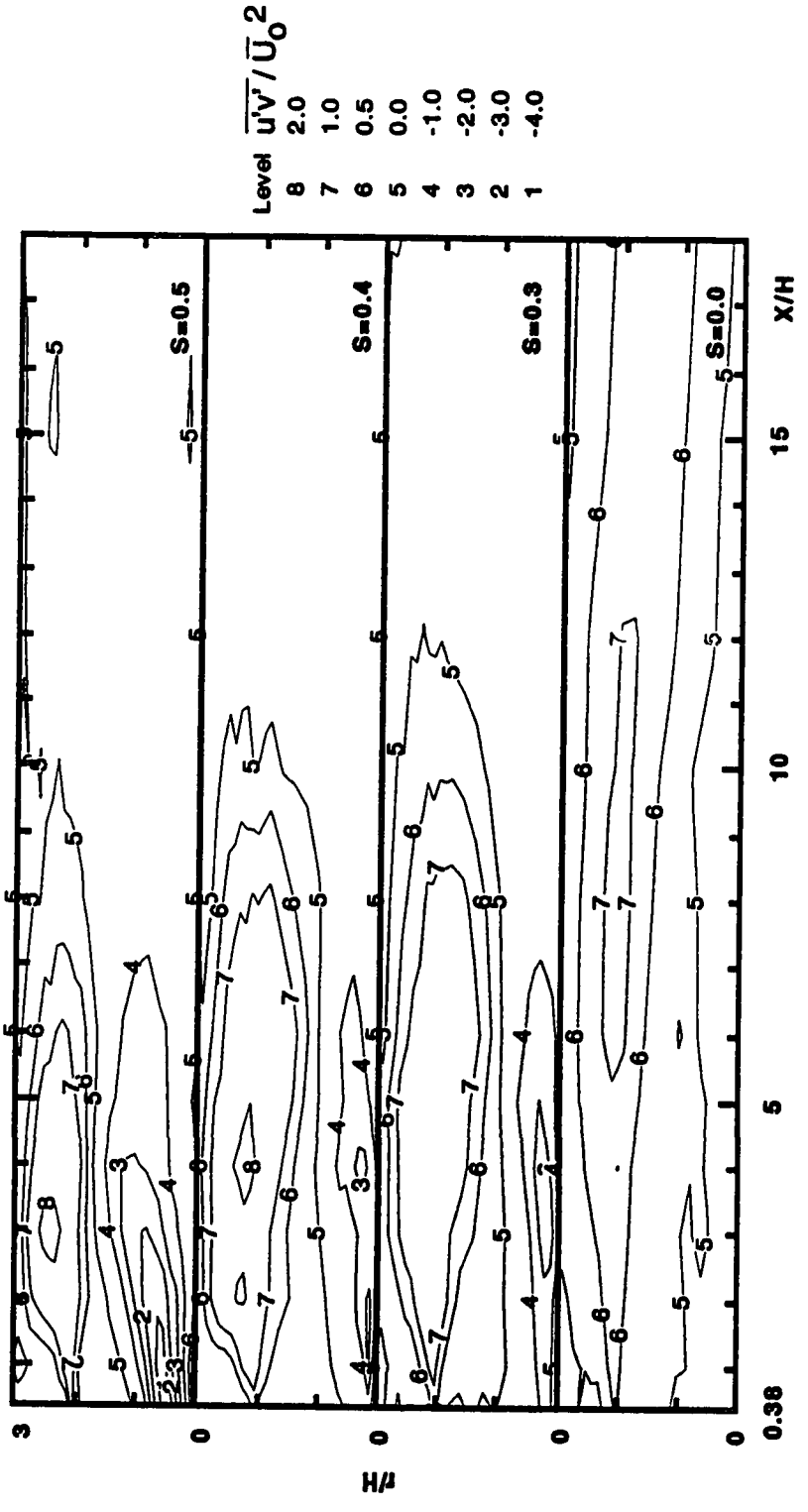

Figure 4.9: Contours of the Shear Stress $\overline{u'v'}/\bar{U}_o^2$, Effects of Inlet Swirl Strength

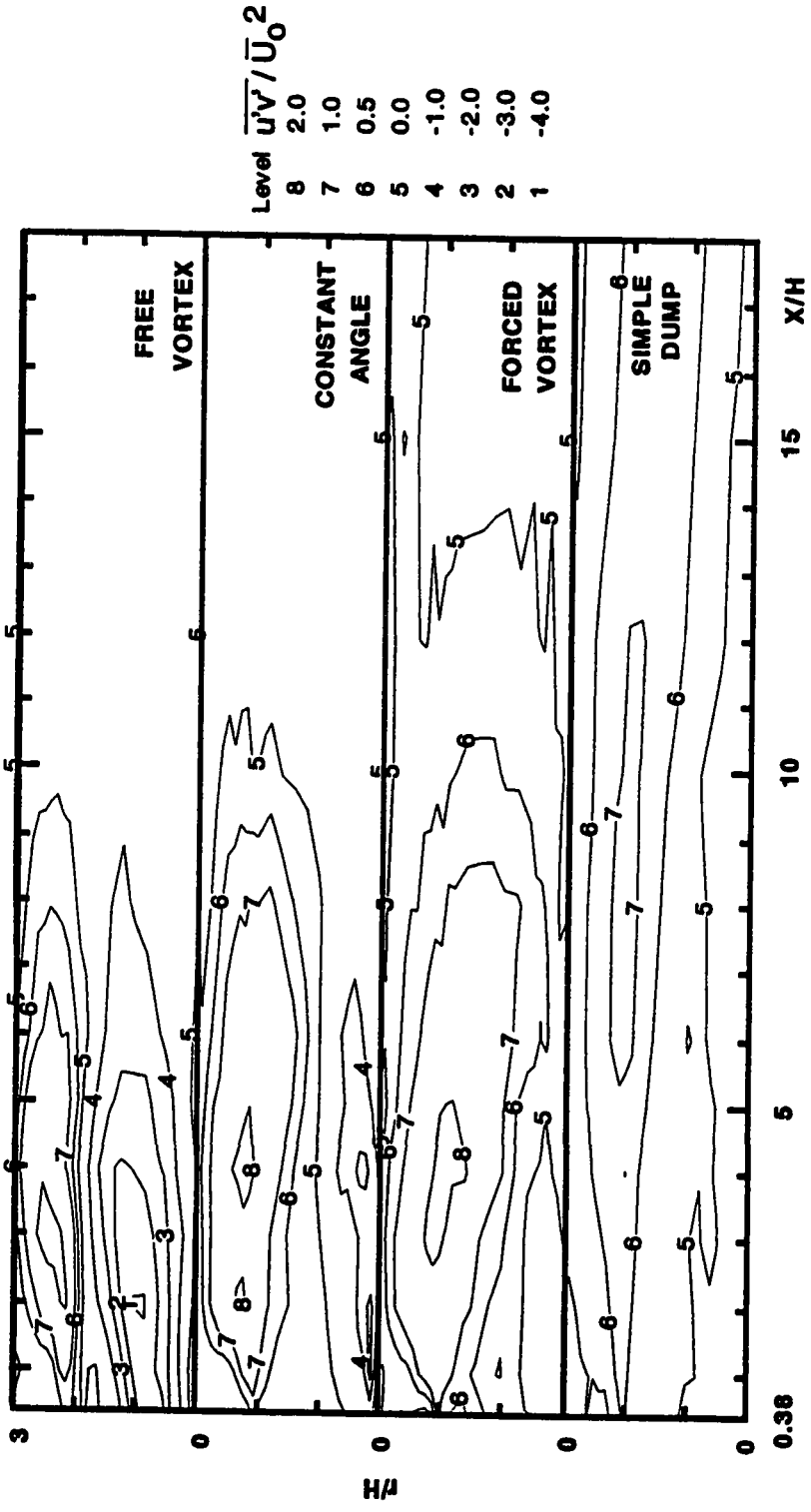

Figure 4.10: Contours of the Shear Stress $\overline{u'v'}/\bar{U}_o^2$, Effects of Inlet Swirl Profile

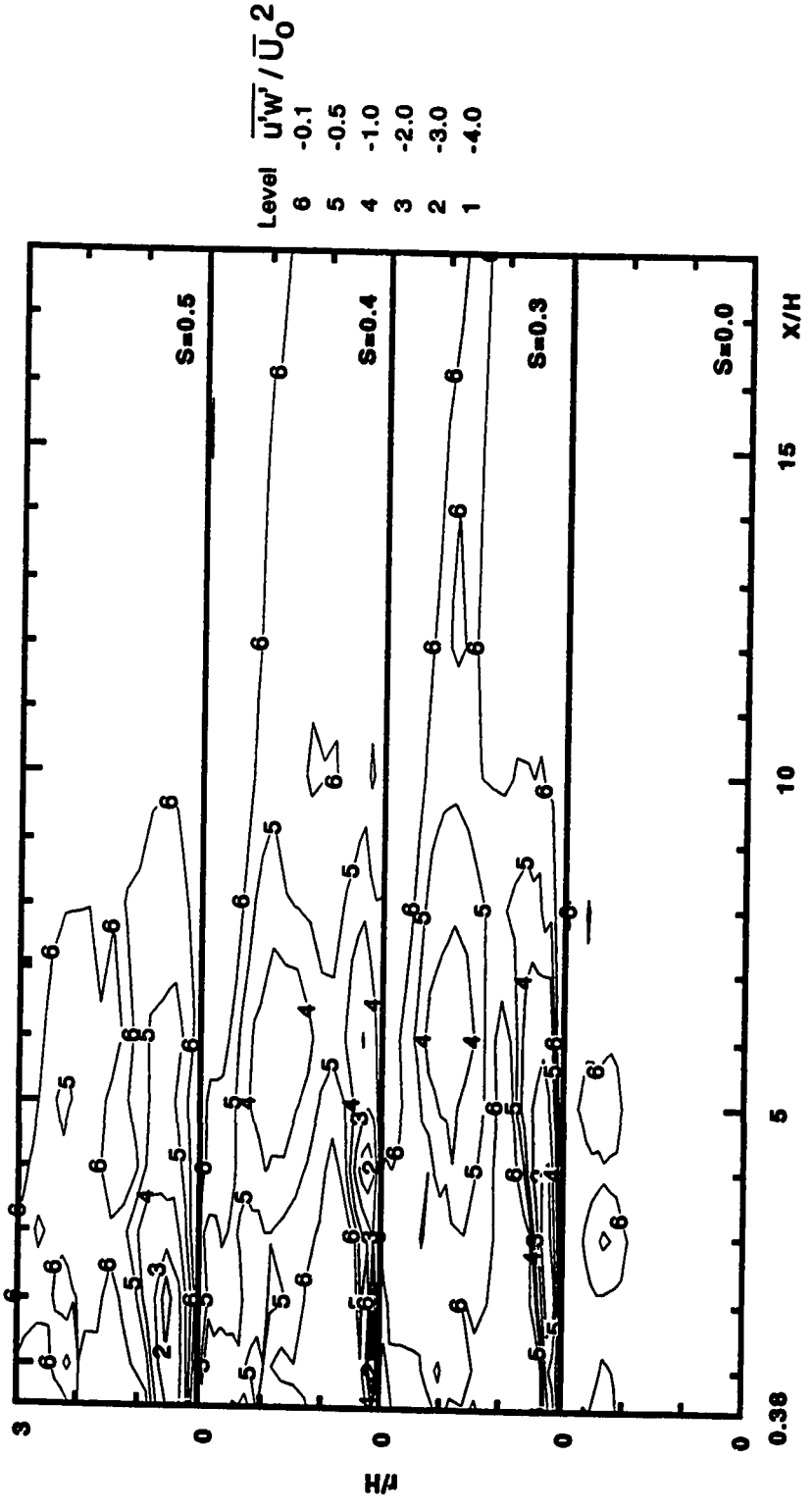

Figure 4.11: Contours of the Shear Stress $\overline{u'w'}/\bar{U}_o^2$, Effects of Inlet Swirl Strength

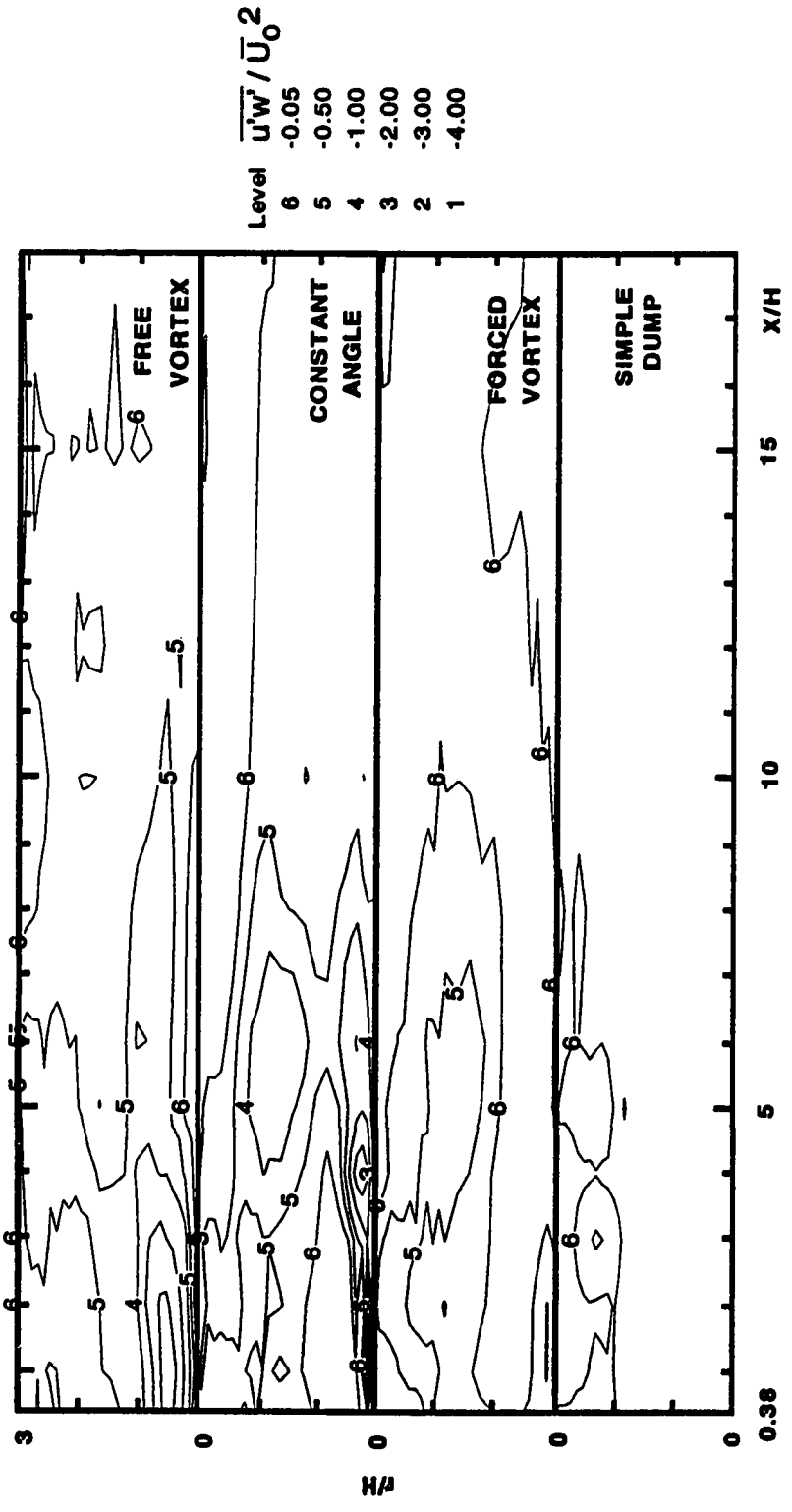

Figure 4.12: Contours of the Shear Stress $\overline{u'w'}/\bar{U}_o^2$, Effects of Inlet Swirl Profile

4.2.1 Effects of inlet swirl strength on TKE terms

The swirl strengths of the swirlers used for this part of the experiment are 0.3, 0.4, and 0.5. These were considered along with the no swirl condition of the inlet flow. The findings made regarding the different terms of the TKE are presented under the following headings.

Production of turbulent kinetic energy

Figure 4.13 shows the production of turbulent kinetic energy variations, at different axial positions along the combustor, in the radial direction from the centerline of the combustor. The production terms, for all the swirl strengths shown, have their highest values close to the centerline of the combustor where steep mean flow gradients exist. The values of these terms diminishes downstream of $x/H = 10$. In particular, the zero swirl case shows highest value of production terms at $r/H = 2.0$. The contour plots of the production terms, Figure 4.14, shows this better. This is at the boundary of the corner recirculation zone CRZ, a region extending from $r/H = 2.0$ to the combustor wall. However, the case is different with the swirling flows. Two peaks, which differ in magnitude, characterizes the swirling flows. One of the peaks is observed near the centerline of the combustor, while the other is close to the border of the CRZ. Generally, all the imparted swirlers demonstrate higher production of turbulence when compared to the zero swirl case. This situation is so in regions up to $x/H = 10$.

For regions beyond $x/H = 10$, values of the production terms are small for all cases considered indicating that there is flow recovery and complete mixing in this region. It is also observed that the high production of turbulent kinetic energy regions, for the $S = 0.5$ case in particular, move towards the combustor wall.

The most significant gain of turbulent kinetic energy production came from the $\rho\overline{u'v'}\frac{\partial\overline{U}}{\partial r}$ component as evident from Figure C.2 in Appendix C. The turbulent shear stress $\rho\overline{u'v'}$, which form part of this component, has a significant mark on the afore-stated behavior of this component of the turbulent kinetic energy production as reported by Ahmed and Nejad[2]. Except for the component of turbulent kinetic energy production referred to in the preceding sentence, all other components of the total production terms have their values, for the zero swirl case, to be comparatively insignificant everywhere in the combustor. In addition, the $\rho\overline{u'v'}\frac{\partial\overline{V}}{\partial x}$ and $\rho\overline{u'w'}\frac{\partial\overline{W}}{\partial x}$ components, shown in Figures C.3 and C.6 respectively in Appendix C, shows relatively no significant value for both the swirled and no-swirl cases everywhere in the combustor. Other components of the turbulent kinetic energy production terms, those of Figures C.1, C.4, C.5, C.7, and C.8 in Appendix C, shows increasing significance with increase in swirl strength.

Convection of turbulent kinetic energy

Figure 4.15 shows the convection of turbulent kinetic energy terms. This is corroborated with its contour plots shown in Figure 4.16. Figure 4.15 shows that the convection of turbulent kinetic energy is more pronounced with the swirled flows. Two peaks of the total convection of turbulent kinetic energy terms are observed. One peak is close to the combustor centerline while the other is at the boundary of CRZ. The contour plots also reveal the high convection of TKE values near centerline of the combustor and in the vicinity of the CRZ. The high values of the convection of TKE at the two regions described indicated that mixing is enhanced in these regions. The turbulent kinetic energy, which is a contributor to the total convection of TKE, demonstrates a similar behavior as stipulated earlier.

The $\rho\overline{U}\frac{\partial k}{\partial x}$ term, axial component of the convection of TKE, made more significant contribution to the gain of the convection of TKE for the swirled flows, its mark on the zero swirl flow being relatively insignificant everywhere in the combustor. However, the radial component contributed more losses of the convection of TKE than the gains. This is most likely due to the less significant radial velocity that is a multiplier in this component. Figures C.9 and C.10 in Appendix C shows the axial and radial component terms of the convection of turbulent TKE.

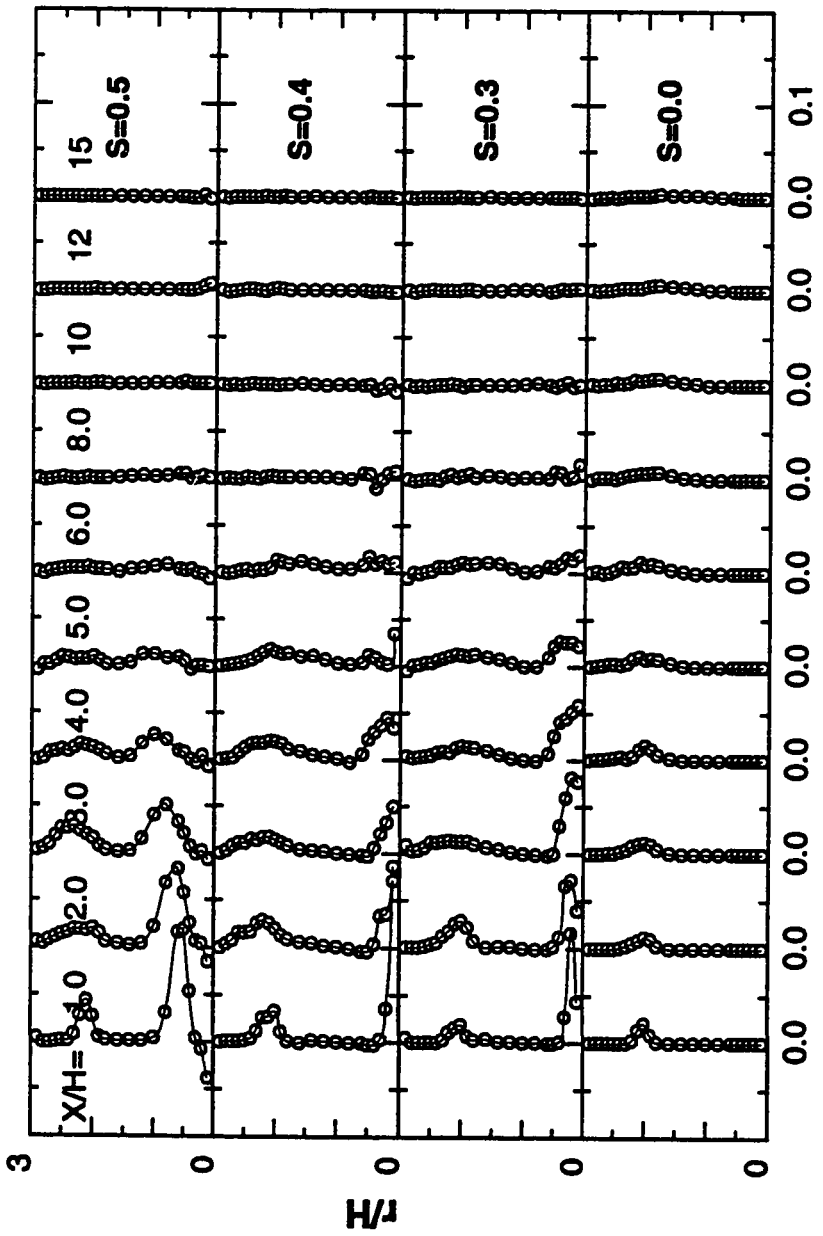

Figure 4.13: Production Terms*H / $\overline{U_o^3}$, Effects of Inlet Swirl Strength

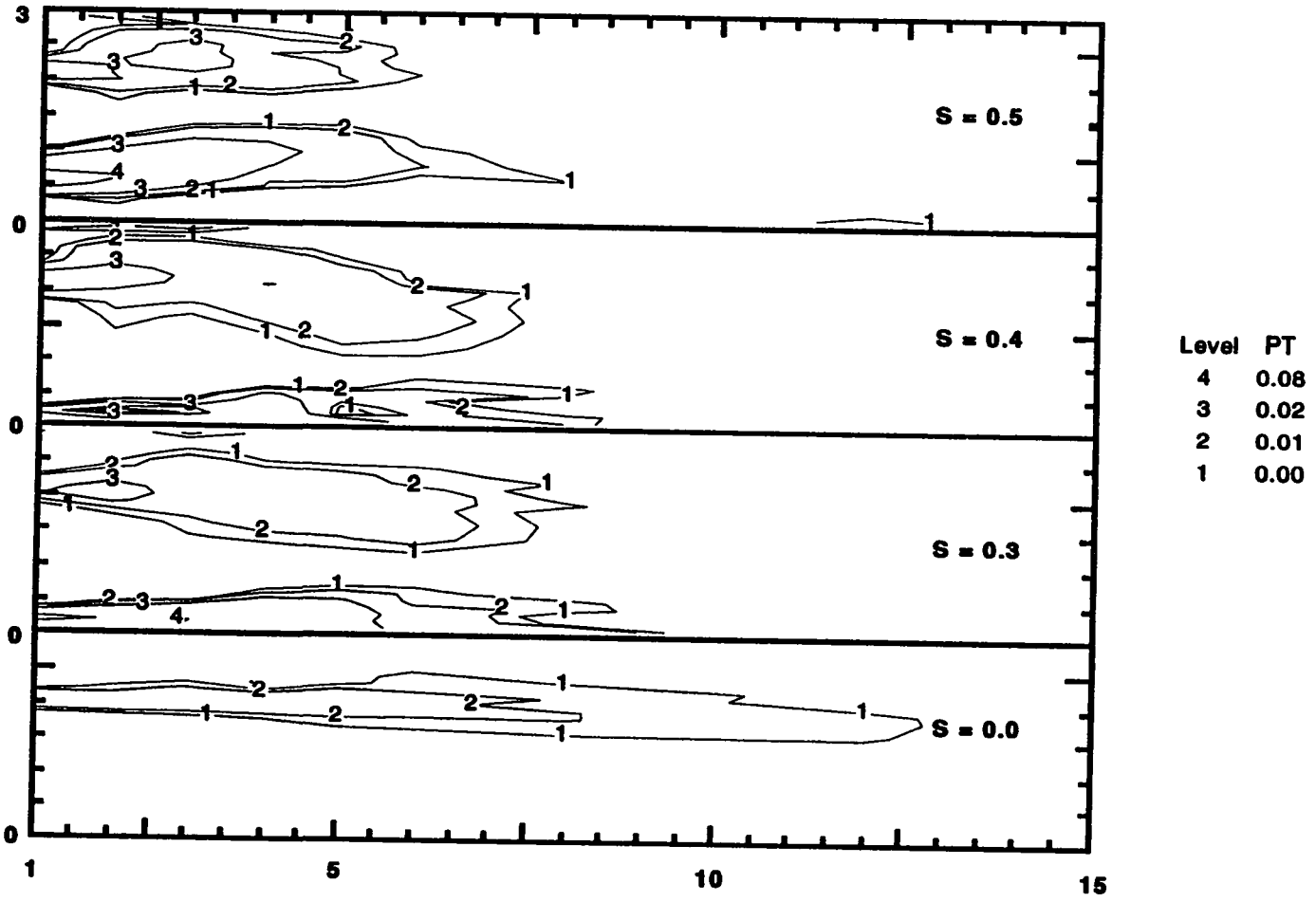

Figure 4.14: Contours of Production Terms, Effects of Inlet Swirl Strength

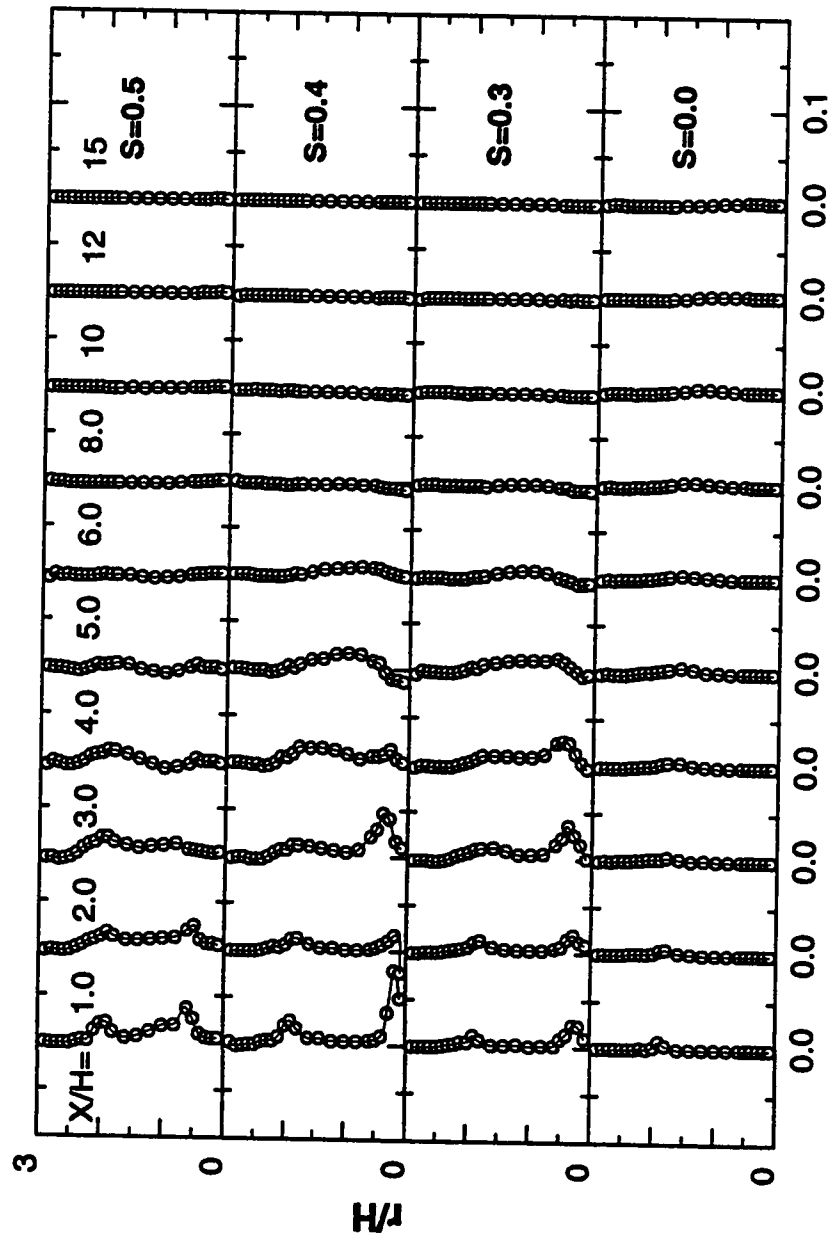

Figure 4.15: Convection Terms* $H / \overline{U_o^3}$, Effects of Inlet Swirl Strength

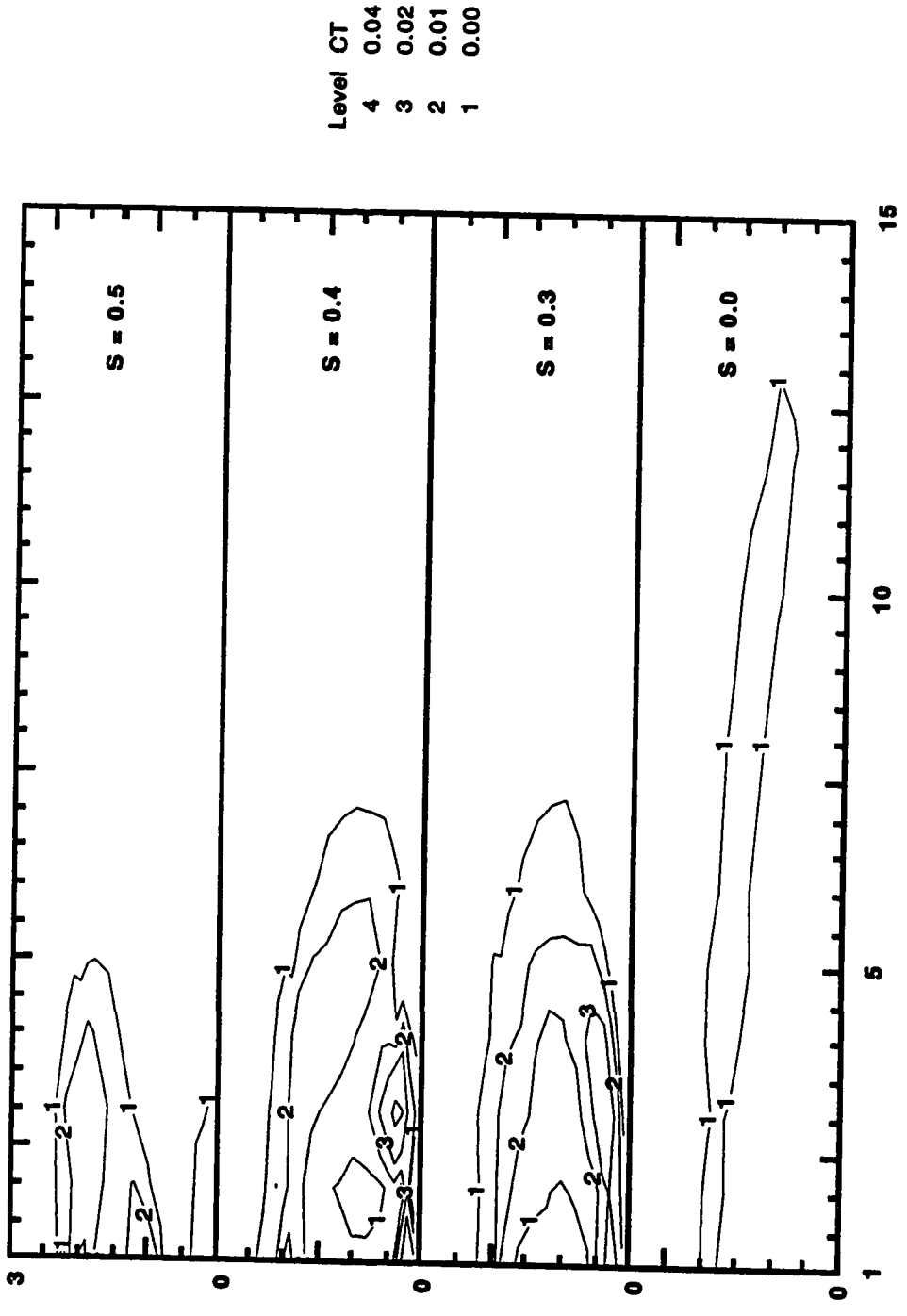

Figure 4.16: Contours of Convection Terms, Effects of Inlet Swirl Strength

Diffusion of turbulent kinetic energy

Figure 4.17 represents the diffusion of TKE. These terms shows antisymmetricity about the centerline of the shear layer. Peak values are observed at either side of the centerline of the shear layer indicating gain and loss of the diffusion of turbulent kinetic energy. Two sets of such activities are observed. As usual, one is close to the centerline of the combustor while the other is at the periphery of the CRZ. These behavior of the diffusion of TKE increases in prominence with increase in swirl strength.

Over 50% of the component terms of the diffusion of TKE make insignificant contribution. This notion is evident from Figures C.11 through C.20 in Appendix C. In particular, the main contribution to the total diffusion term came from the $\frac{1}{r}\frac{\partial}{\partial r}\left(\rho r\frac{\overline{u'^2v'}}{2}\right)$ and $\frac{1}{r}\frac{\partial}{\partial r}\left(\rho r\frac{\overline{v'w'^2}}{2}\right)$ component term as shown in Figures C.13 and C.20 respectively in Appendix C.

Viscous dissipation terms

The viscous dissipation of the turbulent kinetic energy, which was obtained by balance of the turbulent kinetic energy terms, is shown in Figure 4.18. When compared to the production of turbulent kinetic energy, the viscous dissipation terms demonstrate almost the same value as the production of turbulent kinetic energy but opposite in sign. This is an indication that turbulent kinetic energy

production is the most dominant in this type of flow. Similar relationship between the viscous dissipation and the production terms were shown in the earlier works such as those of Driver and Seegmiller[8] and Gould et al.[13]. As was explained earlier, the viscous dissipation term was obtained by difference.

Non-Isotropic Factor

A flow is said to be isotropic if the Reynolds normal stresses are equal. As a result, a non-isotropic flow may be defined as the departure of the Reynolds normal stresses from their mean value. Non-isotropic factors, NIF, are therefore defined as

$$\frac{\overline{u_i'^2} - \frac{2}{3}k}{\frac{2}{3}k}, \quad i = 1..3$$

As it is obvious from the above mathematical expressions, NIF is zero for isotropic flows.

The flow in this study is non-isotropic for most of the combustor flow area. Positive NIF values of 0.2 dominates the combustor flow area. For the swirled flows, the area seen to be nearly isotropic is a region within the CTRZ. The $S = 0.4$ swirler shows no possible isotropy values in within the entire area of the combustor as shown in Figure 4.19.

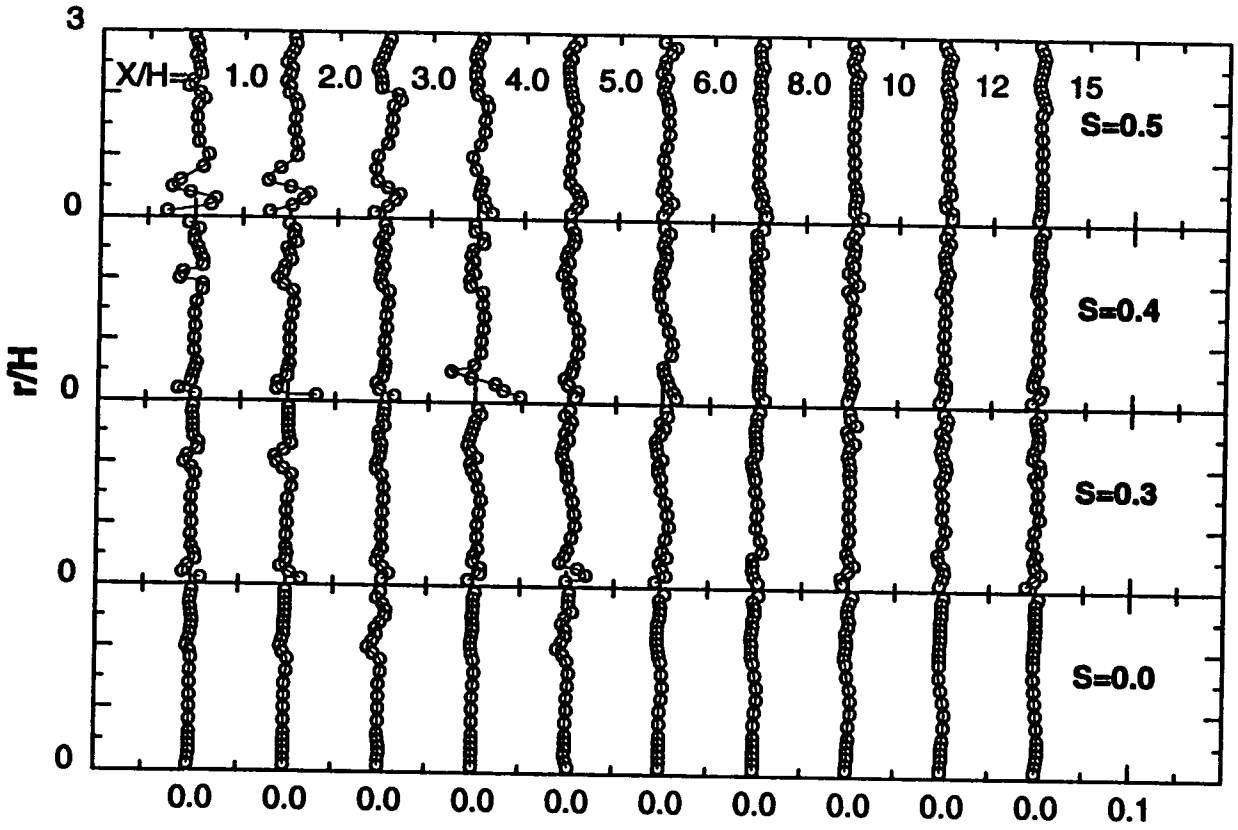

Figure 4.17: Diffusion Terms* H / $\overline{U_0^3}$, Effects of Inlet Swirl Strength

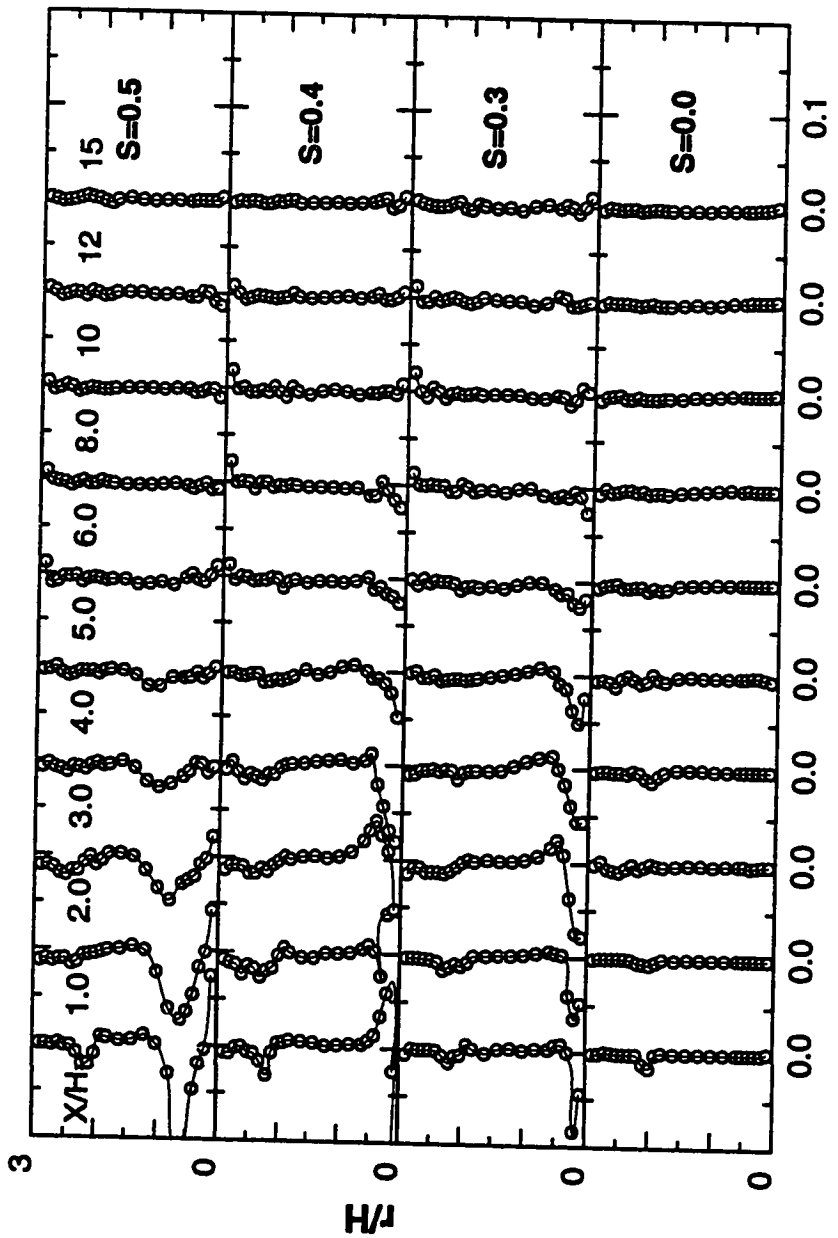

Figure 4.18: Viscous Dissipation Terms* $H / \overline{U_o^3}$; Effects of Inlet Swirl Strength

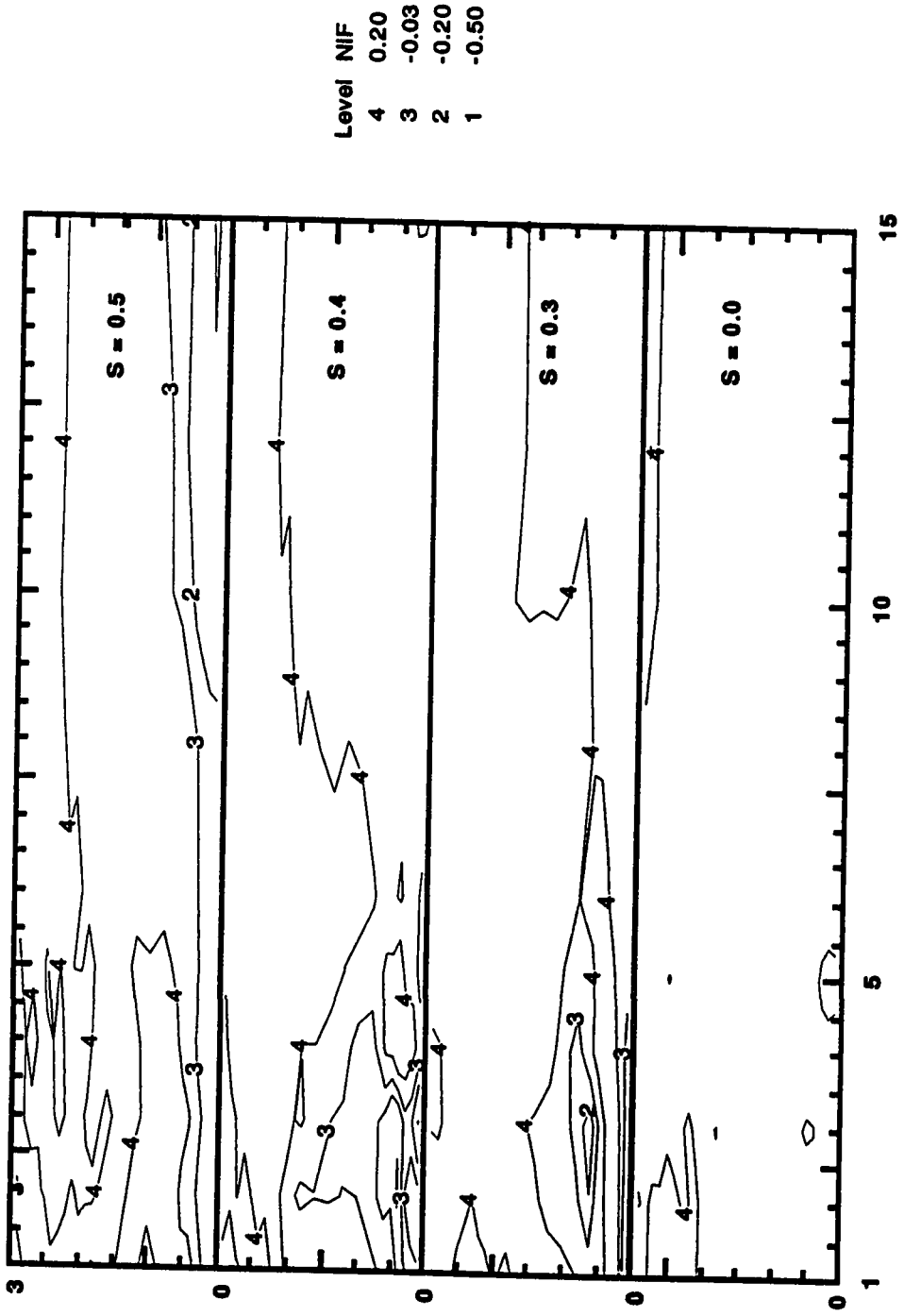

Figure 4.19: Non-Isotropic Factor, Effects of Inlet Swirl Strength

4.2.2 Effects of inlet swirl profile on the TKE terms

The swirl profiles used for this part of the experiment are all of strength 0.4 except for the simple dump which swirl number is synonymous to zero. The simple dump case was included in this analysis in order to see the effect of swirl on the flowfield. The swirl profiles employed for the purpose of this analysis are the forced vortex, the constant angle, and the free vortex profiles. The effect of the inlet swirl profiles on the TKE terms are expounded under the following subheadings.

Production of Turbulent kinetic energy

Figure 4.20 shows the effects of inlet swirl profiles on the combustor flowfield. The contour plots for the effects of inlet swirl profiles on the combustor flowfield is as depicted in Figure 4.21. The features of the free vortex ($S = 0.4$) inlet swirl profiles is basically the same with those of the swirl strength of 0.5 as discussed earlier, despite the difference in their swirl strength. This is an indication that swirl type is as important as swirl number and that swirl type could increase or decrease the effective swirl number on the flow. However, their peak values, that move towards the wall of the combustor as they diminishes downstream, differ in magnitude. For instance, around the combustor inlet at $x/H = 1.0$ and $x/H = 2.0$, the free vortex has peak values of 0.08 and 0.072 respectively at the periphery of the CTRZ, while the peak values of the $S = 0.5$ swirler, for the

same axial position, are 0.12 and 0.08 respectively. The profiles of the simple dump and forced vortex swirl profiles are similar in that they both have one peak each on the boundary of the CRZ. The constant angle swirl profile ($S = 0.4$) and the inlet swirl strength $S = 0.4$ demonstrates similar behavior since they are the same swirler.

For the simple dump and forced vortex cases, the most significant contribution came from the $\rho\overline{u'v'}\frac{\partial \overline{U}}{\partial r}$ component term, while the other component terms made, relative to this term, very little or no contribution at all to the production of turbulent kinetic energy (see Figures D.1 through D.8 in Appendix D). The $\rho\overline{v'w'}\frac{\partial \overline{W}}{\partial r}$ and $\rho\overline{v'w'}\frac{\overline{W}}{r}$ terms, made equal but opposite contributions to the production of the TKE in the case of the free vortex and constant angle swirlers. This mark is seen around the centerline of the combustor. In general, the $\rho\overline{u'v'}\frac{\partial \overline{U}}{\partial r}$ term demonstrates a comparatively significant contribution to the total production of TKE for all the swirlers studied.

Convection of turbulent kinetic energy

Although less obvious than the case of production terms, the imparted swirlers altered the general features of the convection of TKE for the simple dump situation as represented in Figure 4.22. The simple dump case shows only a peak value at the boundary of the CRZ. This peak diminishes downstream of the flowfield

and it is not as prominent as in the swirled cases. For the forced vortex, the only peak value occurred at the CRZ too but more visible when compared to the simple dump case.

In contrast to the simple dump and forced vortex cases, the constant angle and free vortex swirlers caused the convection of the TKE to have two peak values. As can be seen from Figure 4.22, one of the peak values of the convection terms for these swirler inlet conditions occurred at the boundary of the CTRZ and the CRZ. However, the constant angle case shows higher peak values close to the centerline of the combustor.

The peak values of the convection terms described above can be easily discerned from Figure 4.23, which shows the contours of the convection terms being discussed. As convection is known to be the transfer of energy from one location to the other by the movement of molecules, the high values of the convection of TKE at the regions described indicated that mixing is significantly improved in these regions.

The radial and axial convection of TKE, which are the components of the total convection of TKE, both made significant contributions to the gain of total convection of the TKE. In particular, the free vortex got significant contributions

from both components. In the same manner but to a lesser degree compared to the free vortex case, the simple dump and the forced vortex cases had contribution from both the axial and radial components of the convection terms. The axial component contributed more in the case of constant angle inlet swirler. Figures D.9 and D.10 in Appendix D shows the radial and axial components of the convection of TKE terms respectively.

Diffusion of turbulent kinetic energy

The diffusion of TKE, shown in Figure 4.24, revealed two sets of antisymmetric patterns about the centerline of the shear layer for the swirled conditions. In the vicinity of the centerline is one, while the other is around the border of the CRZ. These antisymmetric behavior of the diffusion of TKE, which increases in prominence from the simple dump case to the free vortex case of the inlet swirler condition, have peak values at either side of the centerline of the shear layer. The simple dump inlet flow condition demonstrates its only activity around the CRZ in a comparatively less significant manner.

The main contribution to the total diffusion term came from the $\frac{1}{r}\frac{\partial}{\partial r}\left(\rho r\frac{\overline{u'^2v'}}{2}\right)$ and $\frac{1}{r}\frac{\partial}{\partial r}\left(\rho r\frac{\overline{v'w'^2}}{2}\right)$ component term as shown in Figures D.13 and D.20 respectively in Appendix D. The remaining components, also shown in Appendix D, made very little or no contribution at all.

Viscous dissipation of turbulent kinetic energy

Shown in Figure 4.25 is the viscous dissipation of the turbulent kinetic energy which was obtained by balance of the TKE. For the free vortex inlet swirler condition, the viscous dissipation terms has peak values similar, both in magnitude and location, to those of the production terms but opposite in sign. In the case of the constant angle inlet swirl condition, the peak values of the viscous dissipation terms are visible close to the centerline of the combustor and in the vicinity of the CRZ. However, only one distinct peak value is observed for the simple dump and forced vortex inlet flow conditions. In the case of the simple dump, the peak increases in prominence from the reattachment point upstream of the flowfield while it diminishes downstream of the flowfield from the reattachment point.

Non-Isotropic Factor

Figure 4.26 shows the contour plots of the NIF for the inlet swirl profiles. The free vortex ($S = 0.4$) case indicates the possibility of isotropy within the CTRZ, a region that is not of serious importance as little or no mixing occur there. The forced vortex ($S = 0.4$) case revealed there might be a possible isotropy of the flow in a narrow area of the region where mixing occur. Allowing a ± 0.2 value of NIF for the isotropic region, the isotropic region for the free and forced vortex is only a small fraction of the mixing area of the flow.

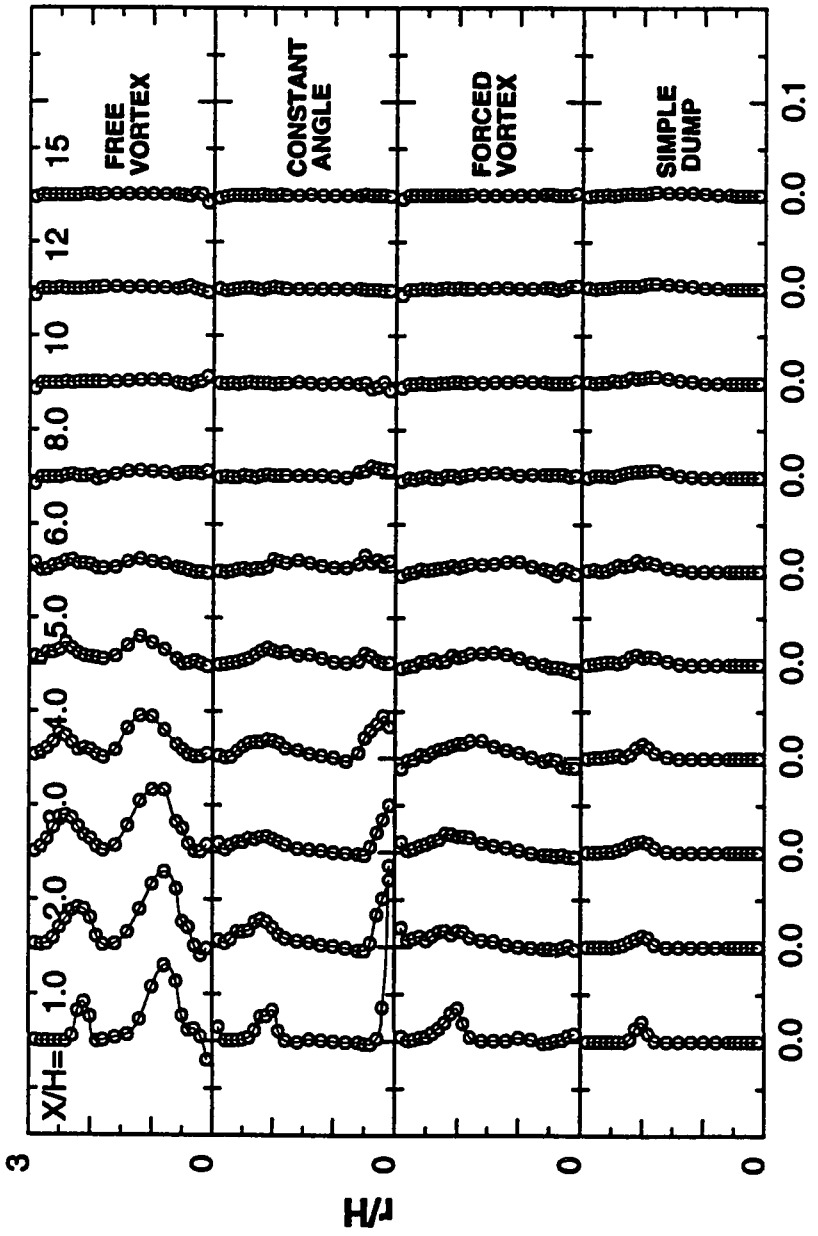

Figure 4.20: Production Terms $^{*}H / \overline{U_o^3}$, Effects of Inlet Swirl Profile

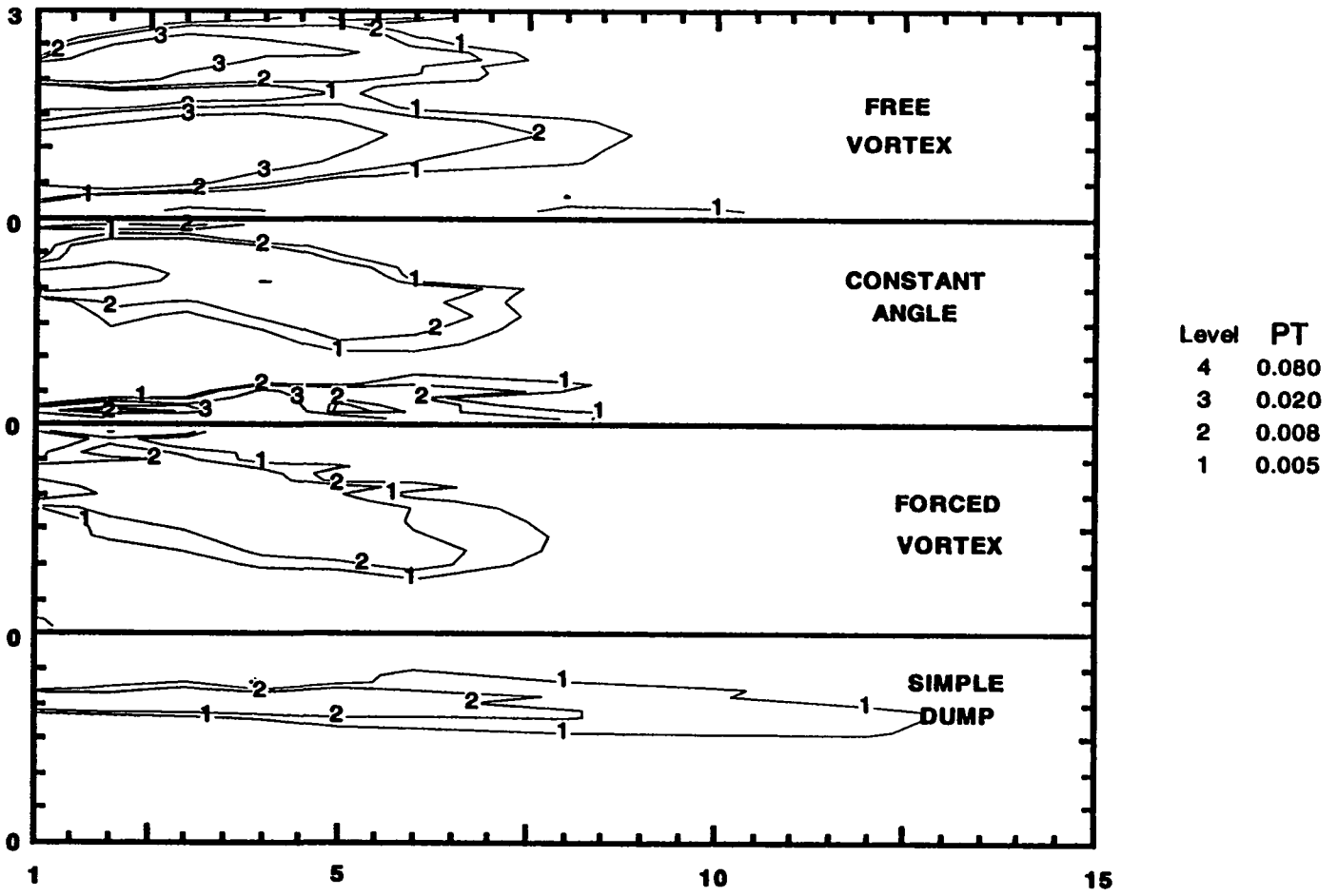

Figure 4.21: Contours of Production Terms, Effects of Inlet Swirl Profile

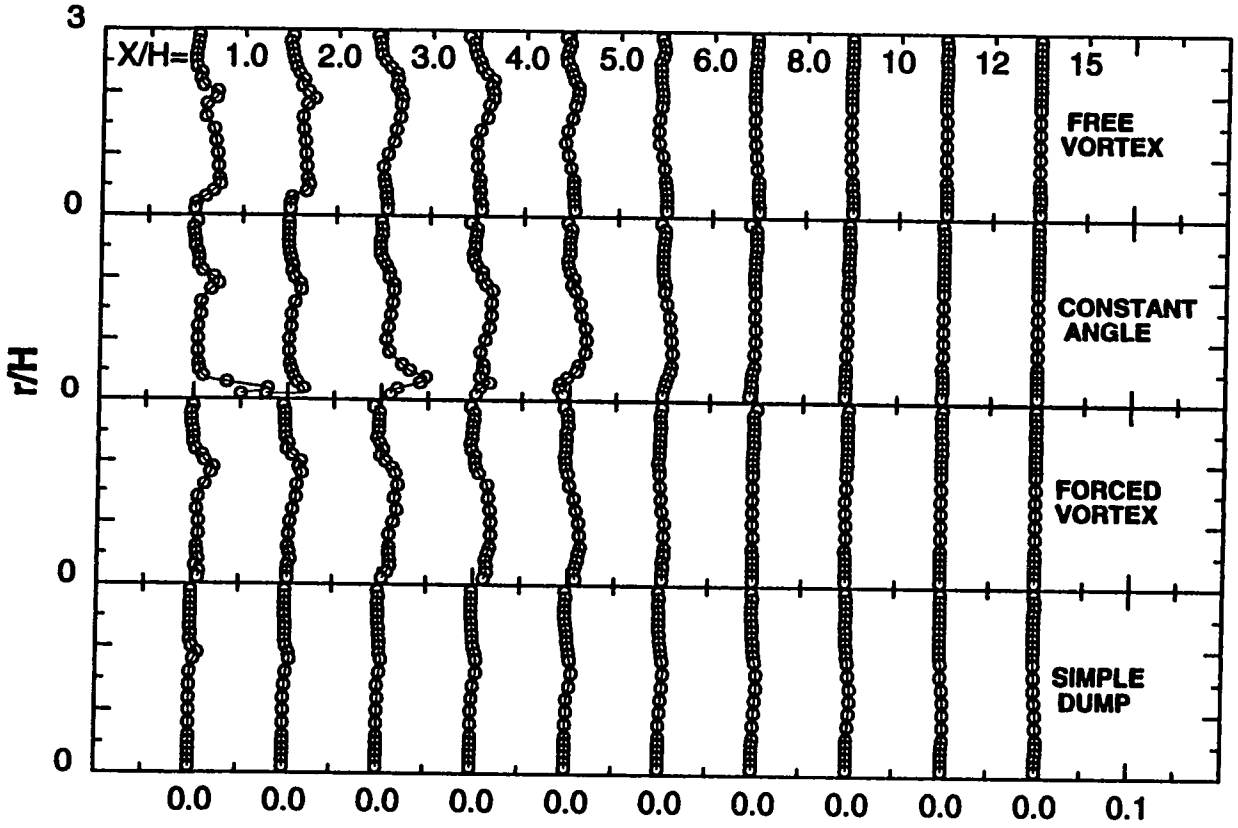

Figure 4.22: Convection Terms*H / $\overline{U_0}^3$, Effects of Inlet Swirl Profile

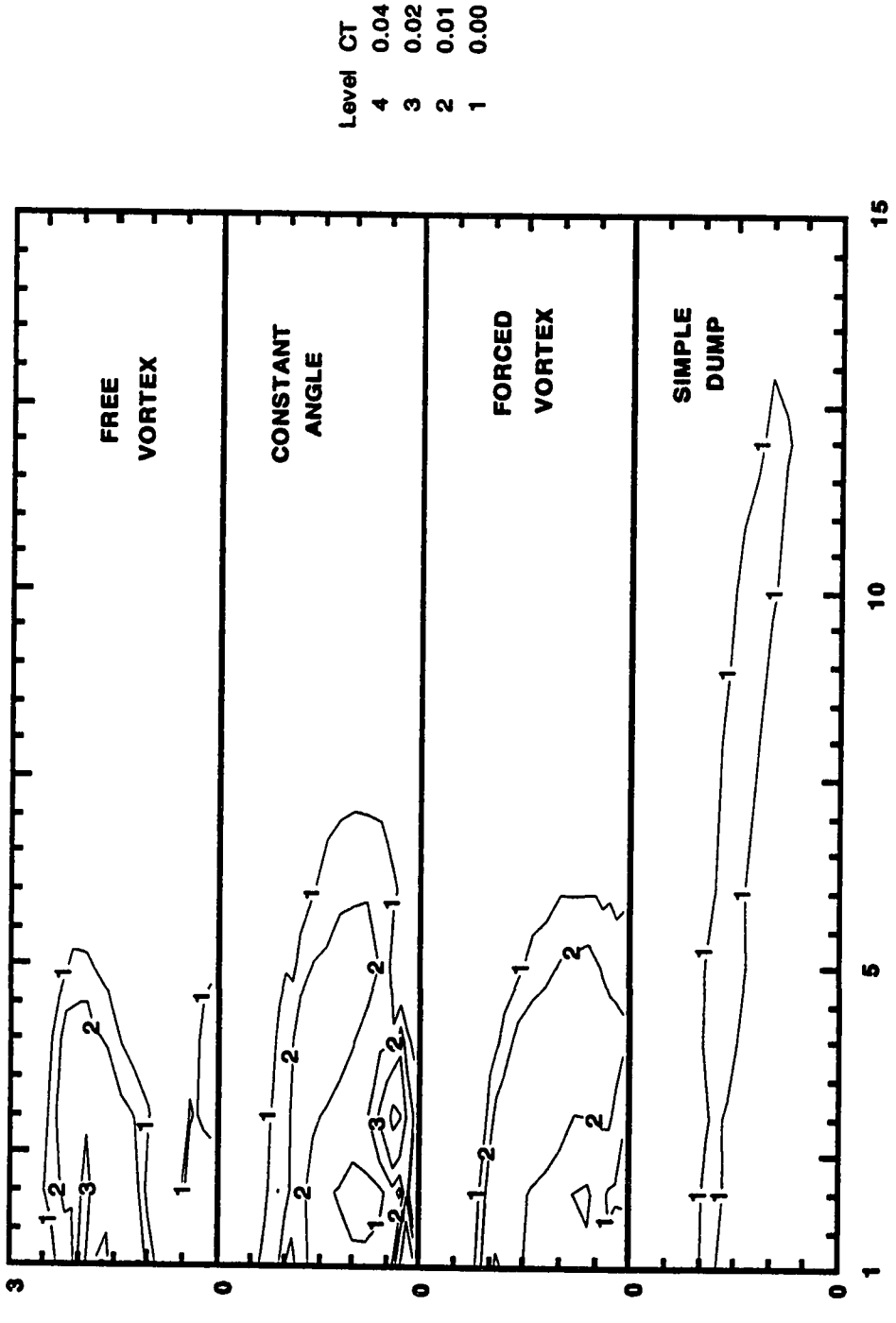

Figure 4.23: Contours of Convection Terms, Effects of Inlet Swirl Profile

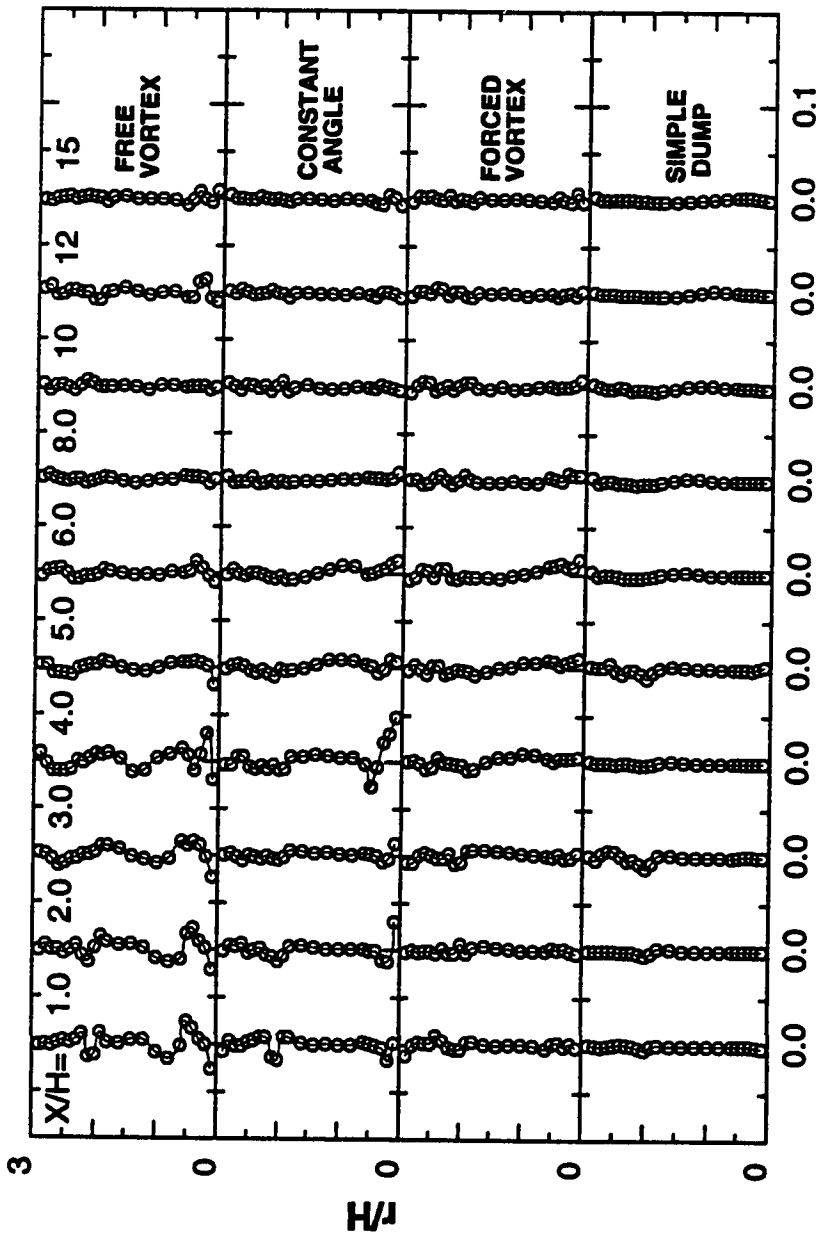

Figure 4.24: Diffusion Terms $\overline{H / U_o^3}$, Effects of Inlet Swirl Profile

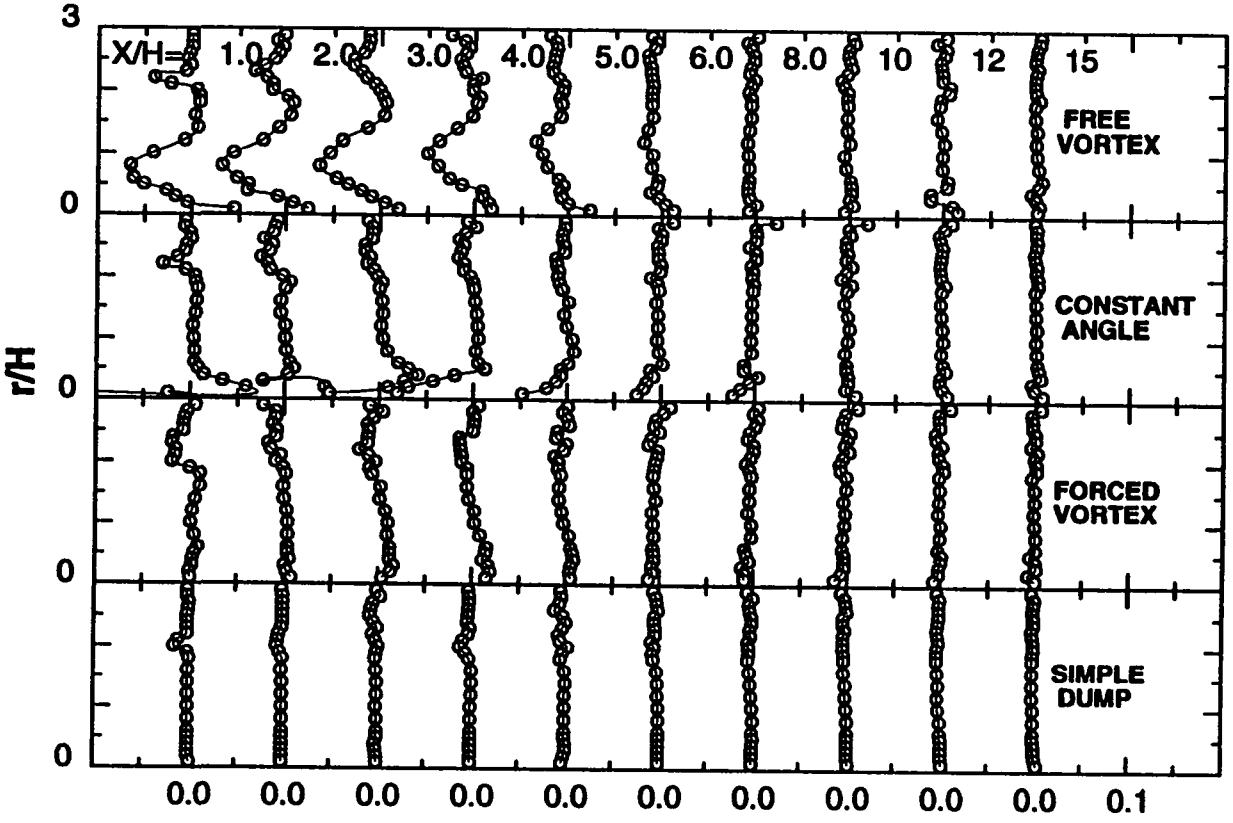

Figure 4.25: Viscous Dissipation Terms* H / $\overline{U_o^3}$, Effects of Inlet Swirl Profile

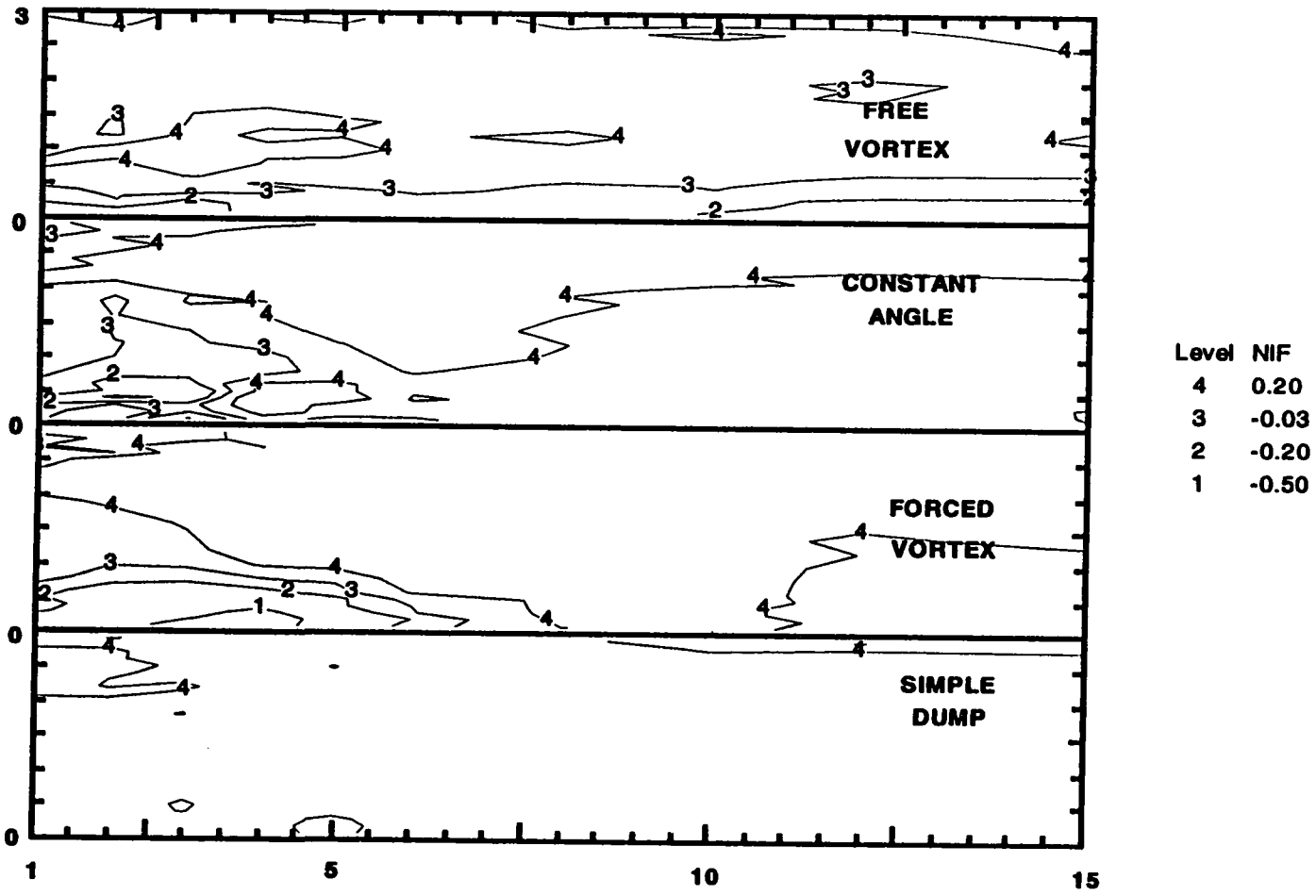

Figure 4.26: Non-Isotropic Factor, Effects of Inlet Swirl Profile

4.3 Comparison of results

The experimental data presented are extensive and detailed. As such, there are no existing works with which this results could be compared in its entirety. However, the simple dump case analysed could be compared to the results of Gould et al.[13]. Figure 4.27 through 30 shows the comparison of the TKE terms from the present work with those of Gould.

The turbulent kinetic energy terms from this result shows similar shapes with those presented by Gould et al. but have different peak values. The $\rho\overline{u'v'}\frac{\partial\overline{U}}{\partial r}$ component term dominates the total production of turbulent kinetic energy term in both studies. Generally, Gould reported peak values that are about 2.5 times the ones reported in this study. The differences in peak values are most likely due to the different expansion ratios used in both studies. Gould used an expansion ratio of 4:1 while an expansion ratio of 2.25:1 was employed in this study. Earlier, Gould reported a similar reason (i.e., difference in expansion ratios) to be responsible for the differences in peak values between his measured quantities and those of Driver and Seegmiller[8]. The positions at which the peak values of the turbulent kinetic energy terms occurred, from these results and those presented by Gould et al., are also at par. For instance, the peak values of the production terms for the present study occurred at $r/R_c = 0.667$, the position of sudden

expansion, while peak values of the same terms presented by Gould et al. also occurred at the position of sudden expansion equivalent to $r/R_c = 0.5$.

The convection terms in both results have their peak values successively moving toward the centerline. For the diffusion terms, where there exist loss and gain of the diffusion of TKE, the loss peak commenced at the position of sudden expansion and died out downstream along the combustor length. The peak for the gain of the diffusion of TKE moved towards the centerline as it varnishes downstream along the combustor length. The peak values of the dissipation terms, which was obtained by balance of the turbulent kinetic equation as mentioned earlier, shows a similar trend when compared to those of the production terms but with opposite sign indicating that the production term is the most dominant term of the TKE. It is worth noting, however, that the peak values of the dissipation terms are not equal to those of the production terms.

The correction lens used by Gould, for the purpose of flow properties measurement, could only allow simultaneous axial-radial velocity measurements up to about 83% of the nondimensional radius, whereas the database used for this study documents axial-radial velocity values for the entire nondimensional radial positions. Hence, the features of the TKE terms from this study were obtained up to the vicinity of the wall whilst Gould's results showed only features at positions

up to about 83% of the nondimensional radius(i.e., a position about 17% of the nondimensional radius away from the wall).

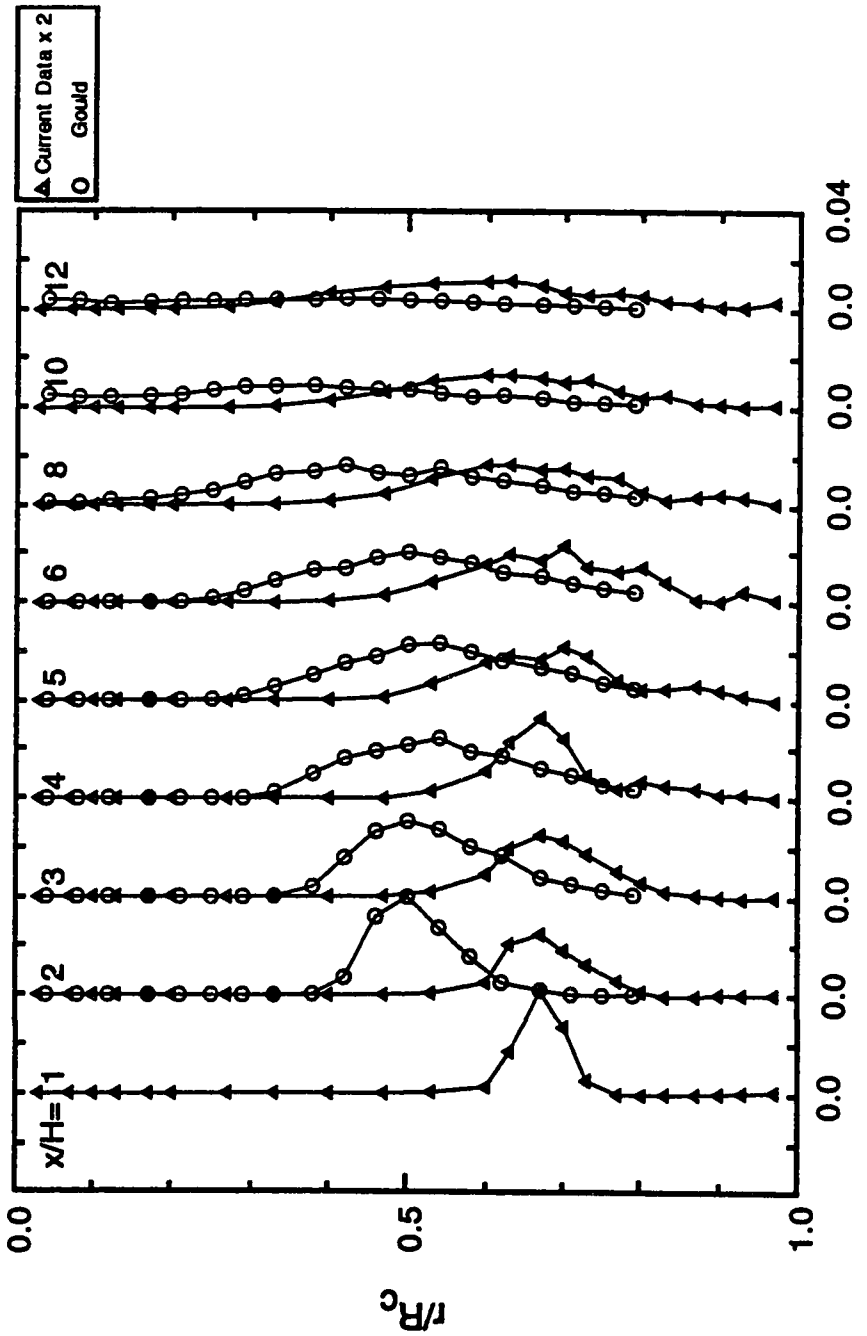

Figure 4.27: Production Terms

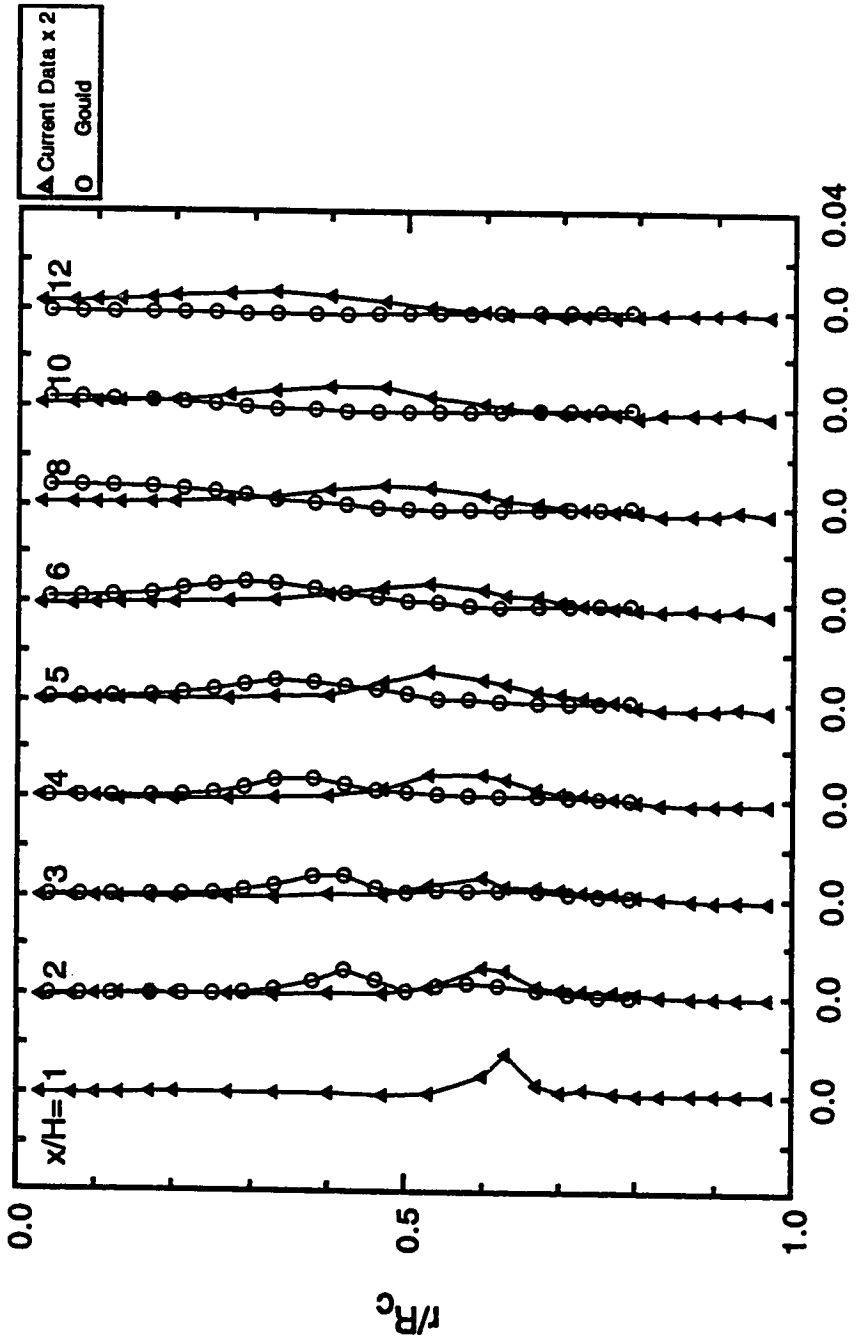

Figure 4.28: Convection Terms

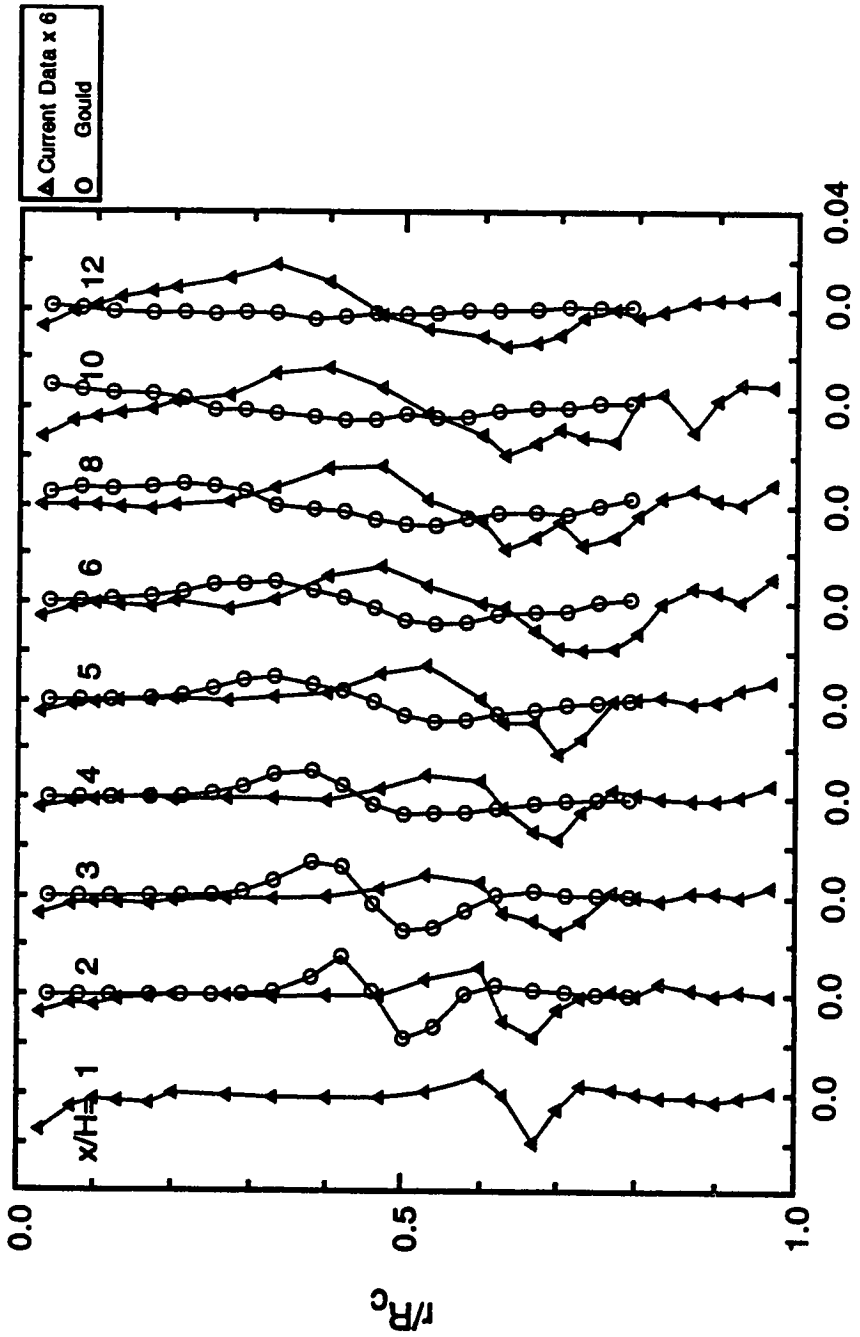

Figure 4.29: Diffusion Terms

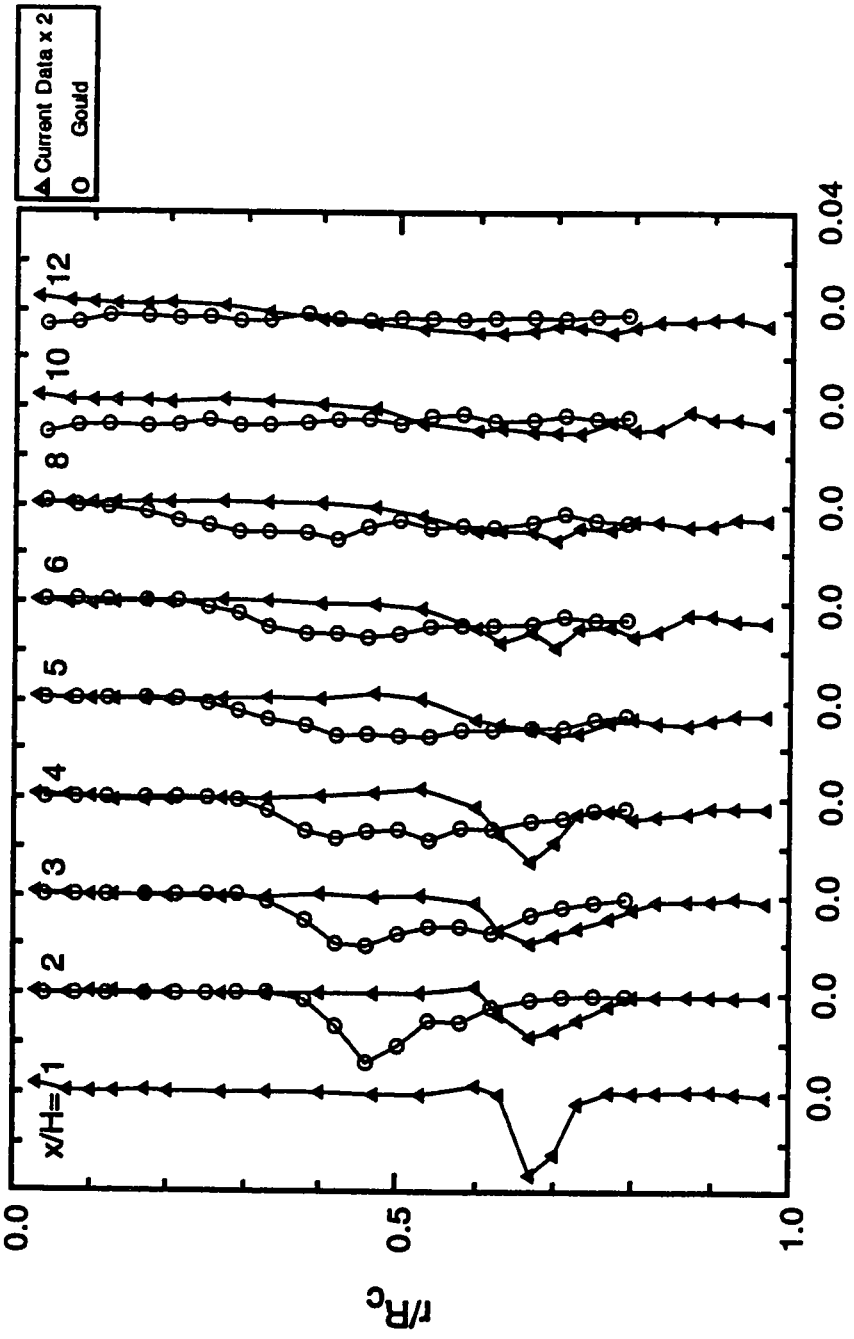

Figure 4.30: Viscous Dissipation Terms

Chapter 5

CONCLUSIONS

From the discussions so far, it is glaring that the inlet swirl affects the development of sudden expansion coaxial dump combustor flowfield. It was shown that all swirlers significantly changed the length of the CRZ. In addition, the high velocity gradients intensified mixing giving room for smaller combustors to be used. Furthermore, the turbulence intensity and shear stress increased significantly with increase in swirl number in the turbulent flowfield. Most often, the $S = 0.5$ (constant angle), and the free vortex ($S = 0.4$) swirlers showed similar features. For instance, both of these cases had similar velocity and turbulence profiles. This behavior is an indication that the flowfield characteristics depend not only on the strength of the swirl, but also on the swirl profile.

Specifically, the following concluding statements could be made from the results

of this study:

1. the mixing layer is small in the case of simple dump flow but quite large in the case of the free vortex flow;

2. CRZ reduces with increase in swirl strength;

3. reverse flow regions of different sizes were generated in the cases of free vortex($S = 0.4$) and $S = 0.5$(constant angle);

4. the free vortex swirler($S = 0.4$), though weaker in strength than the $S = 0.5$ swirler, generated a CTRZ that extended farther away downstream than the $S = 0.5$ swirler(CTRZ extends up to $x/H = 8.0$ in the case of the free vortex swirler while it extends up to $x/H = 5.0$ in the case of the $S = 0.5$ swirler) indicating that the type of swirler used is as important as the swirl strength;

5. there was flow recovery in the far field region for the swirled flows while flow did not recover even far beyond the reattachment point for the simple dump case;

6. relatively insignificant values of $\overline{u'v'}$ shear stress at region $x/H > 10$ for the swirled cases indicate full mixing and flow recovery in this region;

7. all swirlers produced higher turbulent shear stress relative to the zero-swirl flow in the region $x/H \leq 10$;

8. the production term dominates the TKE while the $\rho\overline{u'v'}\frac{\partial \overline{U}}{\partial r}$ component term dominates the production of turbulent kinetic energy;

9. all the component terms of the production of TKE containing the normal stresses make relatively insignificant contribution to the production of the TKE;

10. generally, high values of the TKE terms were observed at the vicinity of the combustor centerline and at the boundary of the CRZ;

11. viscous dissipation term, obtained by balance of TKE, shows similar trend, with different peak values, when compared to the production terms but opposite in sign indicating that the production term is the most dominant among the TKE terms.

APPENDIX

Table 5.1: Abbreviations Used for Component Parts of the TKE Terms

TKE Terms	Abbreviations	Mathematical Expressions
Production	P1	$-\overline{v'^2}\frac{\partial \overline{V}}{\partial r}$
	P2	$-\overline{u'v'}\frac{\partial \overline{U}}{\partial r}$
	P3	$-\overline{u'v'}\frac{\partial \overline{V}}{\partial x}$
	P4	$-\overline{u'^2}\frac{\partial \overline{U}}{\partial x}$
	P5	$-\overline{w'^2}\frac{\overline{V}}{r}$
	P6	$-\overline{u'w'}\frac{\partial \overline{W}}{\partial x}$
	P7	$-\overline{v'w'}\frac{\partial \overline{W}}{\partial r}$
	P8	$-\overline{v'w'}\frac{\overline{W}}{r}$
Convection	C1	$\overline{U}\frac{\partial k}{\partial x}$
	C2	$\overline{V}\frac{\partial k}{\partial r}$
Diffusion	D1	$\frac{1}{\rho r}\frac{\partial}{\partial r}\left(\mu r\frac{\partial k}{\partial r}\right)$
	D2	$\frac{1}{\rho r}\frac{\partial}{\partial r}\left(-\rho r\overline{\frac{v'^3}{2}}\right)$
	D3	$\frac{1}{\rho r}\frac{\partial}{\partial r}\left(-\rho r\overline{\frac{u'^2v'}{2}}\right)$
	D4	$\frac{1}{\rho}\frac{\partial}{\partial x}\left(\mu\frac{\partial k}{\partial x}\right)$
	D5	$\frac{1}{\rho}\frac{\partial}{\partial x}\left(-\rho\overline{\frac{u'^3}{2}}\right)$
	D6	$\frac{1}{\rho}\frac{\partial}{\partial x}\left(-\rho\overline{\frac{u'v'^2}{2}}\right)$
	D7	$\frac{1}{\rho}\frac{\partial}{\partial x}\left(-\rho\overline{\frac{u'w'^2}{2}}\right)$
	D8	$-\frac{\mu}{\rho}\overline{\frac{v'^2}{r^2}}$
	D9	$-\frac{\mu}{\rho}\overline{\frac{w'^2}{r^2}}$
	D10	$\frac{1}{\rho}\frac{\partial}{\partial r}\left(-\rho r\overline{\frac{v'w'^2}{2}}\right)$

Appendix A

Reynolds Equations

Assuming that U, V, and W are the velocity components in the directions of the cylindrical coordinates x, r, and θ; respectively, the conservation of mass equation could be expressed as

$$\frac{\partial \rho}{\partial t} + \frac{\partial (\rho U)}{\partial x} + \frac{1}{r}\frac{\partial (r\rho V)}{\partial r} + \frac{1}{r}\frac{\partial (\rho W)}{\partial \theta} = 0 \tag{A.1}$$

The conservation of momentum equations in the three coordinate directions, axial, radial, and tangential, are as itemized below:

1. Axial momentum equation:

$$\frac{\partial (\rho U)}{\partial t} + \frac{\partial (\rho U^2)}{\partial x} + \frac{1}{r}\frac{\partial (r\rho UV)}{\partial r} + \frac{1}{r}\frac{\partial (\rho UW)}{\partial \theta} = -\frac{\partial P}{\partial x} + \frac{\partial}{\partial x}\left[2\mu\frac{\partial U}{\partial x} - \frac{2}{3}\mu\phi\right] + \frac{1}{r}\frac{\partial}{\partial r}\left[r\mu\left(\frac{\partial U}{\partial r} + \frac{\partial V}{\partial x}\right)\right] + \frac{1}{r}\frac{\partial}{\partial \theta}\left[\mu\left(\frac{\partial V}{\partial x} + \frac{1}{r}\frac{\partial U}{\partial \theta}\right)\right] \tag{A.2}$$

2. Radial momentum equation:

$$\frac{\partial (\rho V)}{\partial t} + \frac{\partial (\rho VU)}{\partial x} + \frac{1}{r}\frac{\partial (r\rho V^2)}{\partial r} + \frac{1}{r}\frac{\partial (\rho VW)}{\partial \theta} - \frac{\rho V^2}{r} = -\frac{\partial P}{\partial r} + \frac{\partial}{\partial x}\left[\mu\left(\frac{\partial U}{\partial r} + \frac{\partial V}{\partial x}\right)\right] + \frac{1}{r}\frac{\partial}{\partial r}\left[r\mu\left(2\frac{\partial V}{\partial r} - \frac{2}{3}\phi\right)\right] + \frac{1}{r}\frac{\partial}{\partial \theta}\left[\mu\left(r\frac{\partial}{\partial x}\frac{V}{r} + \frac{1}{r}\frac{\partial V}{\partial \theta}\right)\right] - \frac{\mu}{r}\left[2\frac{\partial U}{\partial x} + \frac{2V}{r} - \frac{2}{3}\phi\right] \tag{A.3}$$

3. Tangential momentum equation:

$$\frac{\partial (\rho W)}{\partial t} + \frac{\partial (\rho WU)}{\partial x} + \frac{1}{r}\frac{\partial (r\rho WV)}{\partial r} + \frac{1}{r}\frac{\partial (\rho W^2)}{\partial \theta} - \frac{\rho WV}{r} = -\frac{1}{r}\frac{\partial P}{\partial \theta} + \frac{\partial}{\partial x}\left[\mu\left(\frac{\partial W}{\partial x} + \frac{1}{r}\frac{\partial U}{\partial \theta}\right)\right] + \frac{1}{r^2}\frac{\partial}{\partial r}\left[r^2\mu\left(r\frac{\partial}{\partial r}\frac{W}{r} - \frac{1}{r}\frac{\partial V}{\partial \theta}\right)\right] + \frac{1}{r}\frac{\partial}{\partial \theta}\left[2\mu\left(\frac{1}{r}\frac{\partial W}{\partial \theta} + \frac{V}{r}\right) - \frac{2}{3}\phi\right] \tag{A.4}$$

ϕ is defined to be

$$\frac{\partial U}{\partial x}+\frac{1}{r}\frac{\partial}{\partial r}(rV)+\frac{1}{r}\frac{\partial W}{\partial \theta}$$

Reynolds defined the instantaneous values of velocity, pressure, and density to be composed of a mean value and a fluctuating component as follows:

$$U=\overline{U}+u',$$

$$V=\overline{V}+v',$$

$$W=\overline{W}+w',$$

$$P=\overline{P}+p',\ and$$

$$\rho=\overline{\rho}+\rho' \qquad \text{(A.5)}$$

If these instantaneous values are substituted in the conservation of mass, the result is the time averaged continuity equation (time average is performed) as follows:

$$\frac{\partial \overline{\rho}}{\partial t}+\frac{\partial}{\partial x}\left(\overline{\rho}\overline{U}+\overline{\rho' u'}\right)+\frac{1}{r}\frac{\partial}{\partial r}\left(r\overline{\rho}\overline{V}+r\overline{\rho' v'}\right)+\frac{1}{r}\frac{\partial}{\partial \theta}\left(\overline{\rho}\overline{W}+\overline{\rho' w'}\right)=0 \qquad \text{(A.6)}$$

In a similar manner, the time averaged Reynolds equations for turbulent flow in the three coordinates may be obtained by substituting the instantaneous values into the momentum equations and time averaging. The following results are obtained:-

1. Time averaged axial Reynolds equation:

$$\frac{\partial}{\partial t}\left(\overline{\rho}\overline{U}\right)+\frac{1}{r}\frac{\partial}{\partial r}\left(r\overline{\rho}\overline{V}\,\overline{U}\right)+\frac{1}{r}\frac{\partial}{\partial \theta}\left(\overline{\rho}\overline{W}\,\overline{U}\right)+\frac{\partial}{\partial x}\left(\overline{\rho}\overline{U}\,\overline{U}\right)+$$
$$\left[\frac{1}{r}\frac{\partial}{\partial r}\left(r\overline{\rho v'u'}\right)+\frac{1}{r}\frac{\partial}{\partial \theta}\left(\overline{\rho w'u'}\right)+\frac{\partial}{\partial x}\left(\overline{\rho u'u'}\right)\right]+$$
$$\left[\frac{1}{r}\frac{\partial}{\partial r}\left(r\overline{U}\,\overline{\rho'v'}\right)+\frac{1}{r}\frac{\partial}{\partial \theta}\left(\overline{U}\,\overline{\rho'w'}\right)+\frac{\partial}{\partial x}\left(\overline{U}\,\overline{\rho'u'}\right)\right]+$$
$$\left[\frac{1}{r}\frac{\partial}{\partial r}\left(r\overline{V}\,\overline{\rho'u'}\right)+\frac{1}{r}\frac{\partial}{\partial \theta}\left(\overline{W}\,\overline{\rho'u'}\right)+\frac{\partial}{\partial x}\left(\overline{U}\,\overline{\rho'u'}\right)\right]+$$
$$\frac{\partial}{\partial t}\left(\overline{\rho'u'}\right)+\frac{1}{r}\frac{\partial}{\partial r}\left(r\overline{\rho'v'u'}\right)+\frac{1}{r}\frac{\partial}{\partial \theta}\left(\overline{\rho'w'u'}\right)+\frac{\partial}{\partial x}\left(\overline{\rho'u'u'}\right)=-\frac{\partial\overline{P}}{\partial x}+$$
$$\frac{1}{r}\frac{\partial}{\partial r}\left[r\mu\left(\frac{\partial\overline{U}}{\partial r}+\frac{\partial\overline{V}}{\partial x}\right)\right]+\frac{1}{r}\frac{\partial}{\partial \theta}\left[\mu\left(\frac{\partial\overline{W}}{\partial x}+\frac{1}{r}\frac{\partial\overline{U}}{\partial \theta}\right)\right]+\frac{\partial}{\partial x}\left[2\mu\frac{\partial\overline{U}}{\partial x}-\frac{2}{3}\mu\phi\right] \tag{A.7}$$

2. Time averaged radial Reynolds equation:

$$\frac{\partial}{\partial t}\left(\overline{\rho}\overline{V}\right)+\frac{1}{r}\frac{\partial}{\partial r}\left(r\overline{\rho}\overline{V}\,\overline{V}\right)+\frac{1}{r}\frac{\partial}{\partial \theta}\left(\overline{\rho}\overline{W}\,\overline{V}\right)+\frac{\partial}{\partial x}\left(\overline{\rho}\overline{U}\,\overline{V}\right)-\frac{\overline{\rho}\overline{W}\,\overline{W}}{r}+$$
$$\left[\frac{1}{r}\frac{\partial}{\partial r}\left(r\overline{\rho v'v'}\right)+\frac{1}{r}\frac{\partial}{\partial \theta}\left(\overline{\rho w'v'}\right)+\frac{\partial}{\partial x}\left(\overline{\rho u'v'}\right)-\frac{\overline{\rho w'w'}}{r}\right]+$$
$$\left[\frac{1}{r}\frac{\partial}{\partial r}\left(r\overline{V}\,\overline{\rho'v'}\right)+\frac{1}{r}\frac{\partial}{\partial \theta}\left(\overline{V}\,\overline{\rho'w'}\right)+\frac{\partial}{\partial x}\left(\overline{V}\,\overline{\rho'u'}\right)-\frac{\overline{\rho'w'}\,\overline{W}}{r}\right]+$$
$$\left[\frac{1}{r}\frac{\partial}{\partial r}\left(r\overline{V}\,\overline{\rho'v'}\right)+\frac{1}{r}\frac{\partial}{\partial \theta}\left(\overline{W}\,\overline{\rho'v'}\right)+\frac{\partial}{\partial x}\left(\overline{U}\,\overline{\rho'v'}\right)-\frac{\overline{\rho'w'}\,\overline{W}}{r}\right]+$$
$$\frac{\partial}{\partial t}\left(\overline{\rho'v'}\right)+\frac{1}{r}\frac{\partial}{\partial r}\left(r\overline{\rho'v'v'}\right)+\frac{1}{r}\frac{\partial}{\partial \theta}\left(\overline{\rho'w'v'}\right)+\frac{\partial}{\partial x}\left(\overline{\rho'u'v'}\right)-\frac{\overline{\rho'w'w'}}{r}=-\frac{\partial\overline{P}}{\partial r}+$$
$$\frac{1}{r}\frac{\partial}{\partial r}\left[r\mu\left(2\frac{\partial\overline{V}}{\partial r}-\frac{2}{3}\phi\right)\right]+\frac{1}{r}\frac{\partial}{\partial \theta}\left[\mu\left(r\frac{\partial}{\partial x}\frac{\overline{V}}{r}+\frac{1}{r}\frac{\partial\overline{V}}{\partial \theta}\right)\right]-\frac{\mu}{r}\left[2\frac{\partial\overline{U}}{\partial x}+\frac{2\overline{V}}{r}-\frac{2}{3}\phi\right]+$$
$$\frac{\partial}{\partial x}\left[\mu\left(\frac{\partial\overline{U}}{\partial r}+\frac{\partial\overline{V}}{\partial x}\right)\right] \tag{A.8}$$

3. Time averaged tangential Reynolds equation:

$$\frac{\partial}{\partial t}\left(\overline{\rho}\overline{W}\right)+\frac{1}{r}\frac{\partial}{\partial r}\left(r\overline{\rho}\overline{V}\ \overline{W}\right)+\frac{1}{r}\frac{\partial}{\partial\theta}\left(\overline{\rho}\overline{W}\ \overline{W}\right)+\frac{\partial}{\partial x}\left(\overline{\rho}\overline{U}\ \overline{W}\right)+\frac{\overline{\rho}\overline{V}\ \overline{W}}{r}+$$
$$\left[\frac{1}{r}\frac{\partial}{\partial r}\left(r\overline{\rho v'w'}\right)+\frac{1}{r}\frac{\partial}{\partial\theta}\left(\overline{\rho w'w'}\right)+\frac{\partial}{\partial x}\left(\overline{\rho u'w'}\right)+\frac{\overline{\rho v'w'}}{r}\right]+$$
$$\left[\frac{1}{r}\frac{\partial}{\partial r}\left(r\overline{W}\ \overline{\rho'v'}\right)+\frac{1}{r}\frac{\partial}{\partial\theta}\left(\overline{W}\ \overline{\rho'w'}\right)+\frac{\partial}{\partial x}\left(\overline{W}\ \overline{\rho'u'}\right)+\frac{\overline{\rho'v'}\ \overline{W}}{r}\right]+$$
$$\left[\frac{1}{r}\frac{\partial}{\partial r}\left(r\overline{V}\ \overline{\rho'w'}\right)+\frac{1}{r}\frac{\partial}{\partial\theta}\left(\overline{W}\ \overline{\rho'w'}\right)+\frac{\partial}{\partial x}\left(\overline{U}\ \overline{\rho'w'}\right)+\frac{\overline{\rho'w'}\ \overline{V}}{r}\right]+$$
$$\frac{\partial}{\partial t}\left(\overline{\rho'w'}\right)+\frac{1}{r}\frac{\partial}{\partial r}\left(r\overline{\rho'w'w'}\right)+\frac{1}{r}\frac{\partial}{\partial\theta}\left(\overline{\rho'w'w'}\right)+\frac{\partial}{\partial x}\left(\overline{\rho'u'w'}\right)-$$
$$\frac{\overline{\rho'v'w'}}{r}=-\frac{1}{r}\frac{\partial\overline{P}}{\partial\theta}+\frac{1}{r^2}\frac{\partial}{\partial r}\left[r^2\mu\left(r\frac{\partial}{\partial r}\frac{\overline{W}}{r}-\frac{1}{r}\frac{\partial\overline{V}}{\partial\theta}\right)\right]+\frac{1}{r}\frac{\partial}{\partial\theta}\left[2\mu\left(\frac{1}{r}\frac{\partial\overline{W}}{\partial\theta}+\frac{\overline{V}}{r}\right)-\frac{2}{3}\phi\right]+$$
$$\frac{\partial}{\partial x}\left[\mu\left(\frac{\partial\overline{W}}{\partial x}+\frac{1}{r}\frac{\partial\overline{U}}{\partial\theta}\right)\right] \qquad \text{(A.9)}$$

The Reynolds equations in tensor form could be written as:

$$\frac{\partial}{\partial t}\left(\overline{\rho}\overline{U_i}\right)+\frac{\partial}{\partial t}\left(\overline{\rho'u_i'}\right)+\frac{\partial}{\partial x_j}\left(\overline{\rho}\ \overline{U_i}\ \overline{U_j}\right)+\frac{\partial}{\partial x_j}\left(\overline{U_i}\ \overline{\rho'u'}\right)+\frac{\partial}{\partial x_j}\left(\overline{U_j}\ \overline{\rho'u_i'}\right)+\frac{\partial}{\partial x_j}\left(\overline{\rho}\ \overline{u_i'u_j'}\right)+$$
$$\frac{\partial}{\partial x_j}\left(\overline{\rho'u_i'u_j'}\right)=-\frac{\partial\overline{P}}{\partial x_i}+\frac{\partial}{\partial x_j}\left[\mu\left(\frac{\partial\overline{U_i}}{\partial x_j}+\frac{\partial\overline{U_j}}{\partial x_i}-\frac{2}{3}\delta_{ij}\frac{\partial\overline{U_k}}{\partial x_k}\right)\right] \qquad \text{(A.10)}$$

For constant density flow (or neglecting the fluctuations in the density), the above equation reduces to the following form:-

$$\frac{\partial}{\partial t}\left(\overline{\rho}\overline{U_i}\right)+\frac{\partial}{\partial x_j}\left(\overline{\rho}\ \overline{U_i}\ \overline{U_j}\right)+\frac{\partial}{\partial x_j}\left(\overline{\rho}\ \overline{u_i'u_j'}\right)=-\frac{\partial\overline{P}}{\partial x_i}+\frac{\partial}{\partial x_j}\left[\mu\frac{\partial\overline{U_i}}{\partial x_j}\right]+\frac{\partial\overline{U_j}}{\partial x_i}\frac{\partial\mu}{\partial x_j} \qquad \text{(A.11)}$$

if cartesian coordinates were used instead of cylindrical coordinates, these coordinate transformation equations could be utilized:

$$x=x,\ y=r\ and\ z=r\theta$$

and the equations in rectangular coordinates could be evaluated.

Appendix B

Turbulence Energy Equation

The turbulence energy equation could be derived by multiplying the i*th* Reynolds equation by u_i' ($i = 1, 2$ *and* 3) and then summing all the equations. The new equation in tensor form is as follows:-

$$\overline{\rho' u_i'}\frac{\partial \overline{U}_i}{\partial t} + \frac{\partial}{\partial t}\left(\overline{\rho} k\right) + \frac{\partial}{\partial t}\left(\overline{\rho' k}\right) + \frac{\partial}{\partial x_j}\left(\overline{\rho}\,\overline{U}_j k\right) + \frac{\partial}{\partial x_j}\left(\overline{U}_j\,\overline{\rho' k}\right) +$$

$$\left[\frac{\partial}{\partial x_j}\left(\overline{\rho u_j' k}\right) + \frac{\partial}{\partial x_j}\left(\overline{\rho' u_j' k}\right) + \overline{\rho u_i' u_j'}\frac{\partial \overline{U}_i}{\partial x_j} + \overline{\rho' u_i'}\,\overline{U}_j\frac{\partial \overline{U}_i}{\partial x_j}\right] + \overline{\rho' u_i' u_j'}\frac{\partial \overline{U}_i}{\partial x_j} = -\frac{\partial}{\partial x_i}\left(\overline{u_i' \rho'}\right) + \overline{\rho' \frac{\partial u_i'}{\partial x_i}} +$$

$$\frac{\partial}{\partial x_j}\left[\mu\frac{\partial}{\partial x_j}(k)\right] - \mu\overline{\left[\frac{\partial u_i'}{\partial x_j}\right]^2} + \overline{u_i'\frac{\partial u_j'}{\partial x_i}\frac{\partial \mu}{\partial x_j}} + \frac{1}{3}\mu\overline{u_i'\frac{\partial}{\partial x_i}\left[\frac{\partial u_k'}{\partial x_k}\right]} - \frac{2}{3}\overline{u_j'\frac{\partial \mu}{\partial x_j}\left[\frac{\partial u_k'}{\partial x_k}\right]} \quad \text{(B.1)}$$

For constant density flow (or neglecting the fluctuations in the density), the above equation becomes:

$$\frac{\partial}{\partial t}\left(\overline{\rho} k\right) + \frac{\partial}{\partial x_j}\left(\overline{\rho}\,\overline{U}_j k\right) + \frac{\partial}{\partial x_j}\left(\overline{\rho u_j' k}\right) + \overline{\rho u_i' u_j'}\frac{\partial \overline{U}_i}{\partial x_j} = -\frac{\partial}{\partial x_i}\left(\overline{u_i' \rho'}\right) + \frac{\partial}{\partial x_j}\left[\mu\frac{\partial}{\partial x_j}(k)\right] -$$

$$\mu\overline{\left[\frac{\partial u_i'}{\partial x_j}\right]^2} + \overline{u_i'\frac{\partial u_j'}{\partial x_i}\frac{\partial \mu}{\partial x_j}} \quad \text{(B.2)}$$

This equation in cylindrical coordinates (for steady, axisymmetric, and constant density flow) could be written as

$$\overline{U}\frac{\partial k}{\partial x} + \overline{V}\frac{\partial k}{\partial r} = \frac{1}{\rho}\frac{\partial}{\partial x}\left[\mu\frac{\partial k}{\partial x} - \rho\frac{\overline{u'v'v'}}{2} - \rho\frac{\overline{u'w'w'}}{2} - \rho\frac{\overline{u'u'u'}}{2} - \overline{u'p'}\right] +$$

$$\frac{1}{\rho r}\frac{\partial}{\partial r}\left[\mu r\frac{\partial k}{\partial r} - \rho r\frac{\overline{v'v'v'}}{2} - \rho r\frac{\overline{v'w'w'}}{2} - \rho r\frac{\overline{u'u'v'}}{2} - r\overline{v'p'}\right] - \left[\frac{2}{\rho}\mu\frac{\overline{v'v'}}{r^2} - \frac{\mu}{\rho}\frac{\overline{w'w'}}{r^2}\right] -$$

$$\left[\overline{v'v'}\frac{\partial \overline{V}}{\partial r} + \overline{u'v'}\frac{\partial \overline{U}}{\partial r} + \overline{u'v'}\frac{\partial \overline{V}}{\partial x} + \overline{u'u'}\frac{\partial \overline{U}}{\partial x} + \overline{w'w'}\frac{\overline{V}}{r}\right] -$$

$$\frac{\mu}{\rho}\left[\overline{\left(\frac{\partial v'}{\partial r}\right)^2} + \overline{\left(\frac{\partial w'}{\partial r}\right)^2} + \overline{\left(\frac{\partial u'}{\partial r}\right)^2} + \overline{\left(\frac{\partial v'}{\partial x}\right)^2} + \overline{\left(\frac{\partial w'}{\partial x}\right)^2} + \overline{\left(\frac{\partial u'}{\partial x}\right)^2}\right] \quad \text{(B.3)}$$

Appendix C

Components of TKE Terms, Effects of Swirl Strength

Components of Production Terms

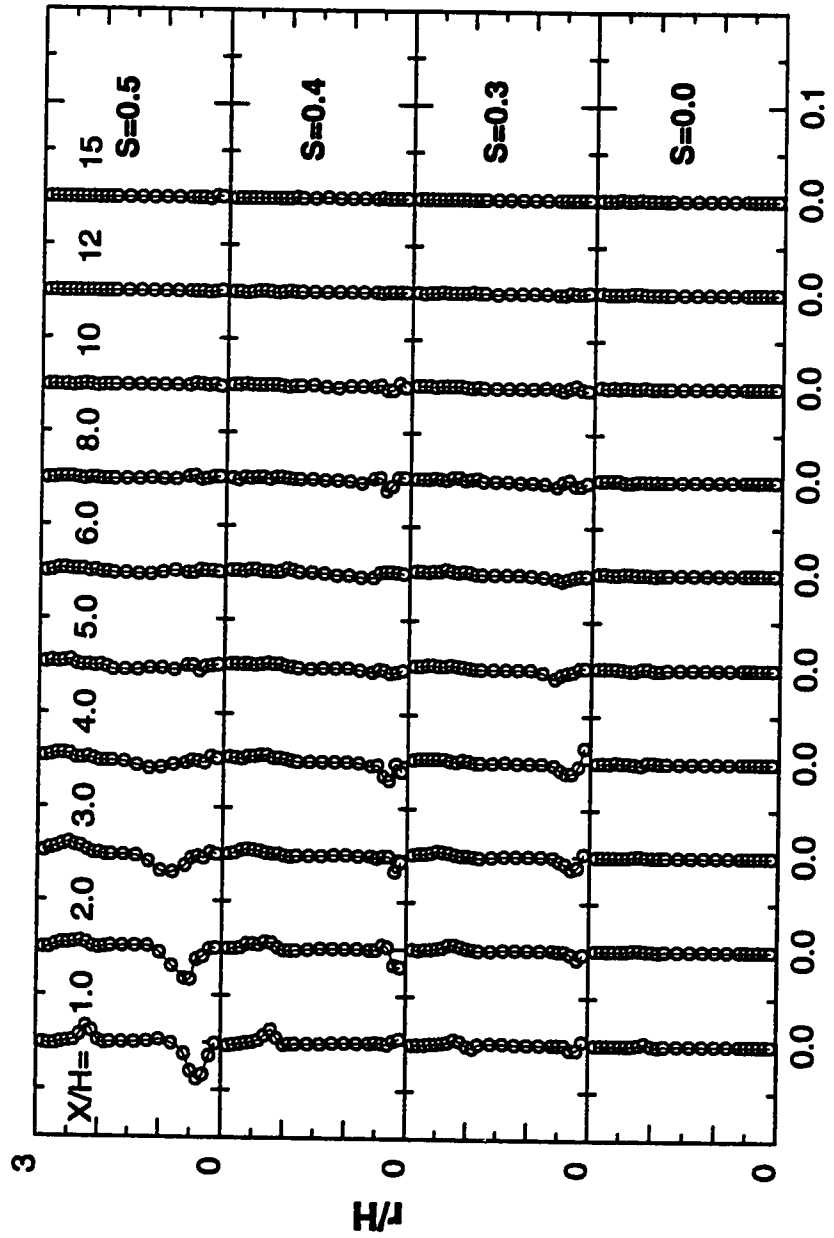

Figure C.1: First Component Term of Production, P1

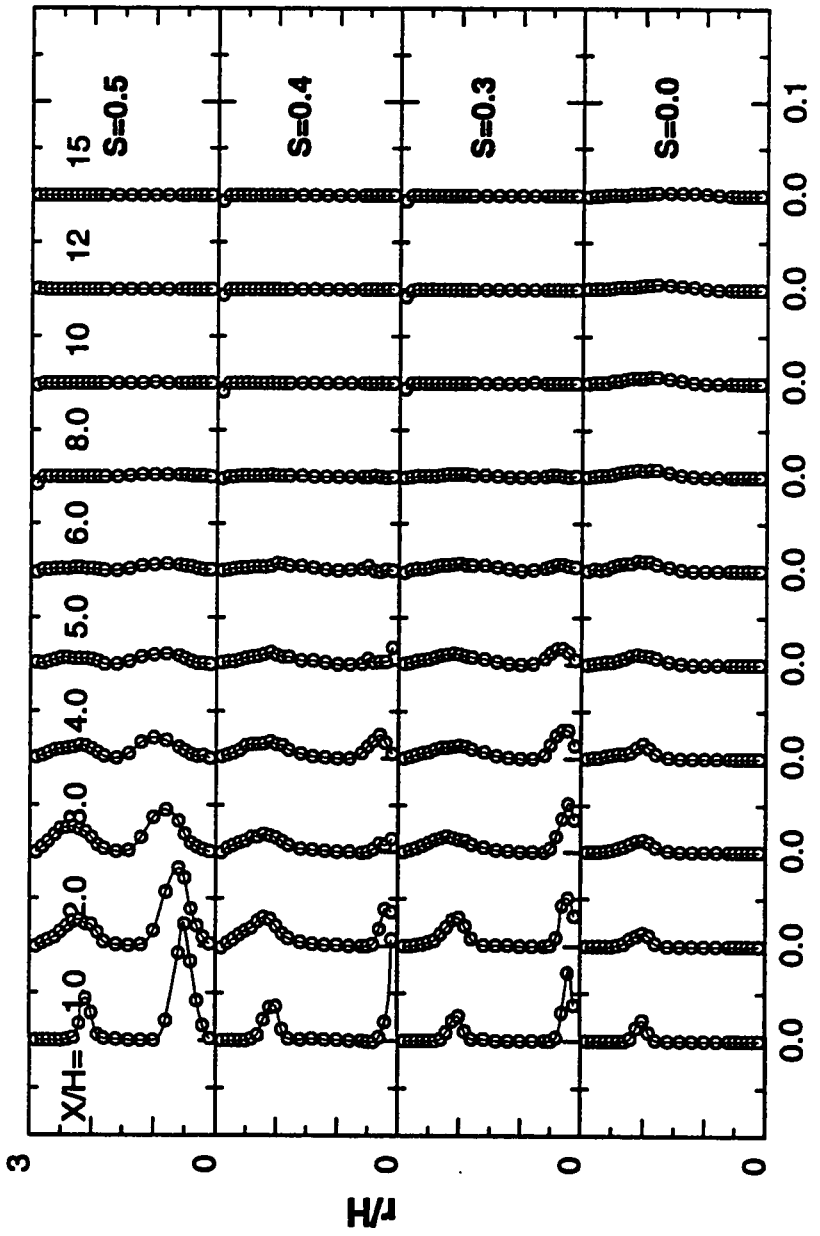

Figure C.2: Second Component Term of Production, P2

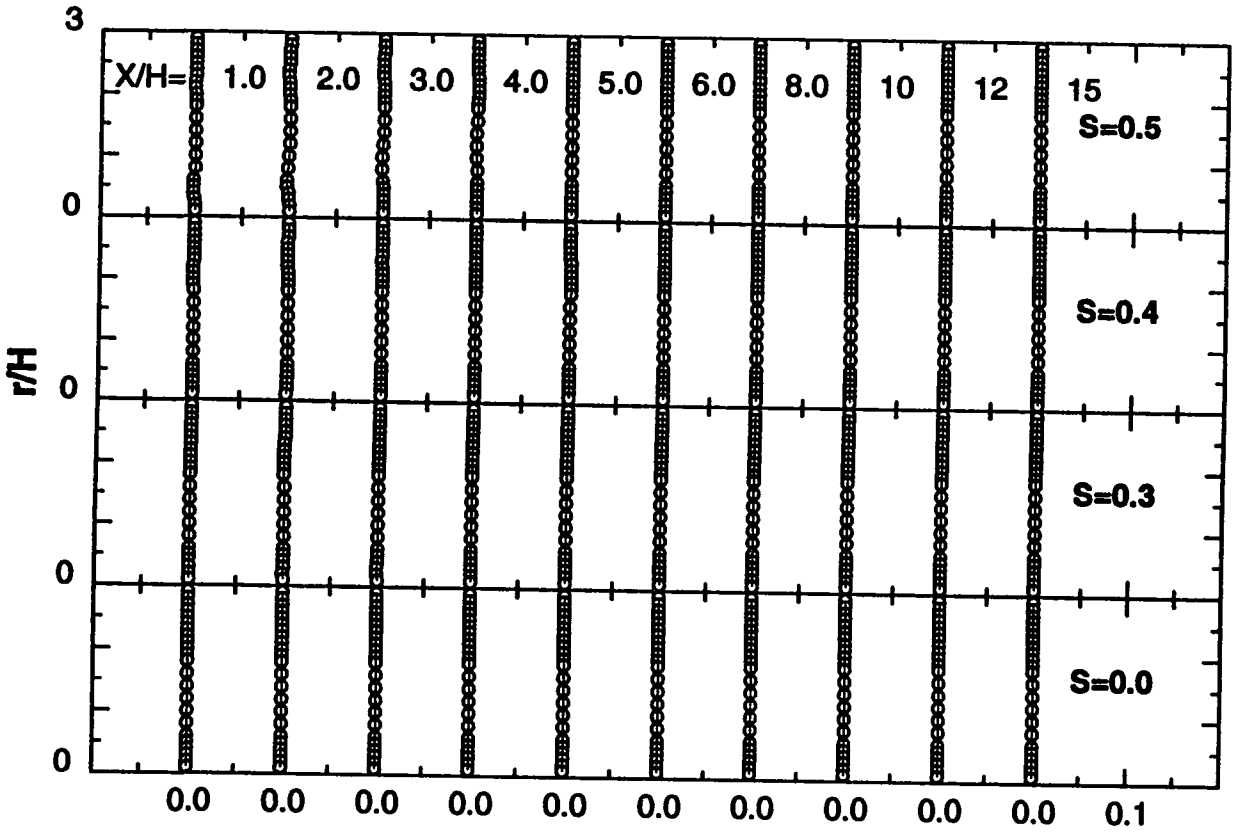

Figure C.3: Third Component Term of Production, P3

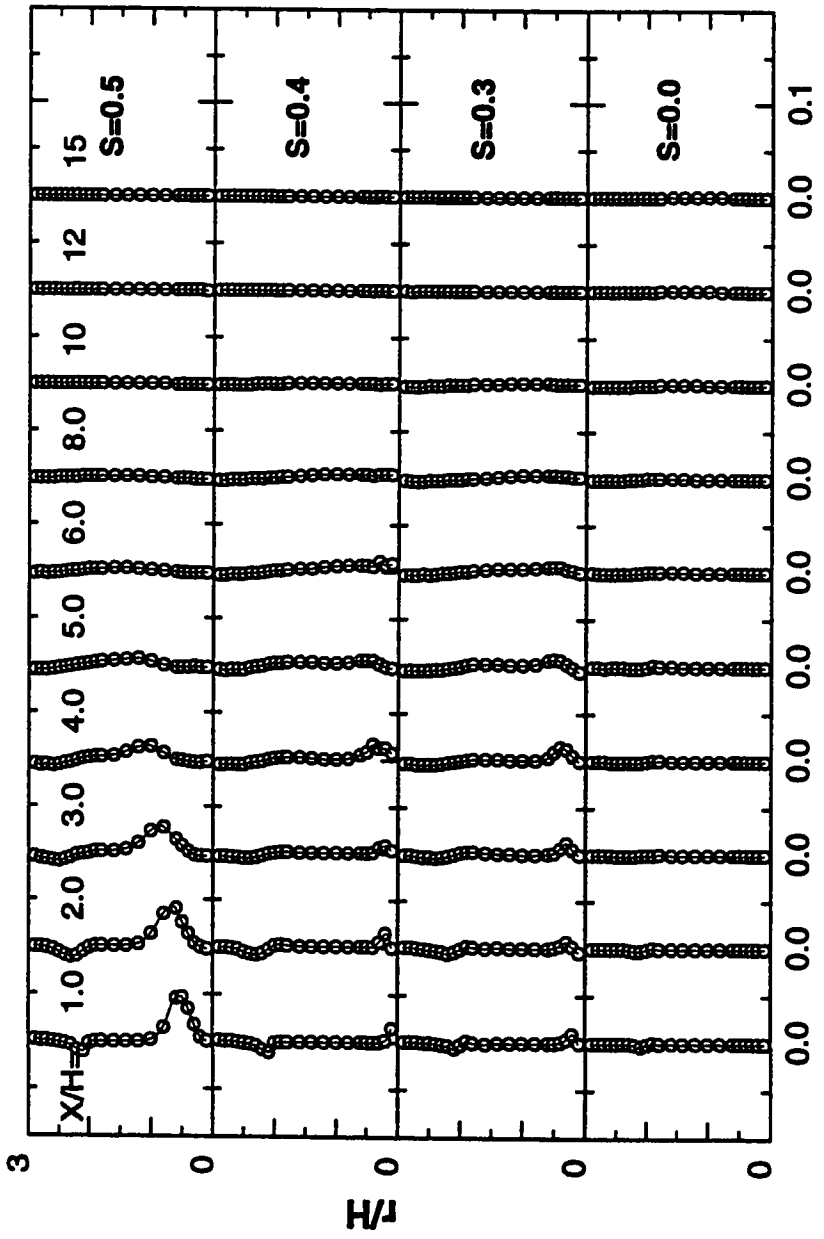

Figure C.4: Fourth Component Term of Production, P4

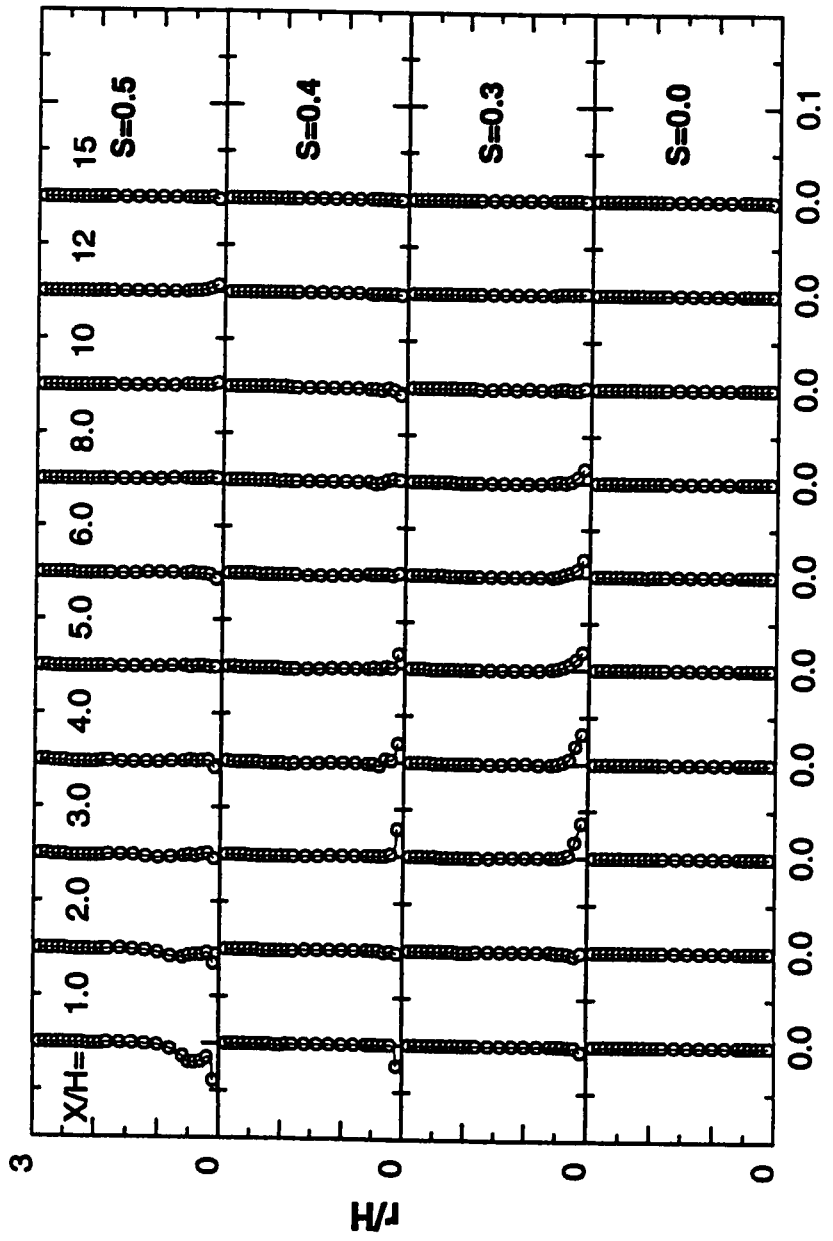

Figure C.5: Fifth Component Term of Production, P5

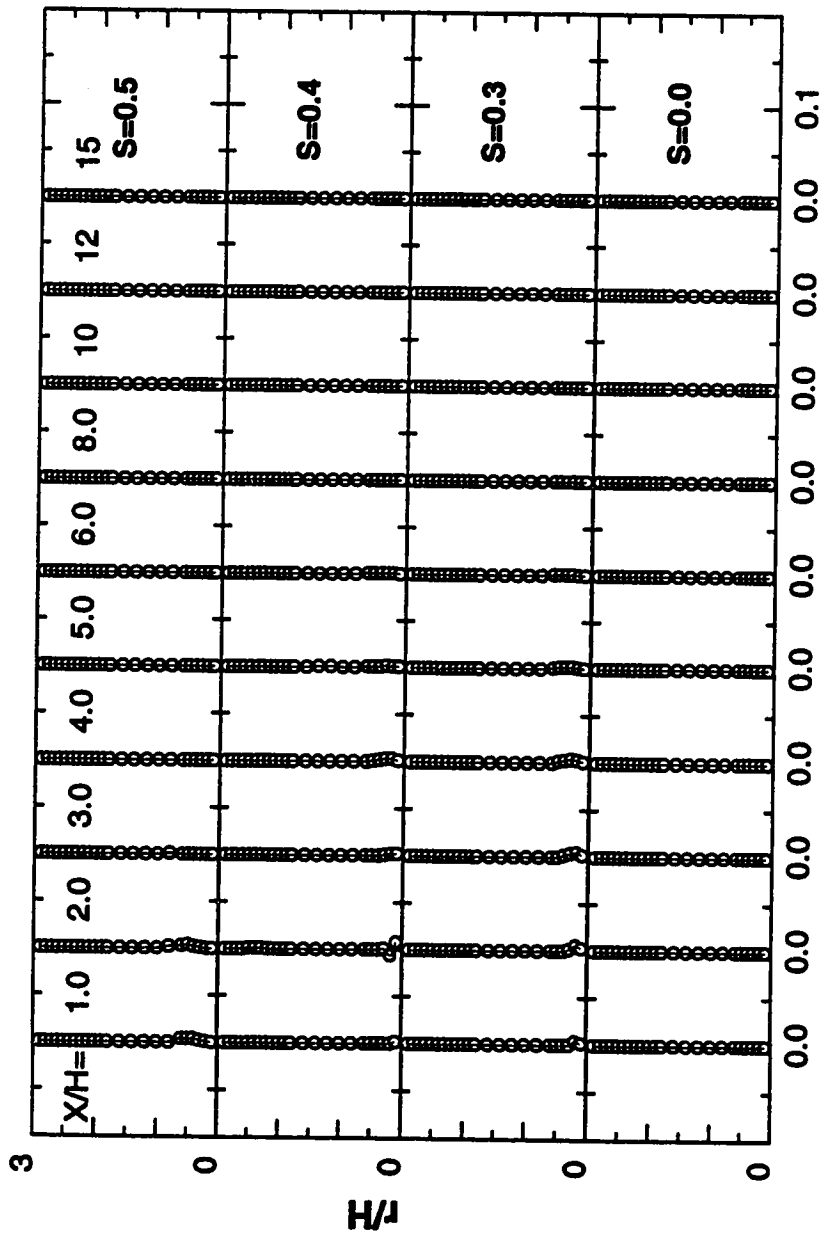

Figure C.6: Sixth Component Term of Production, P6

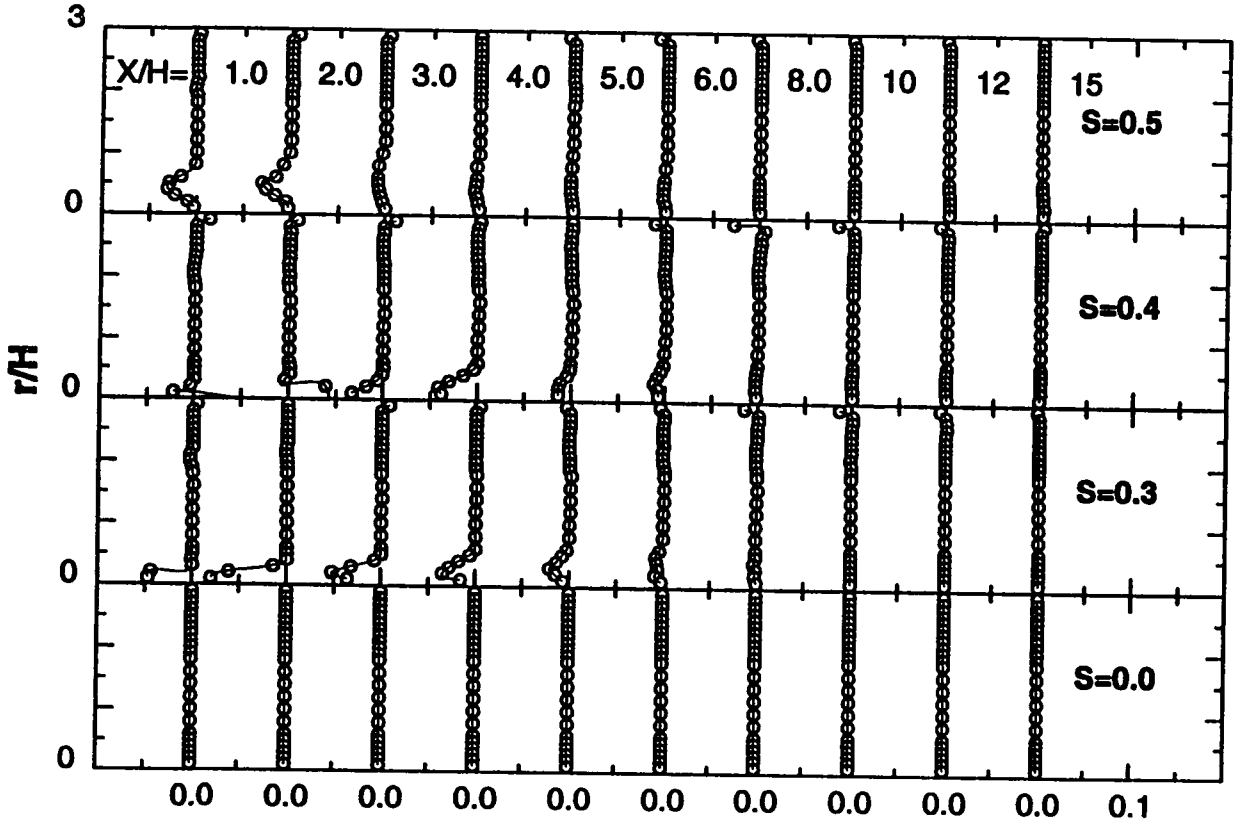

Figure C.7: Seventh Component Term of Production, P7

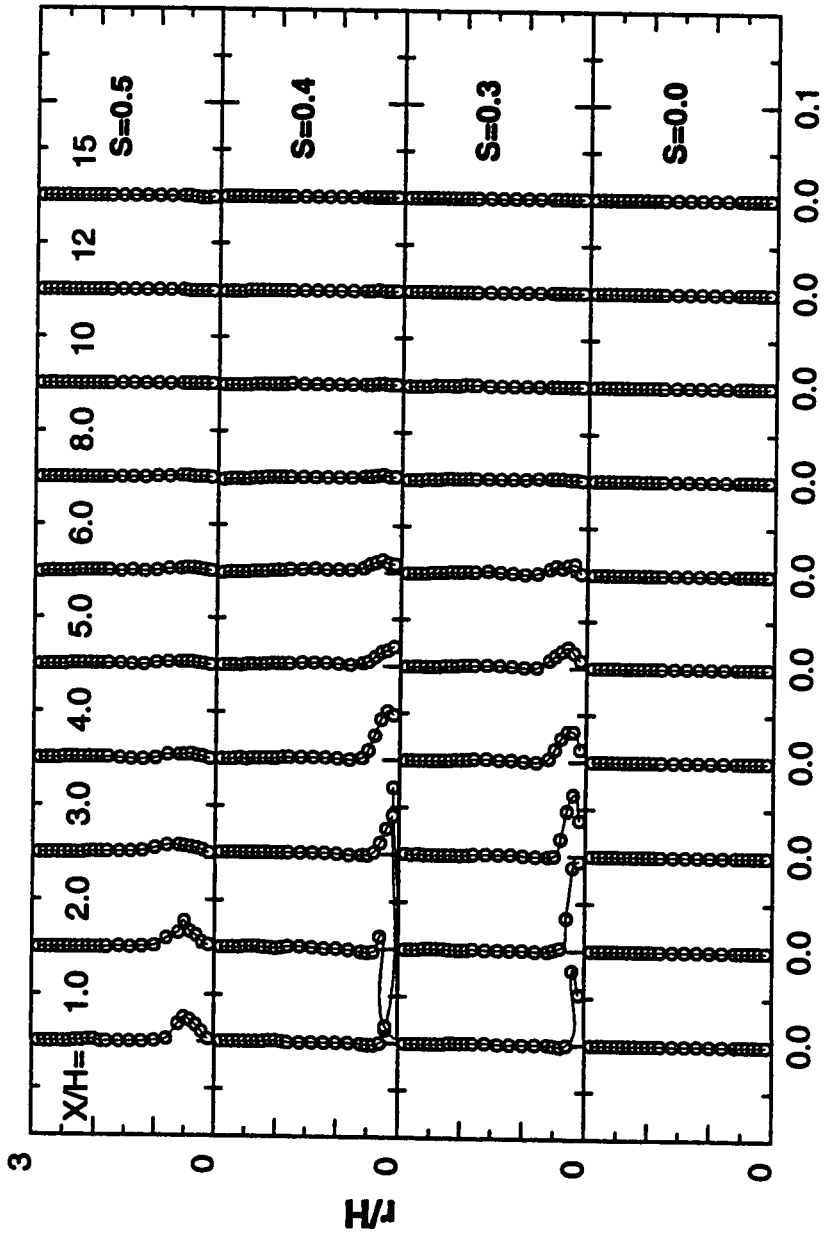

Figure C.8: Eighth Component Term of Production, P8

Components of Convection Terms

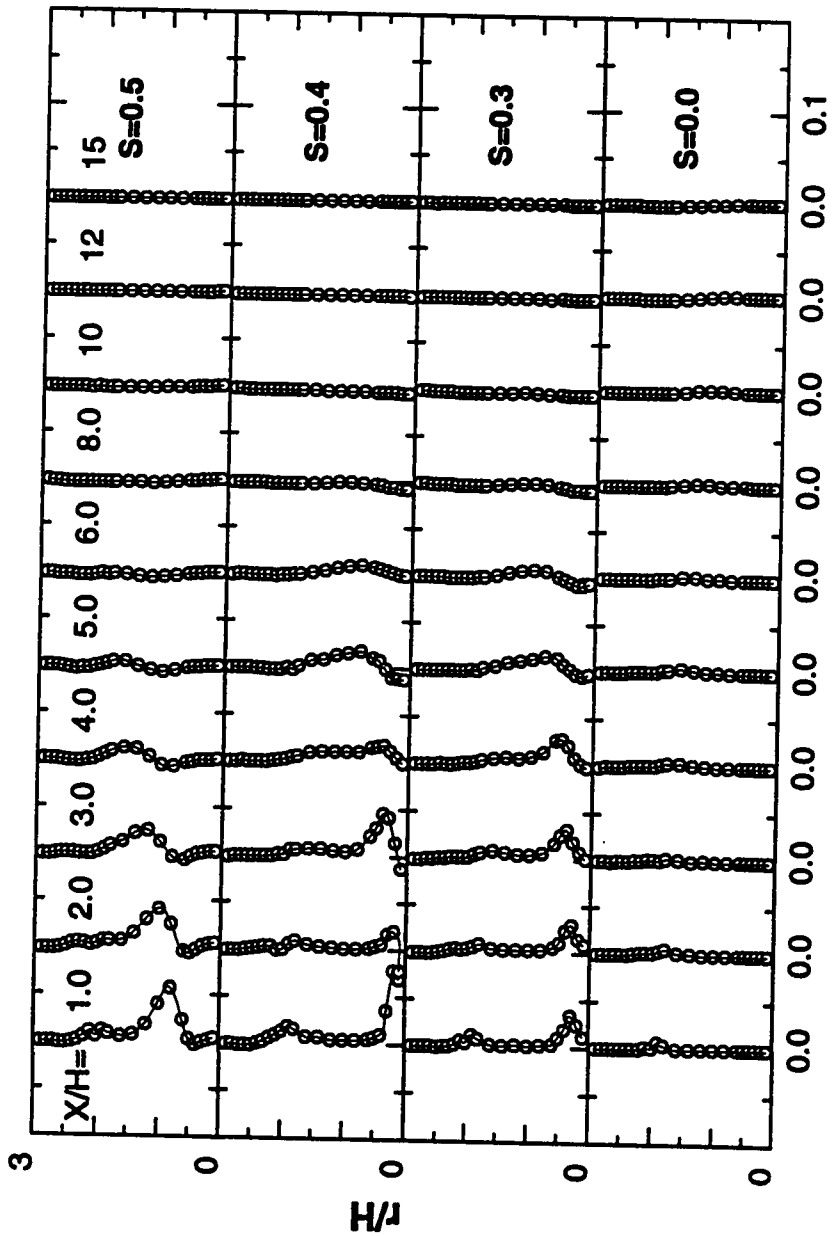

Figure C.9: First Component Term of Convection, C1

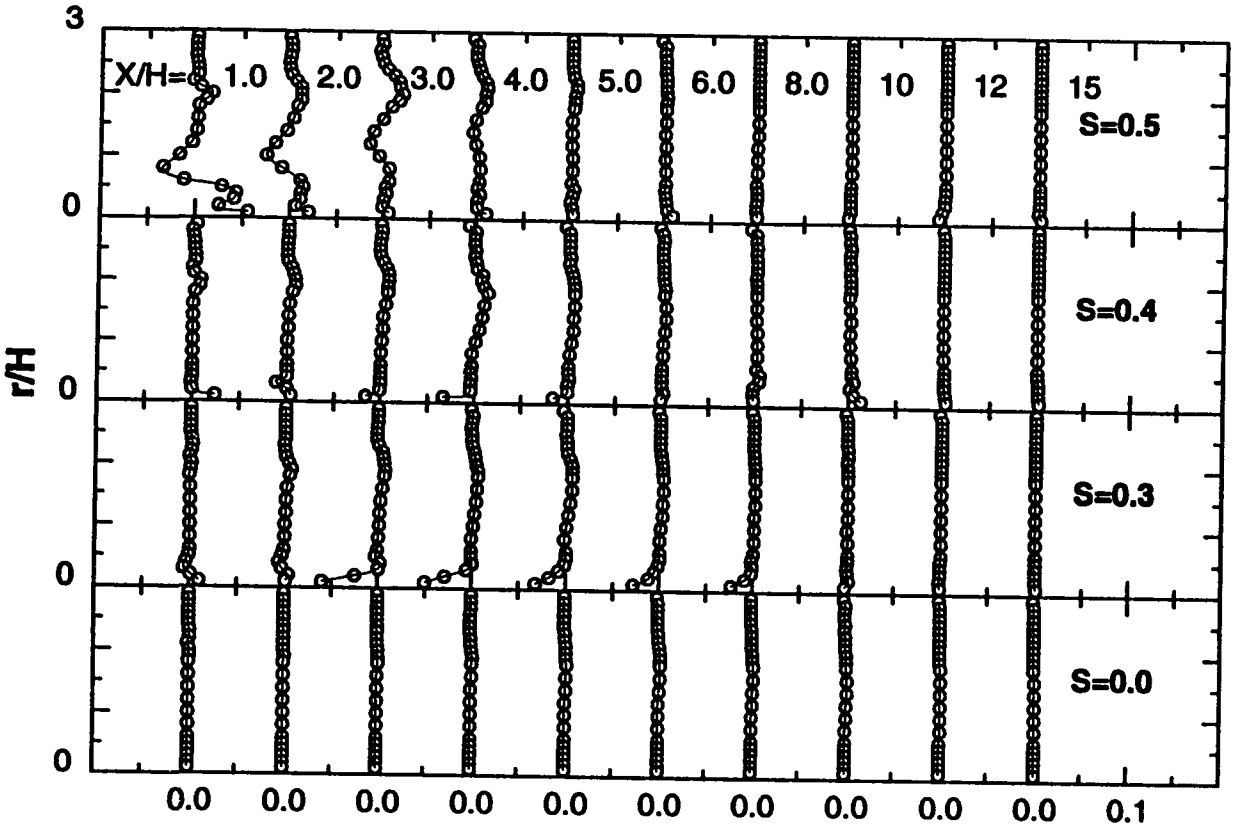

Figure C.10: Second Component Term of Convection, C2

Components of Diffusion Terms

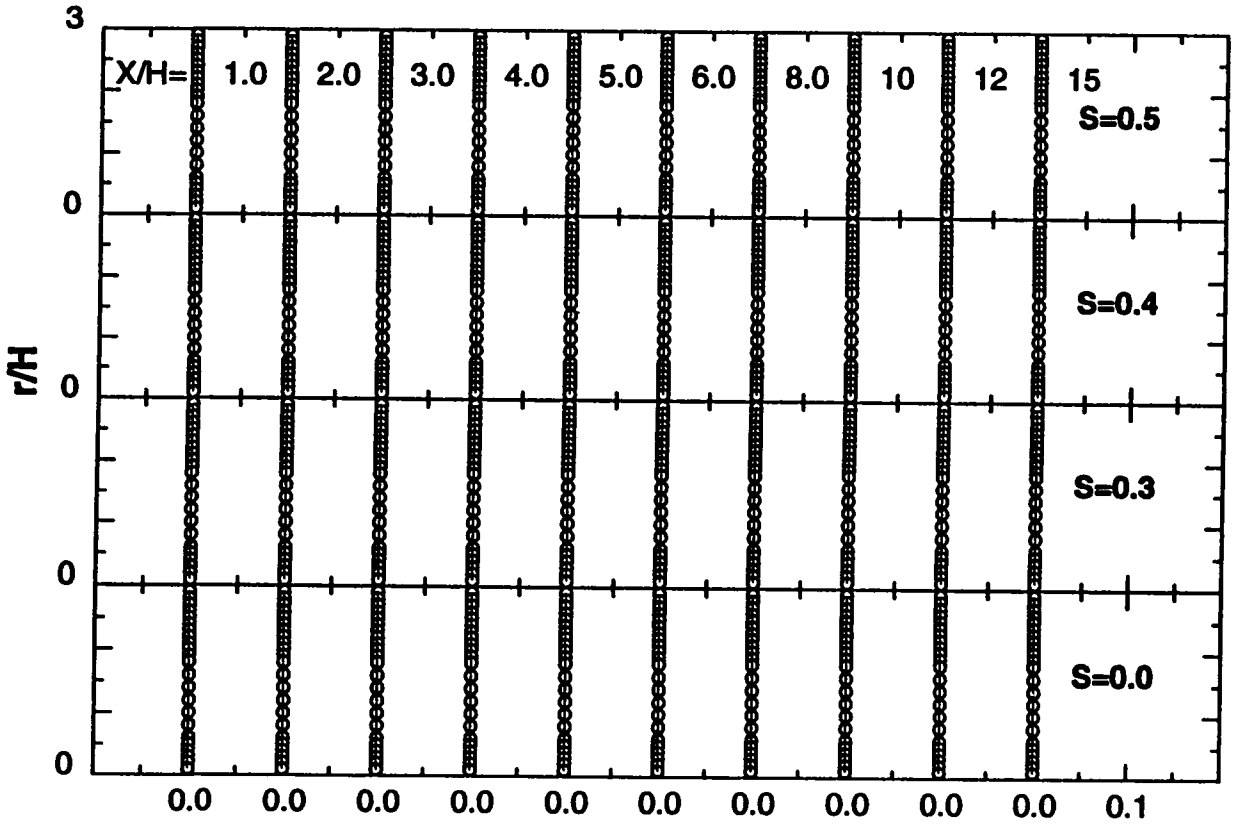

Figure C.11: First Component Term of Diffusion, D1

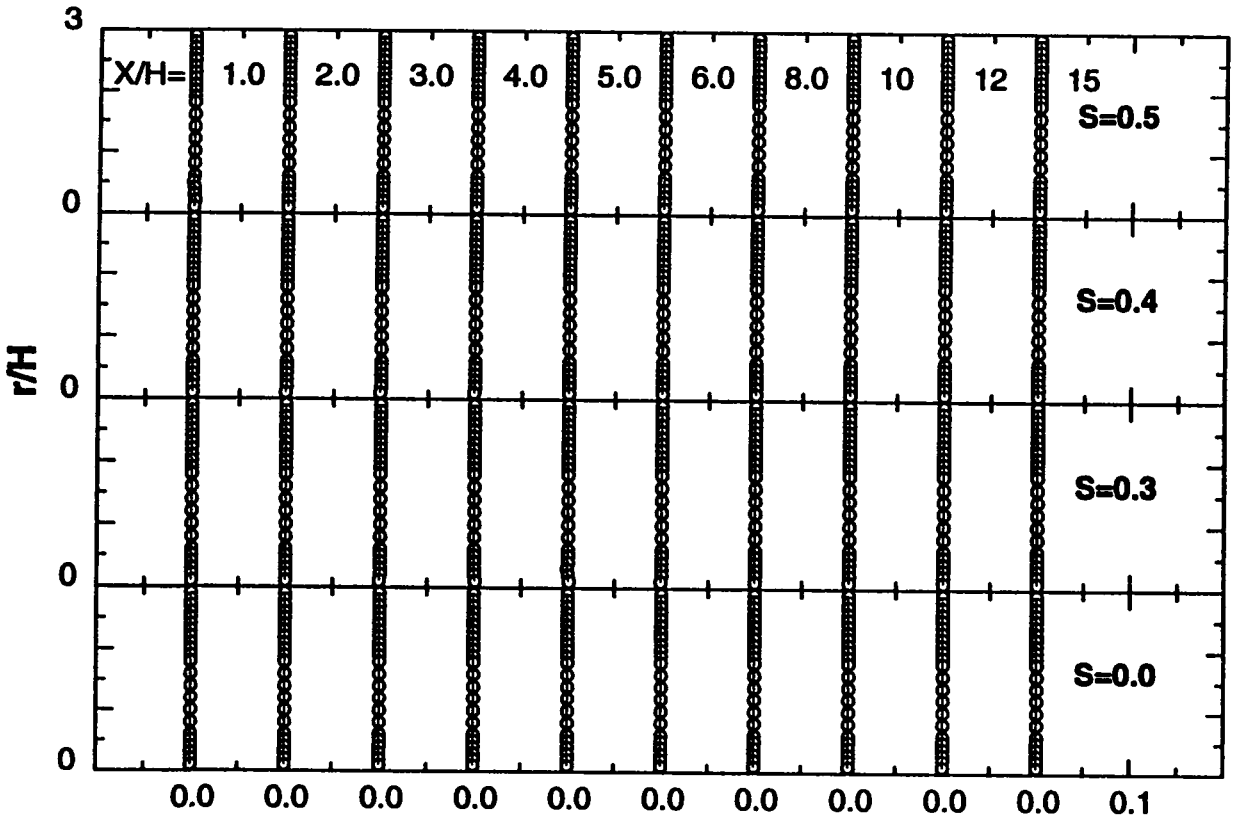

Figure C.12: Second Component Term of Diffusion, D2

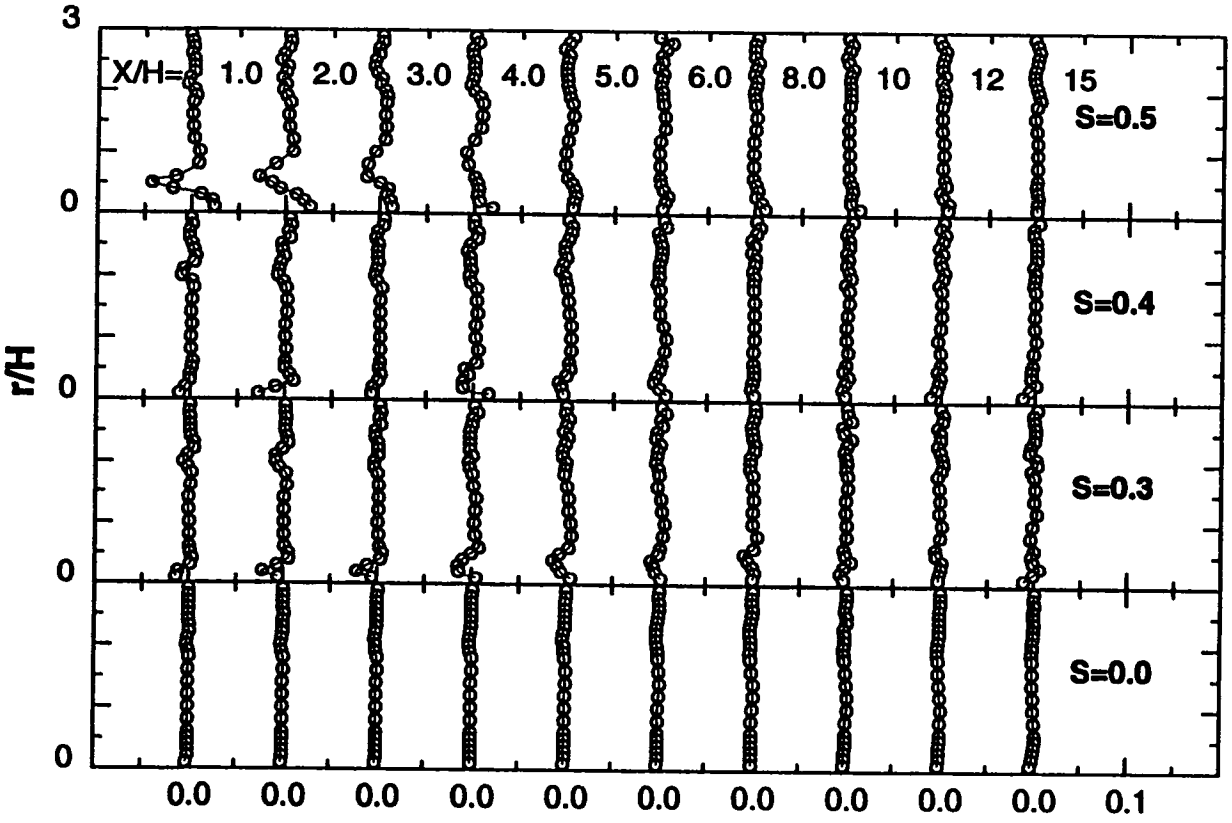

Figure C.13: Third Component Term of Diffusion, D3

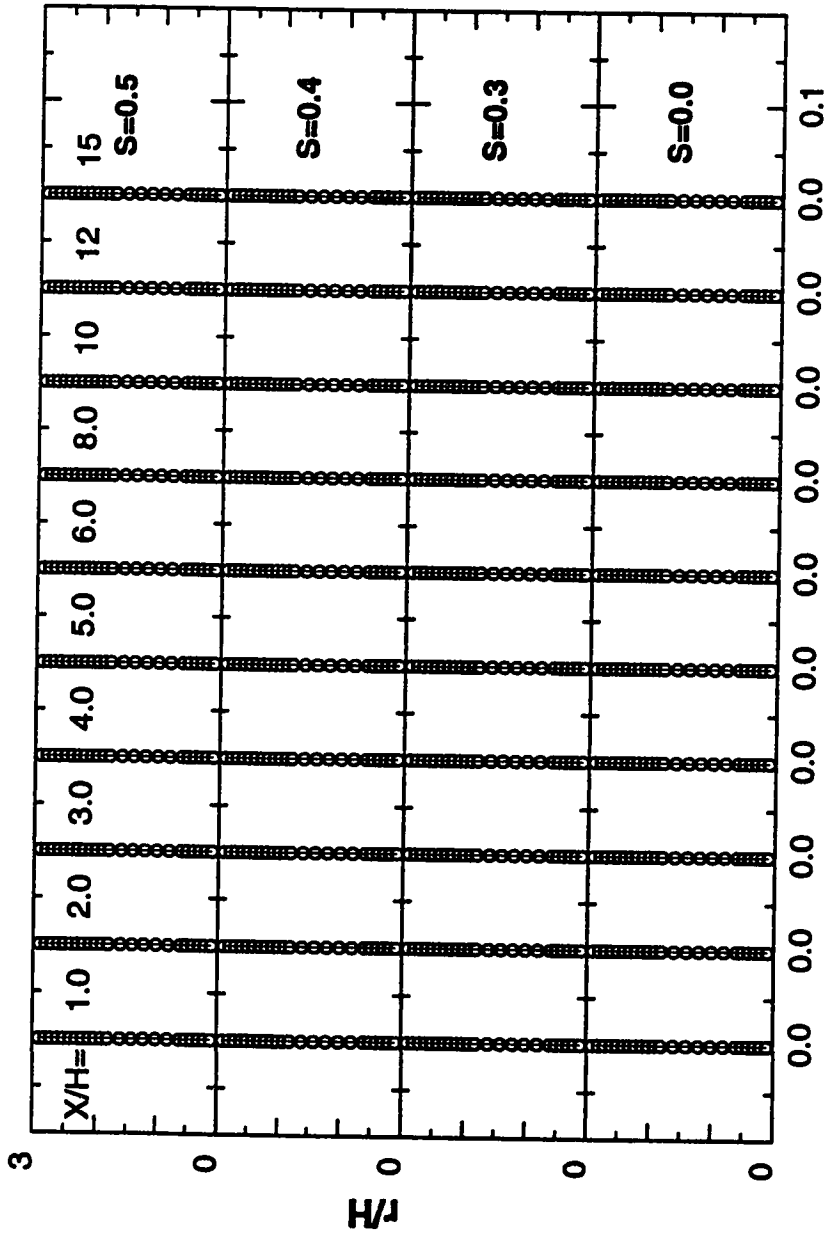

Figure C.14: Fourth Component Term of Diffusion, D4

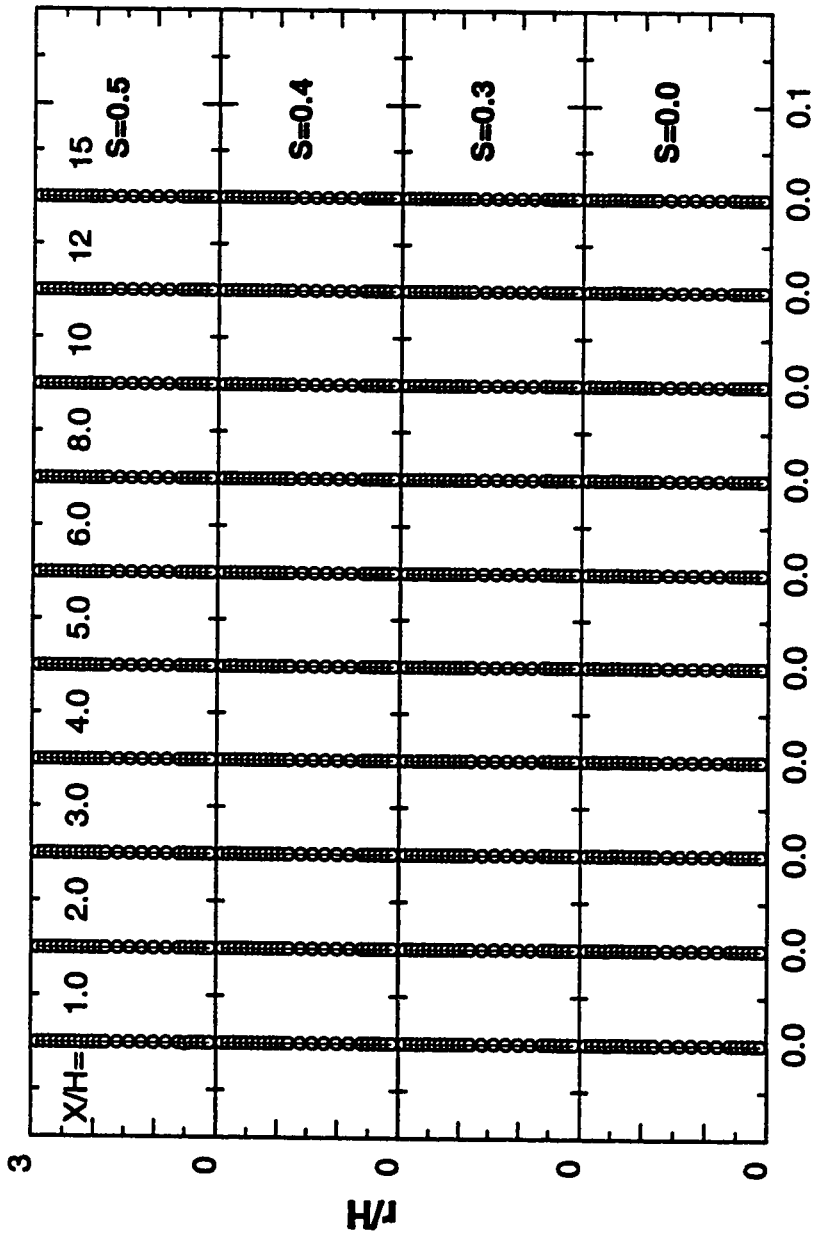

Figure C.15: Fifth Component Term of Diffusion, D5

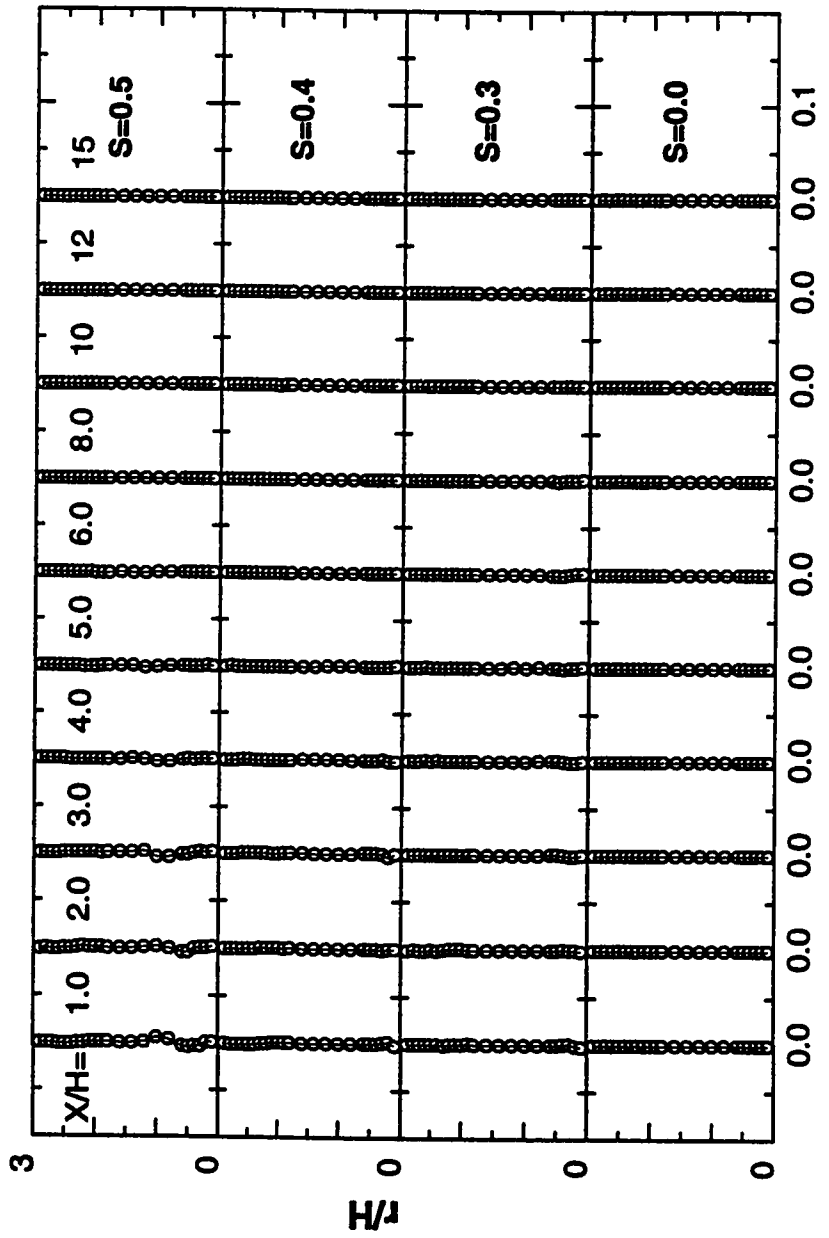

Figure C.16: Sixth Component Term of Diffusion, D6

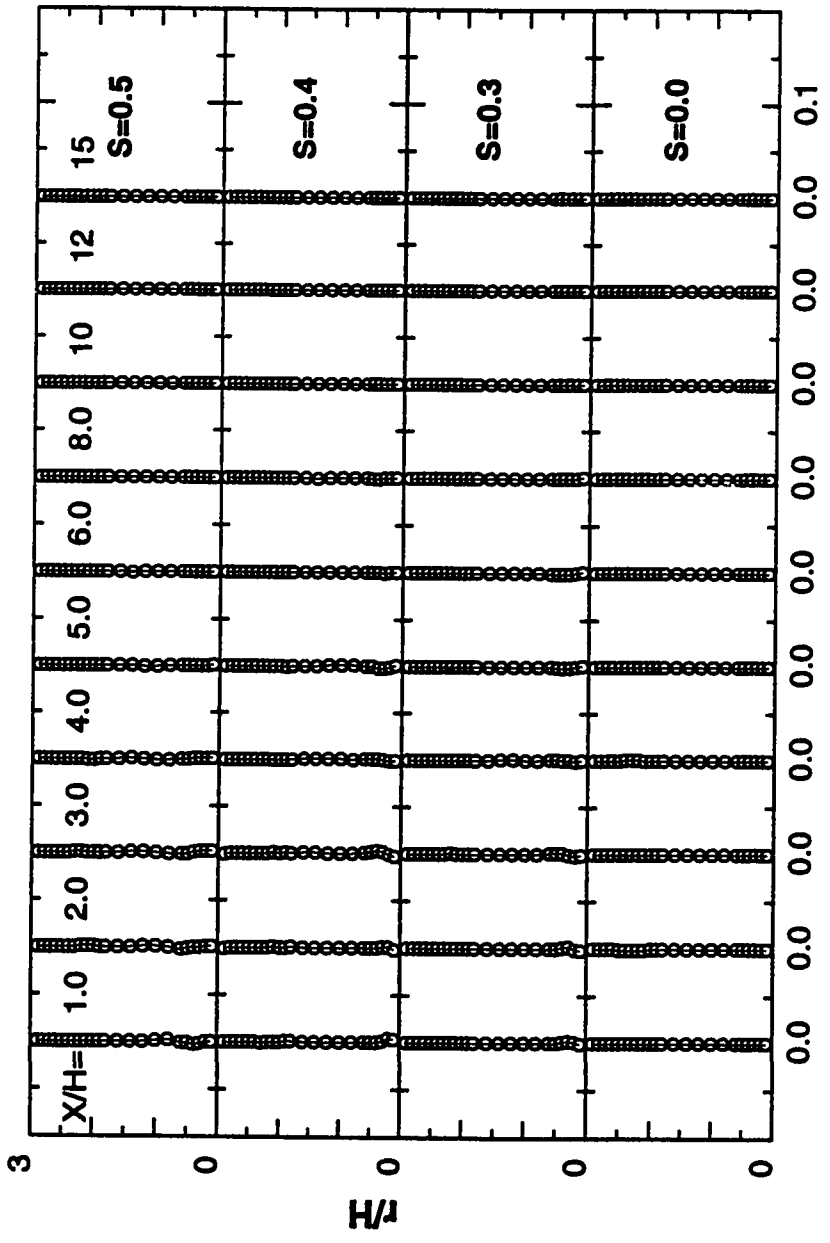

Figure C.17: Seventh Component Term of Diffusion, D7

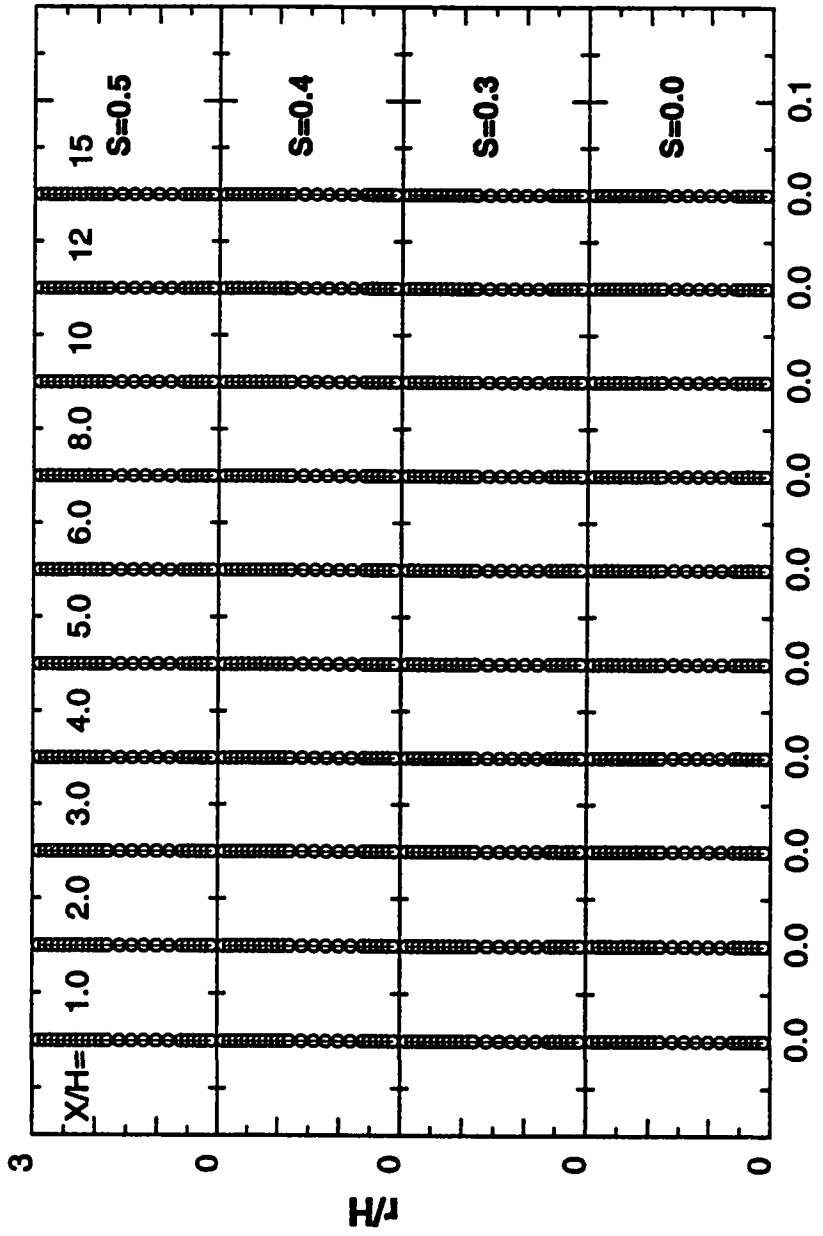

Figure C.18: Eighth Component Term of Diffusion, D8

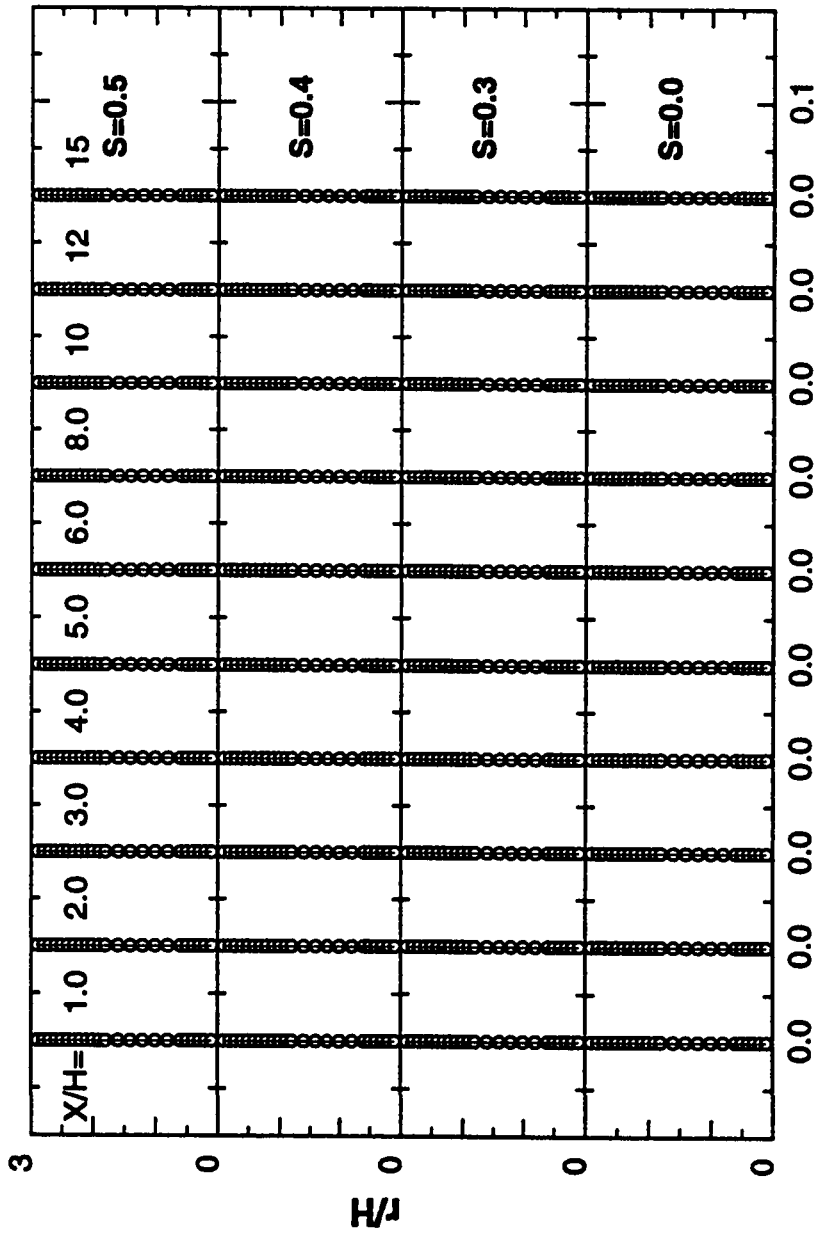

Figure C.19: Ninth Component Term of Diffusion, D9

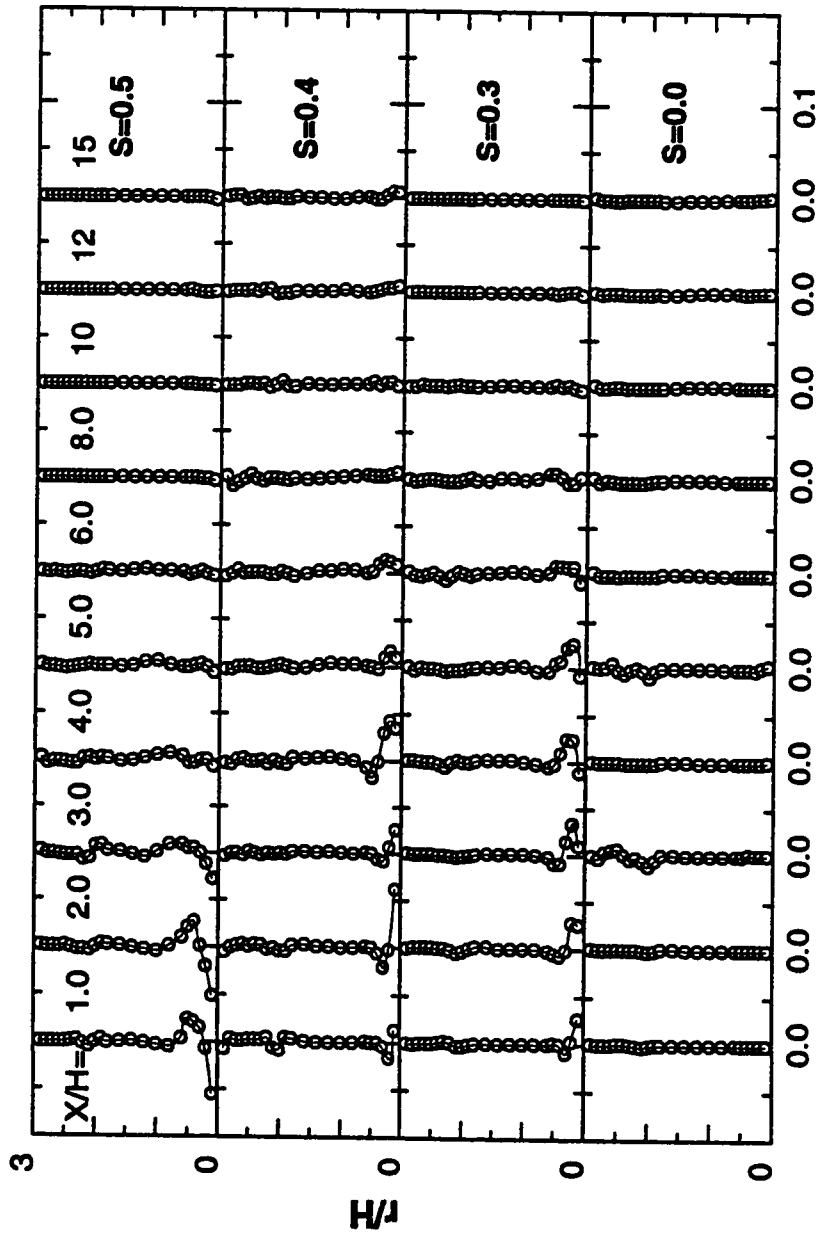

Figure C.20: Tenth Component Term of Diffusion, D10

Appendix D

Components of TKE Terms,

Effects of Swirl Profile

Components of Production Terms

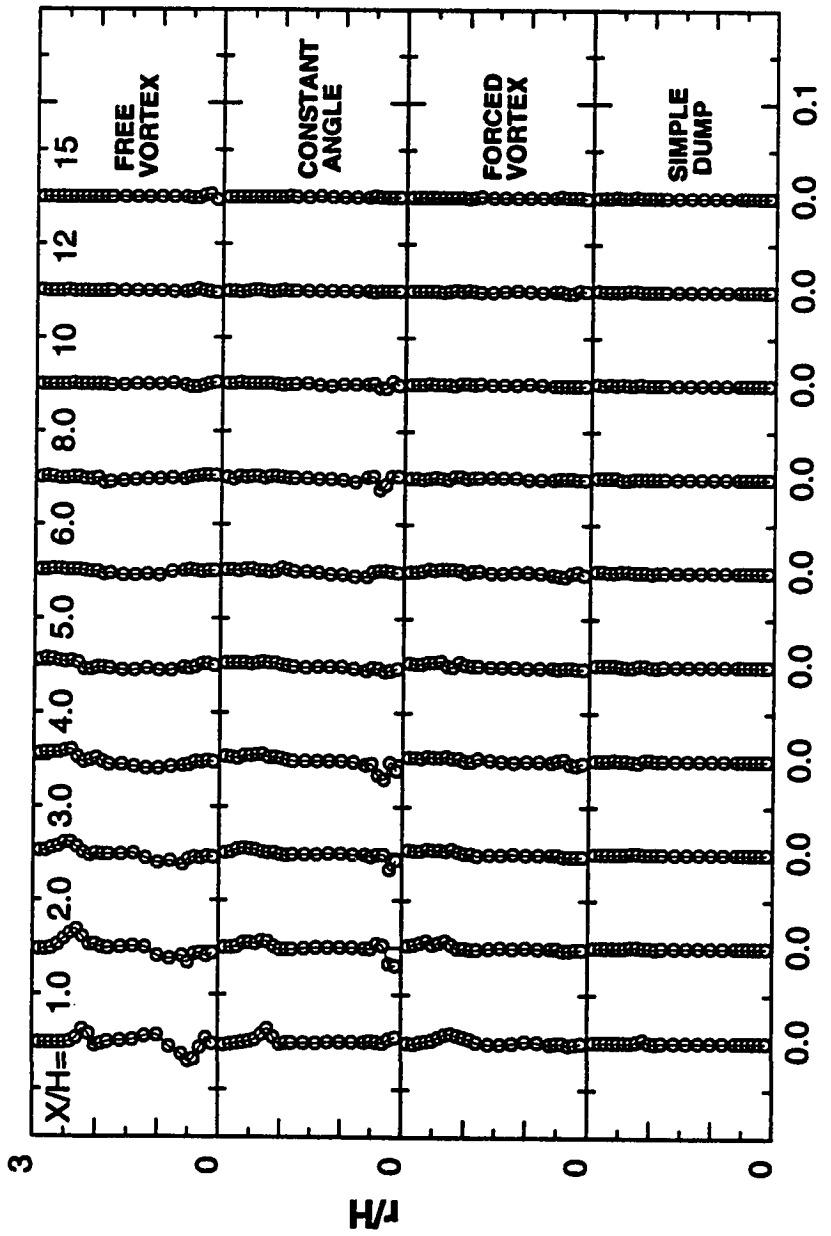

Figure D.1: First Component Term of Production, P1

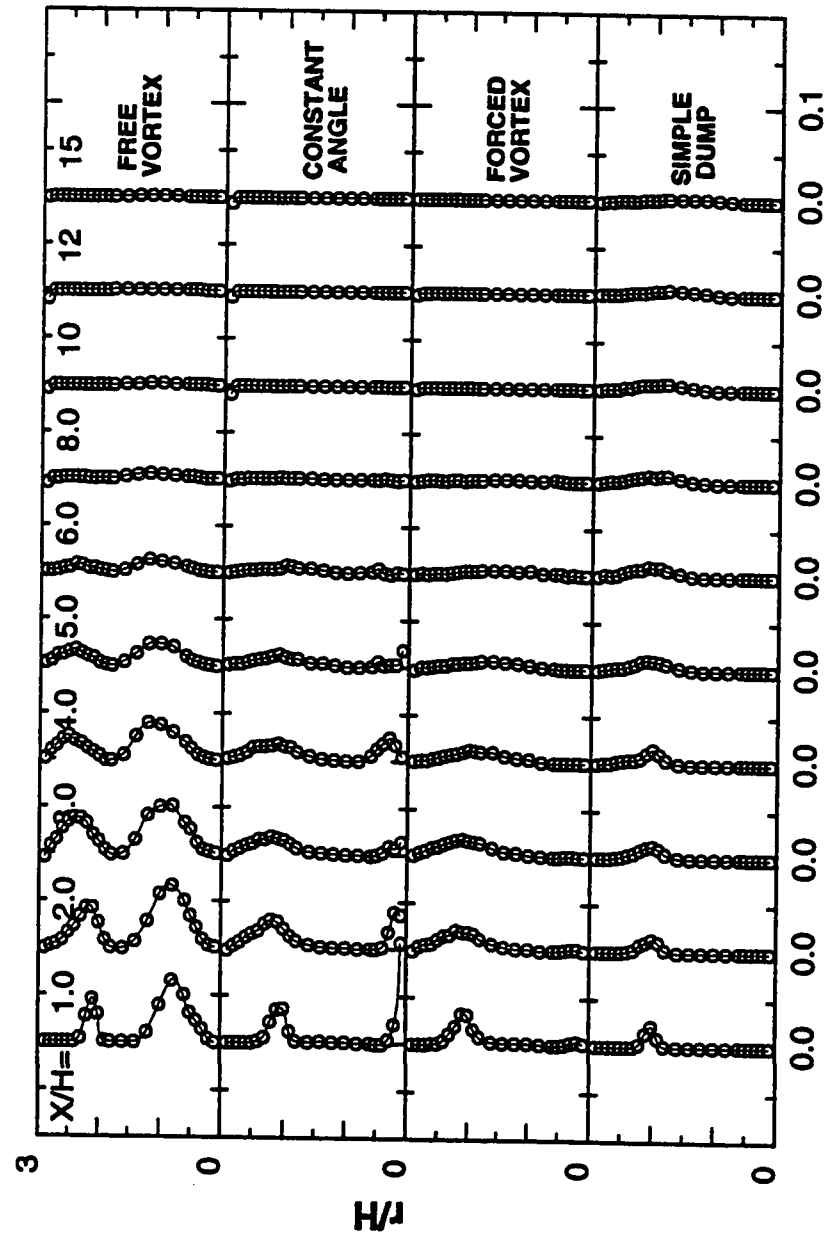

Figure D.2: Second Component Term of Production, P2

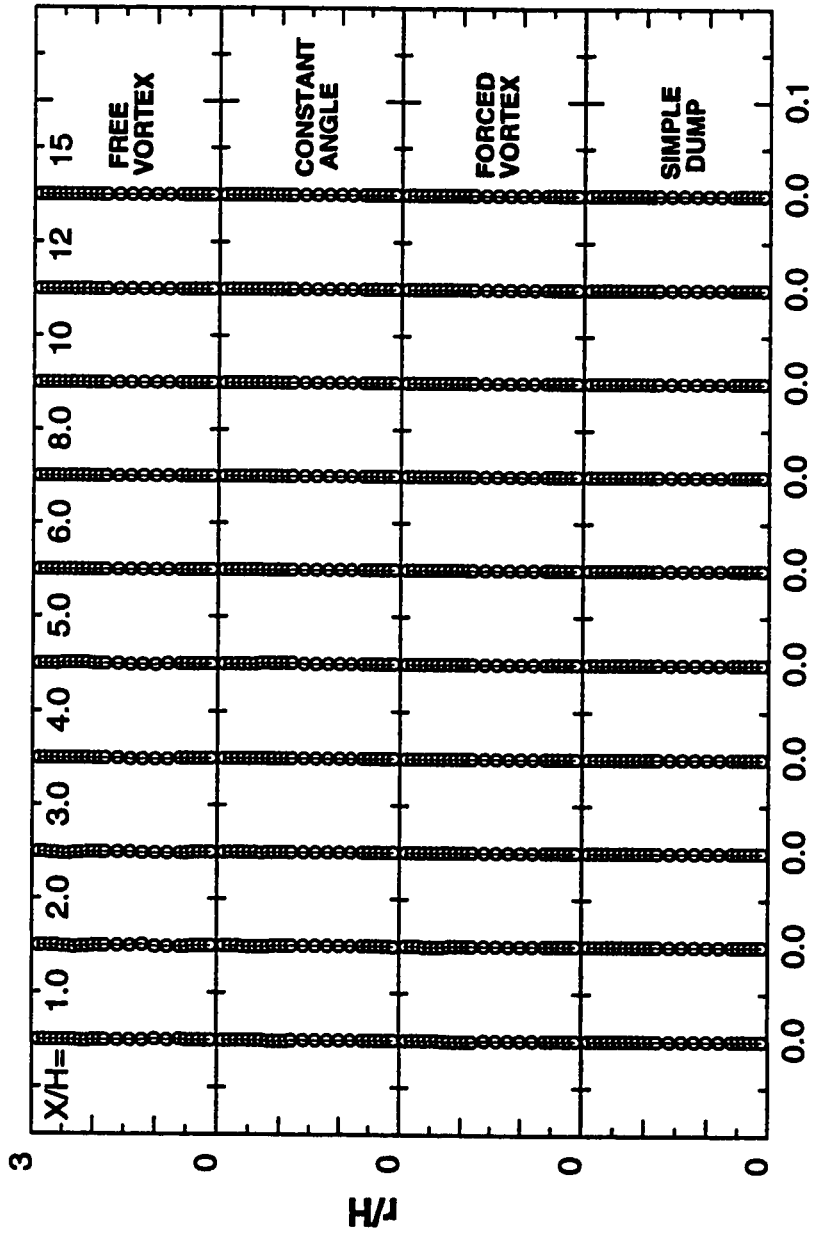

Figure D.3: Third Component Term of Production, P3

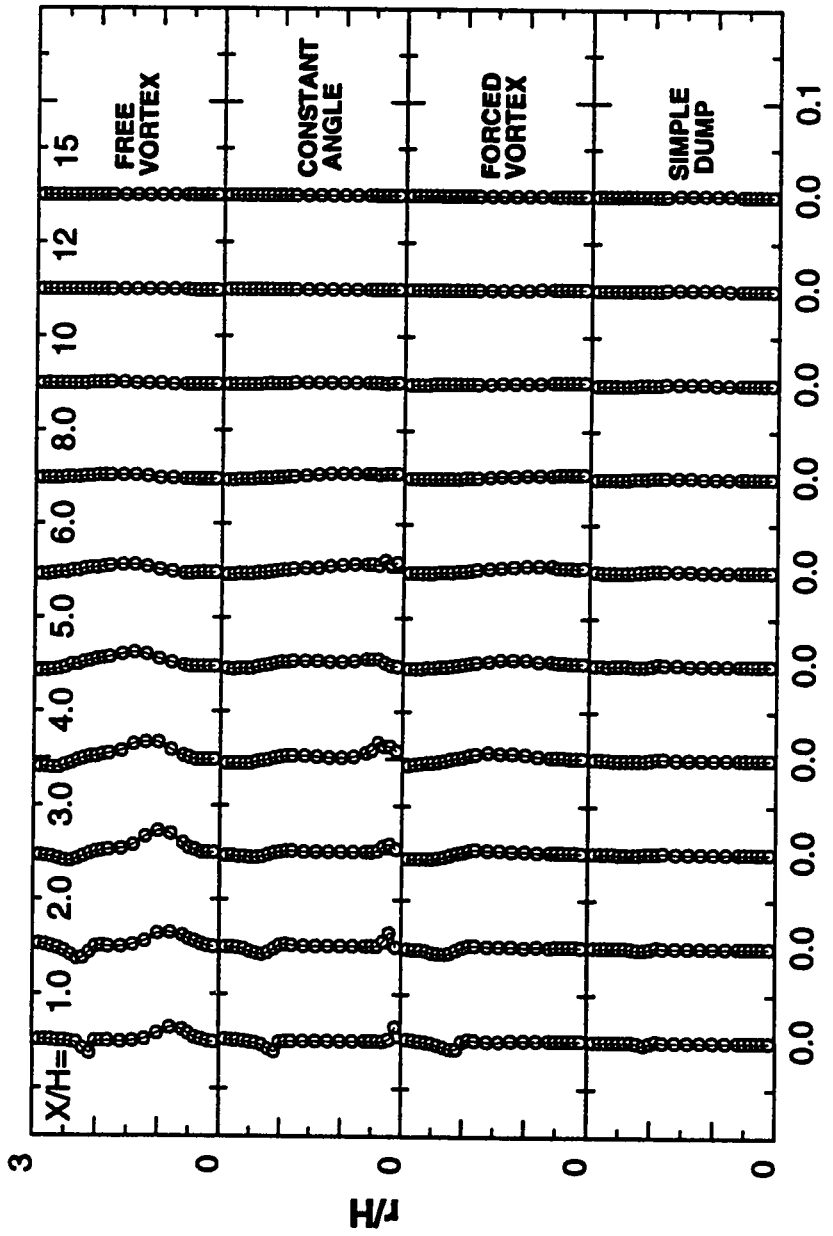

Figure D.4: Fourth Component Term of Production, P4

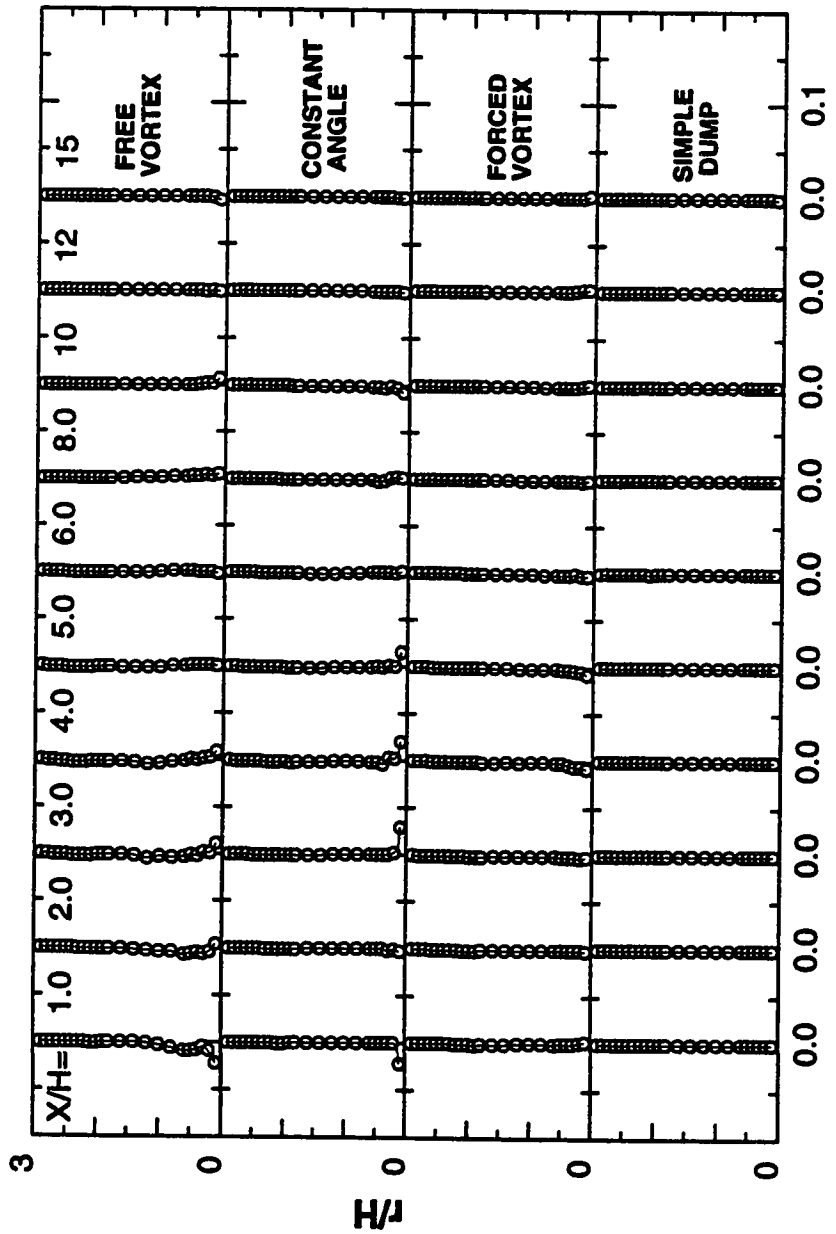

Figure D.5: Fifth Component Term of Production, P5

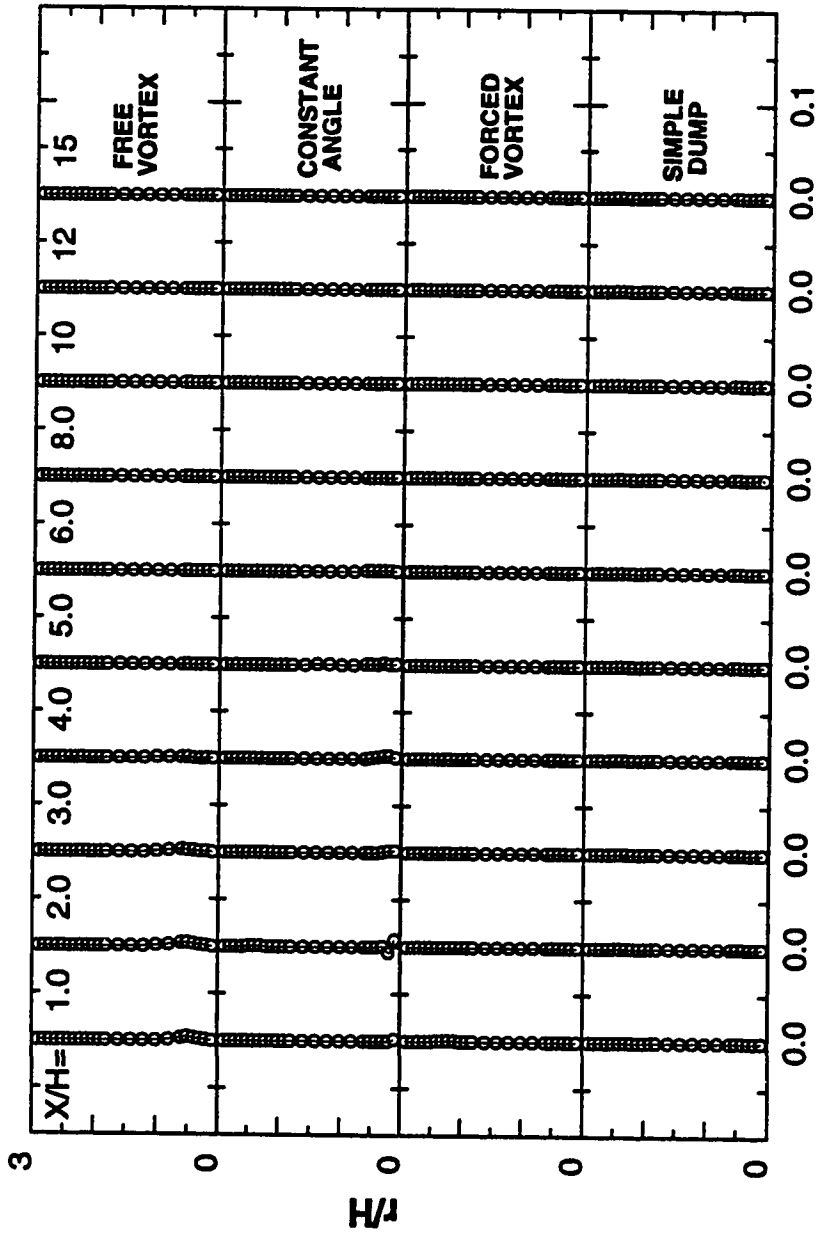

Figure D.6: Sixth Component Term of Production, P6

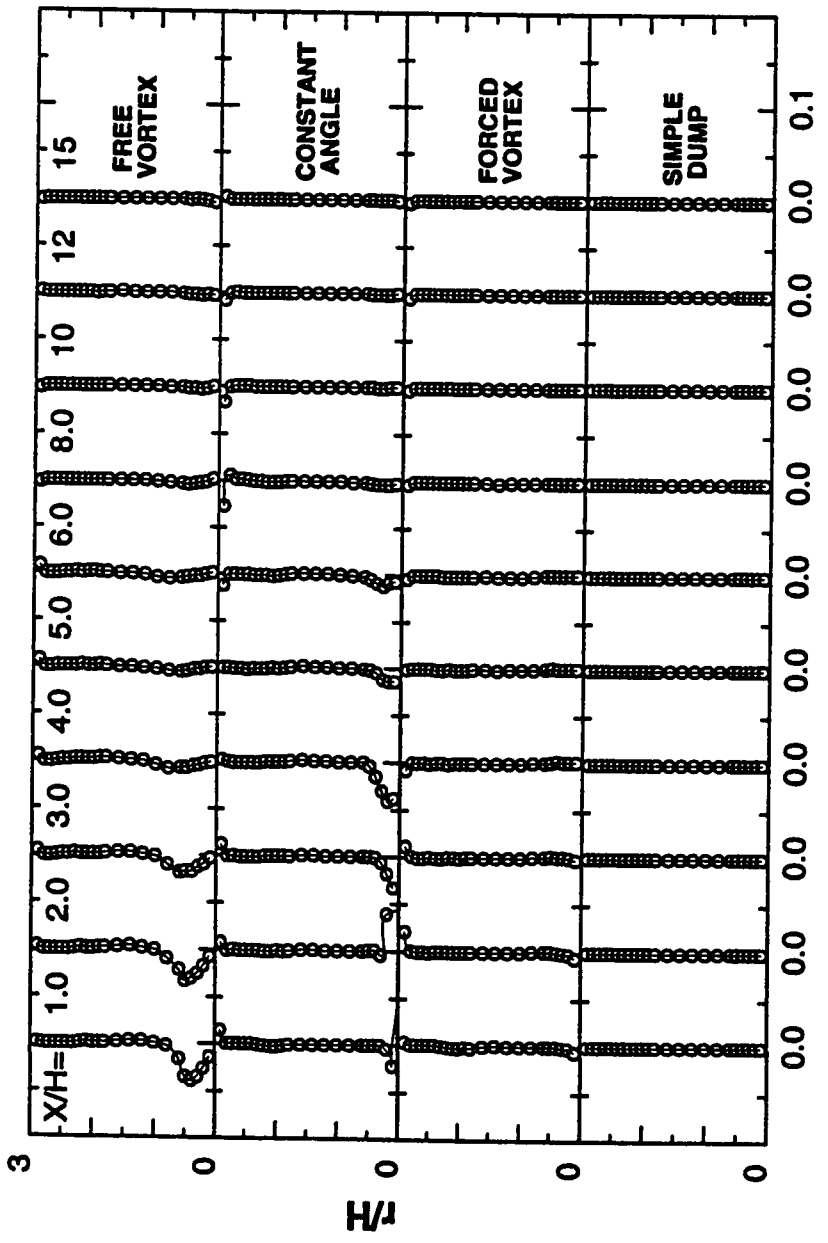

Figure D.7: Seventh Component Term of Production, P7

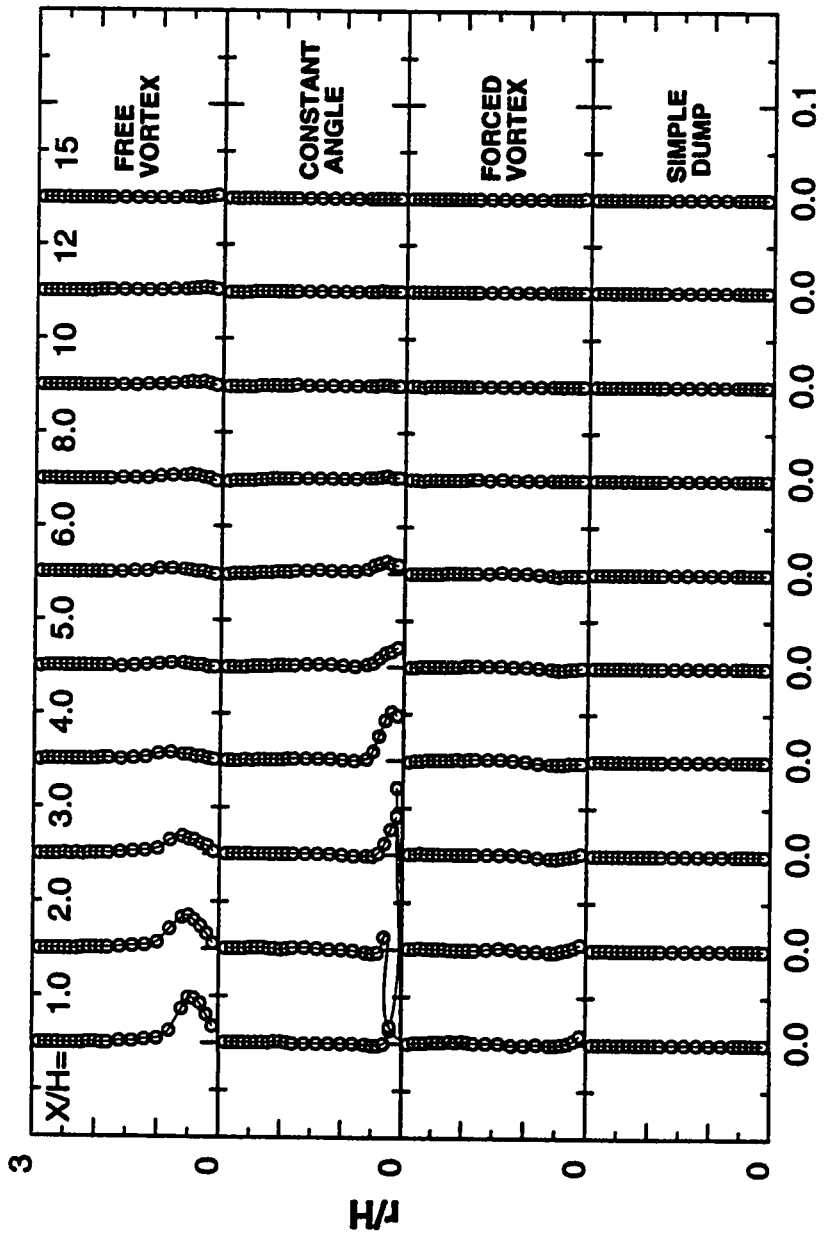

Figure D.8: Eighth Component Term of Production, P8

Components of Convection Terms

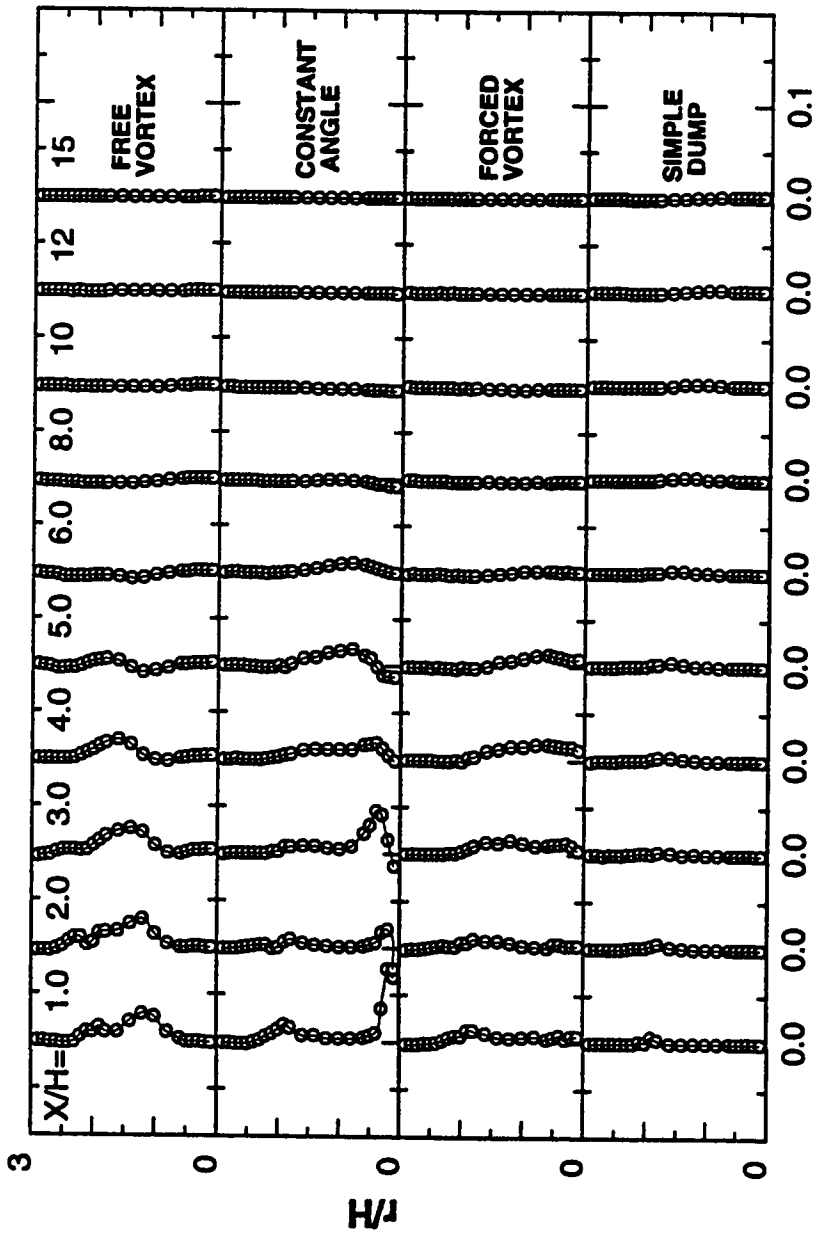

Figure D.9: First Component Term of Convection, C1

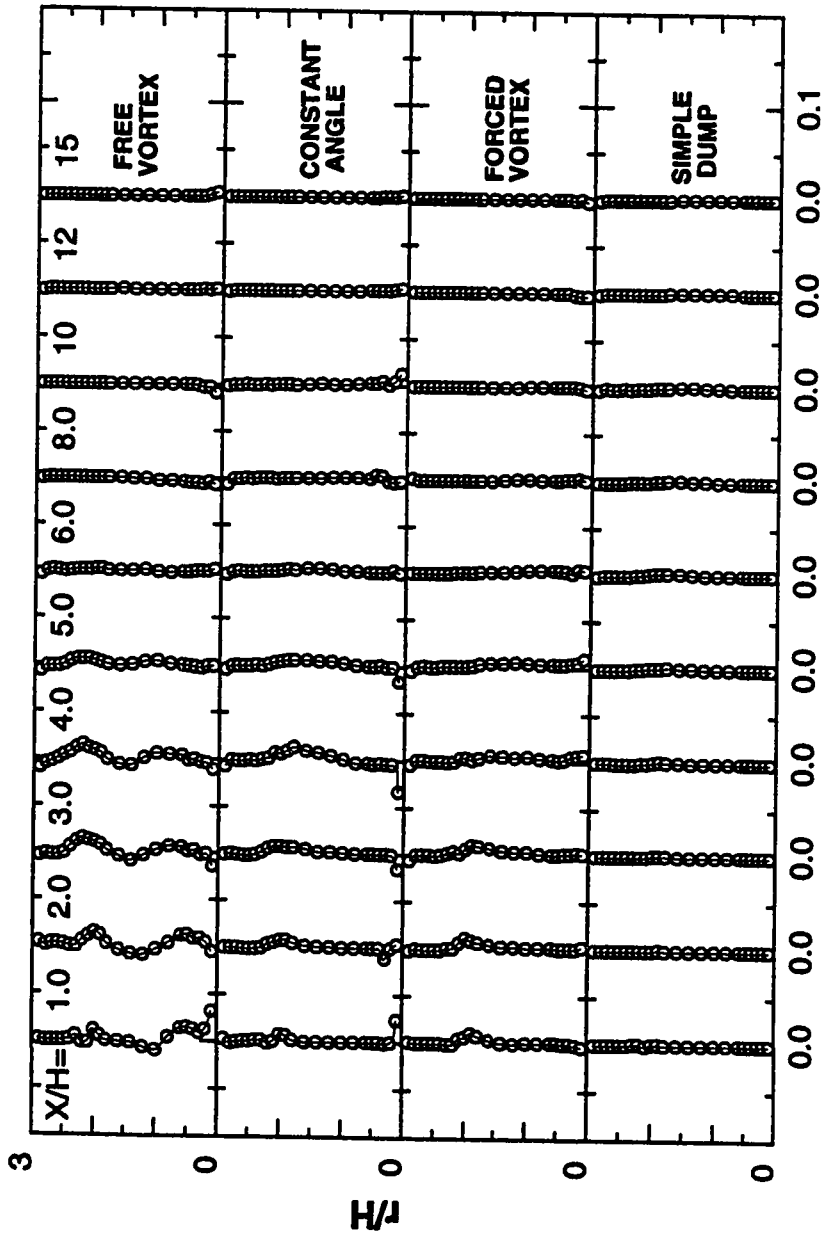

Figure D.10: Second Component Term of Convection, C2

Components of Diffusion Terms

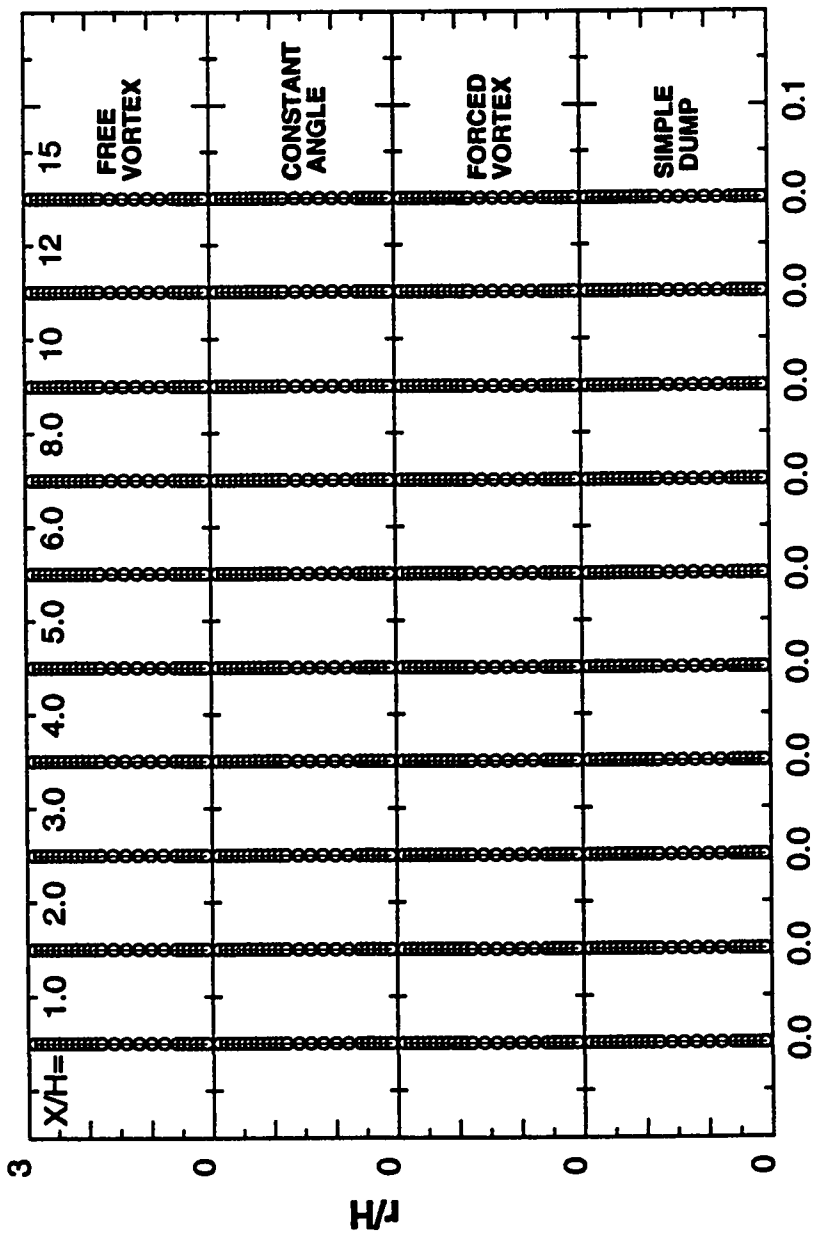

Figure D.11: First Component Term of Diffusion, D1

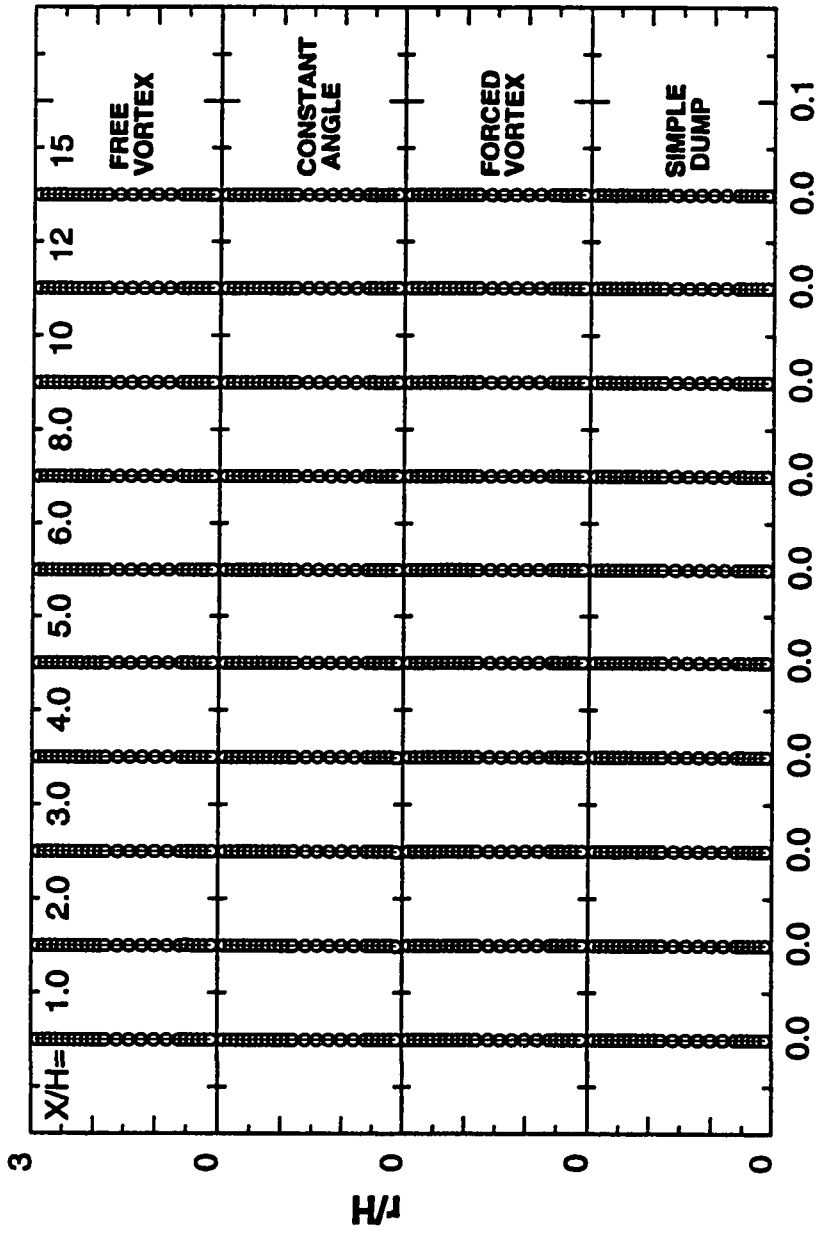

Figure D.12: Second Component Term of Diffusion, D2

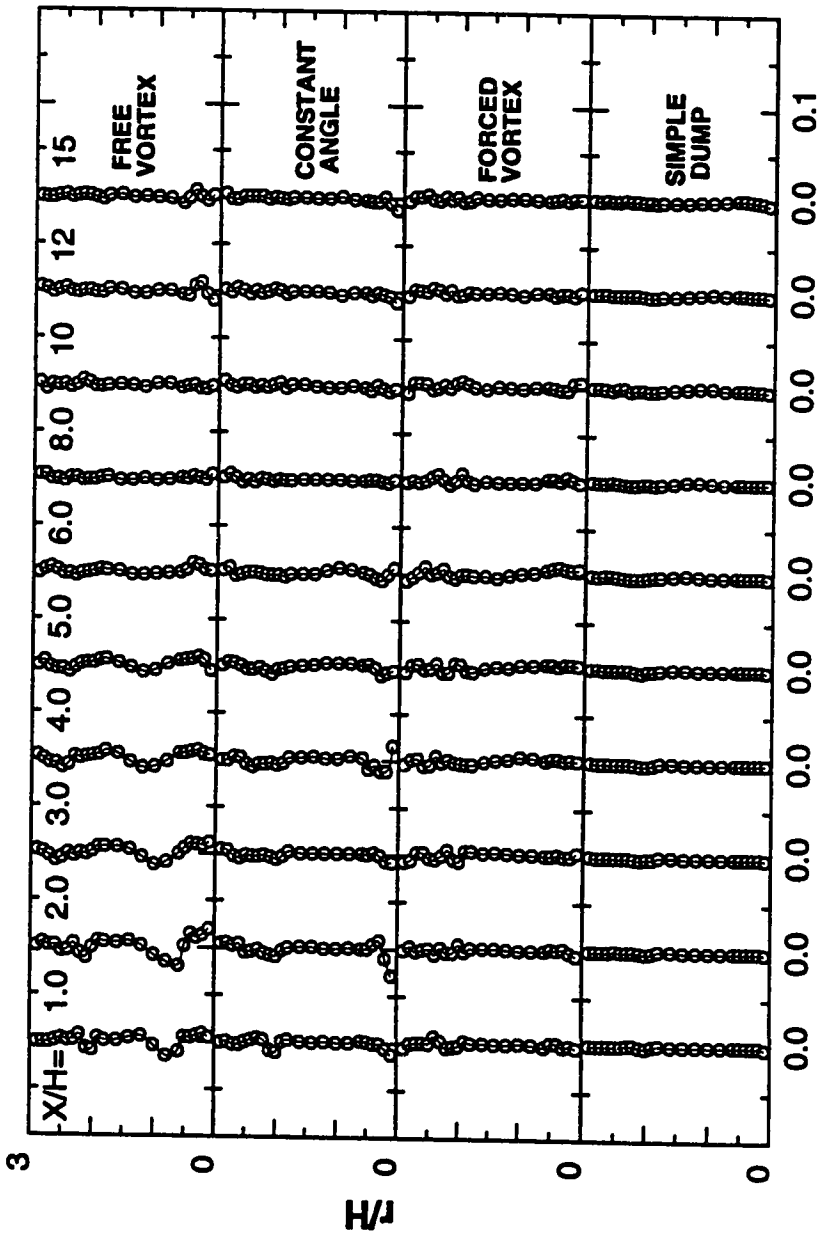

Figure D.13: Third Component Term of Diffusion, D3

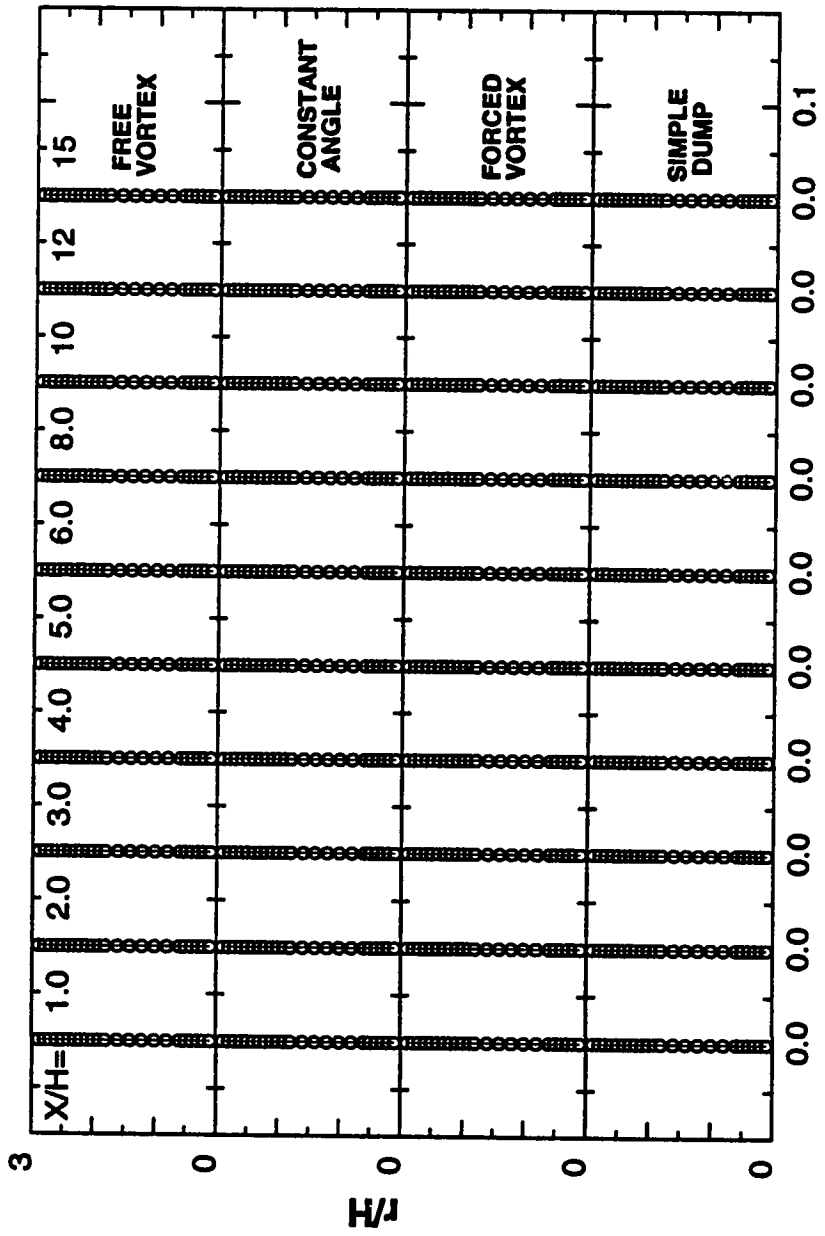

Figure D.14: Fourth Component Term of Diffusion, D4

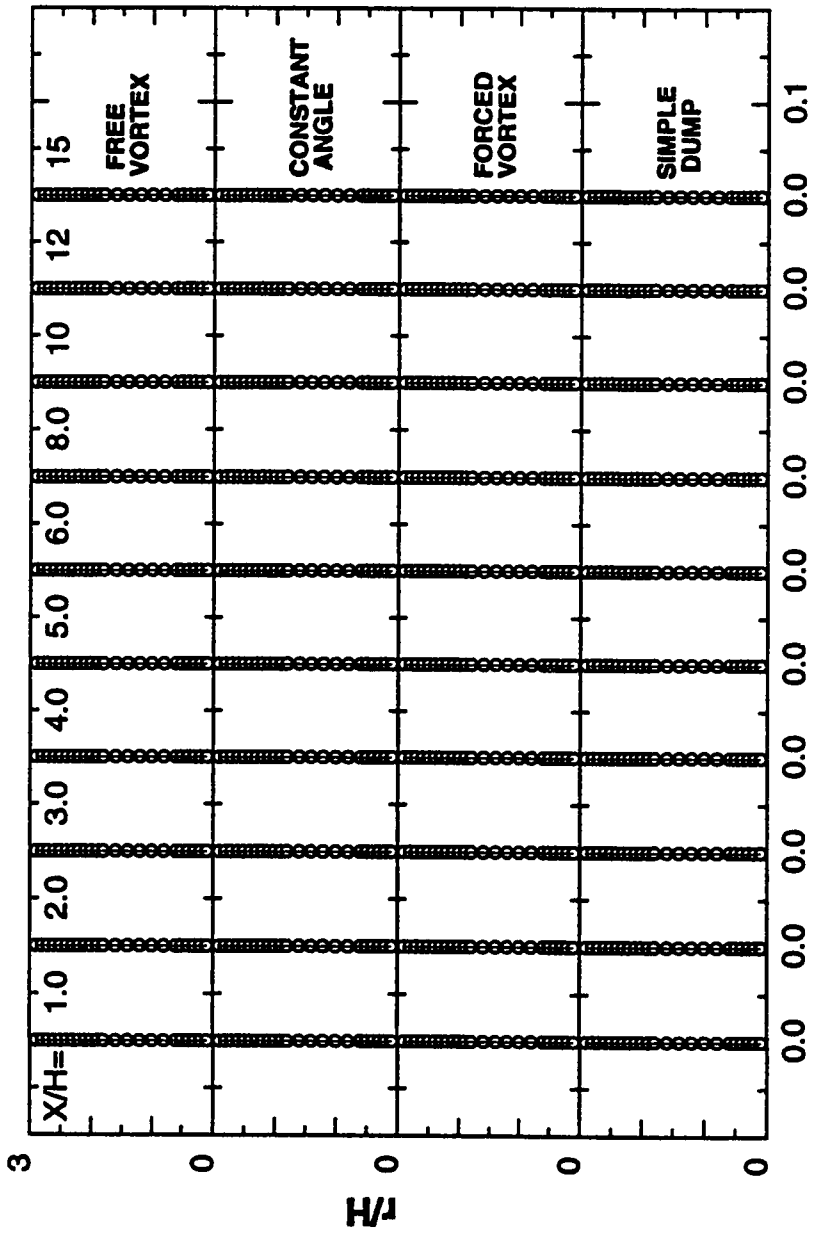

Figure D.15: Fifth Component Term of Diffusion, D5

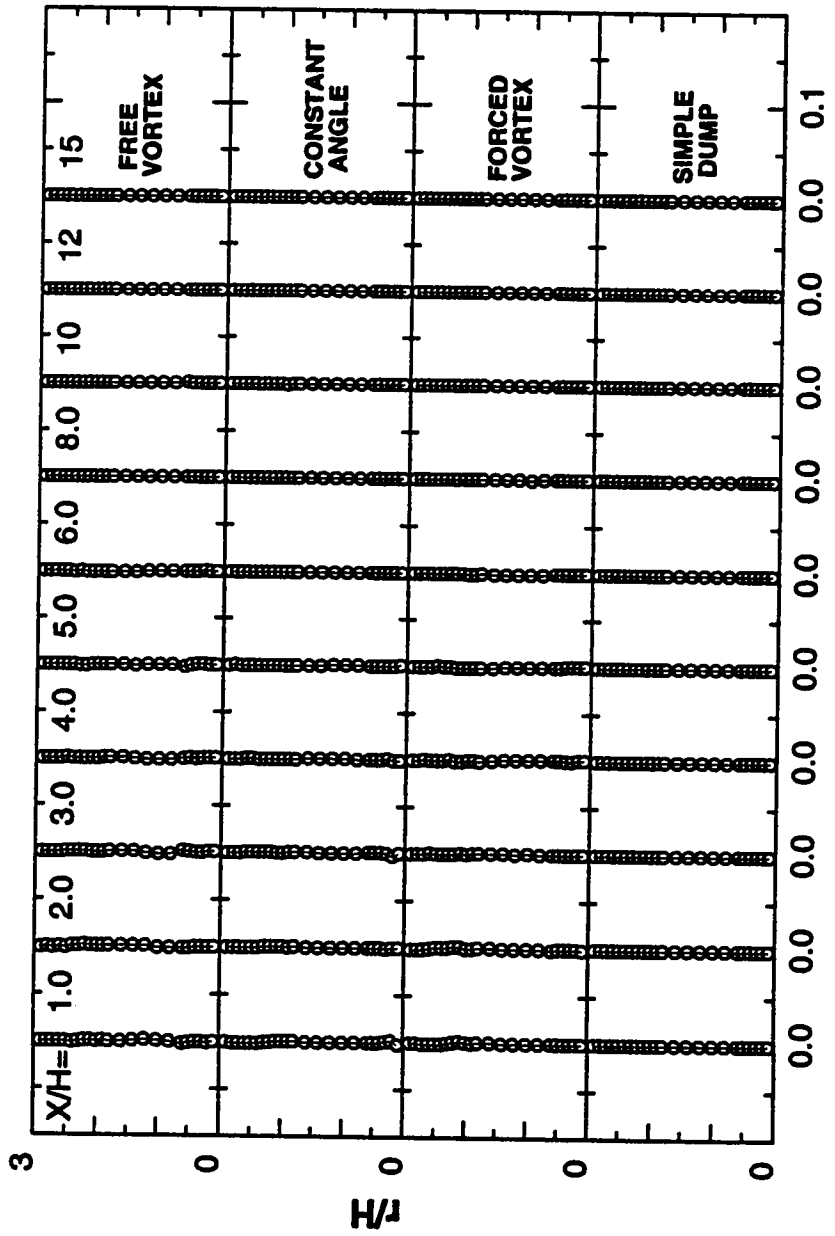

Figure D.16: Sixth Component Term of Diffusion, D6

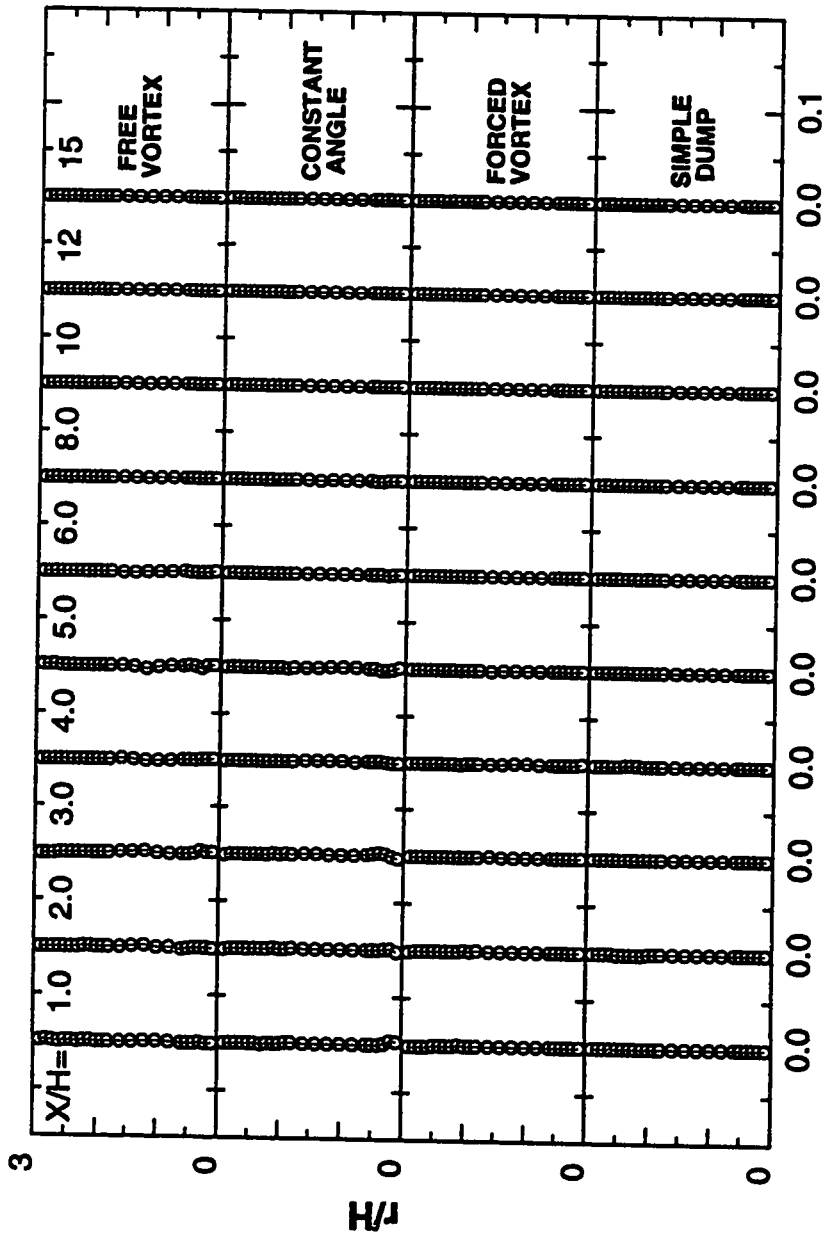

Figure D.17: Seventh Component Term of Diffusion, D7

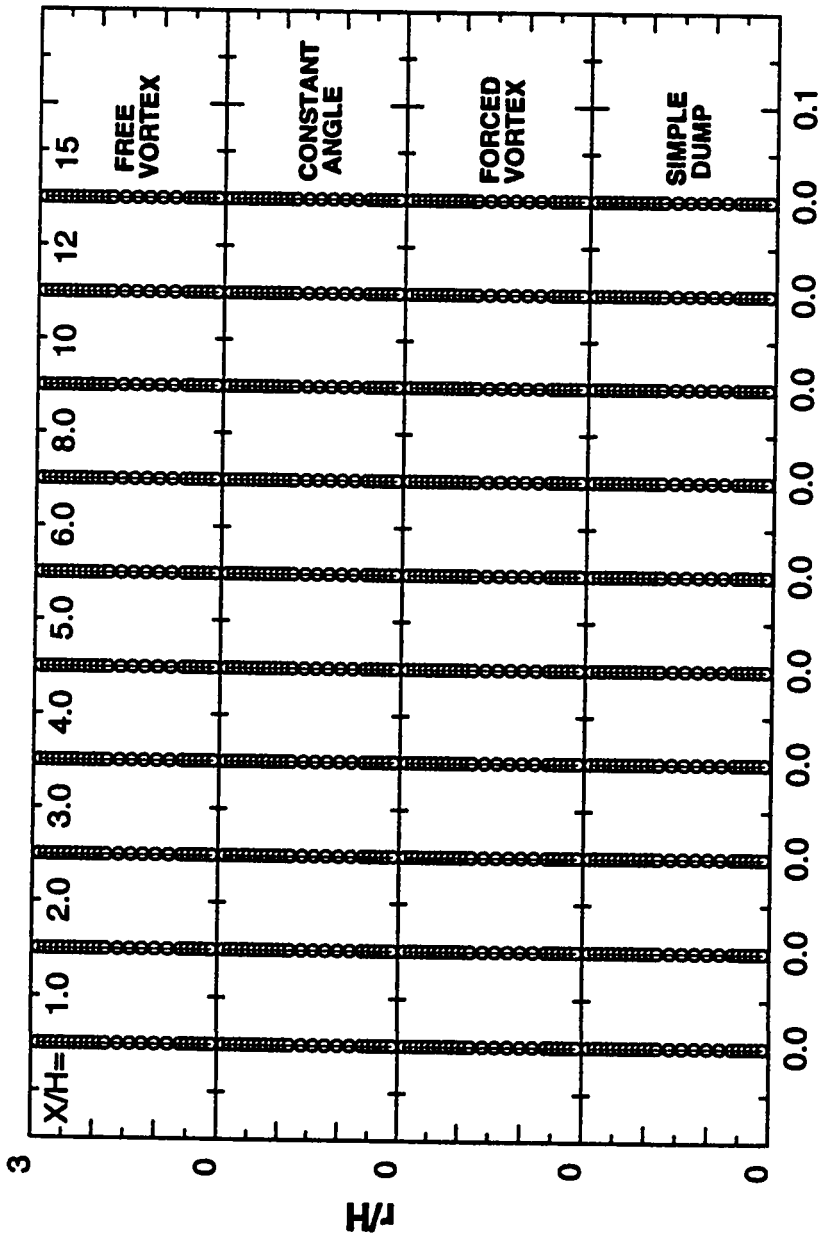

Figure D.18: Eighth Component Term of Diffusion, D8

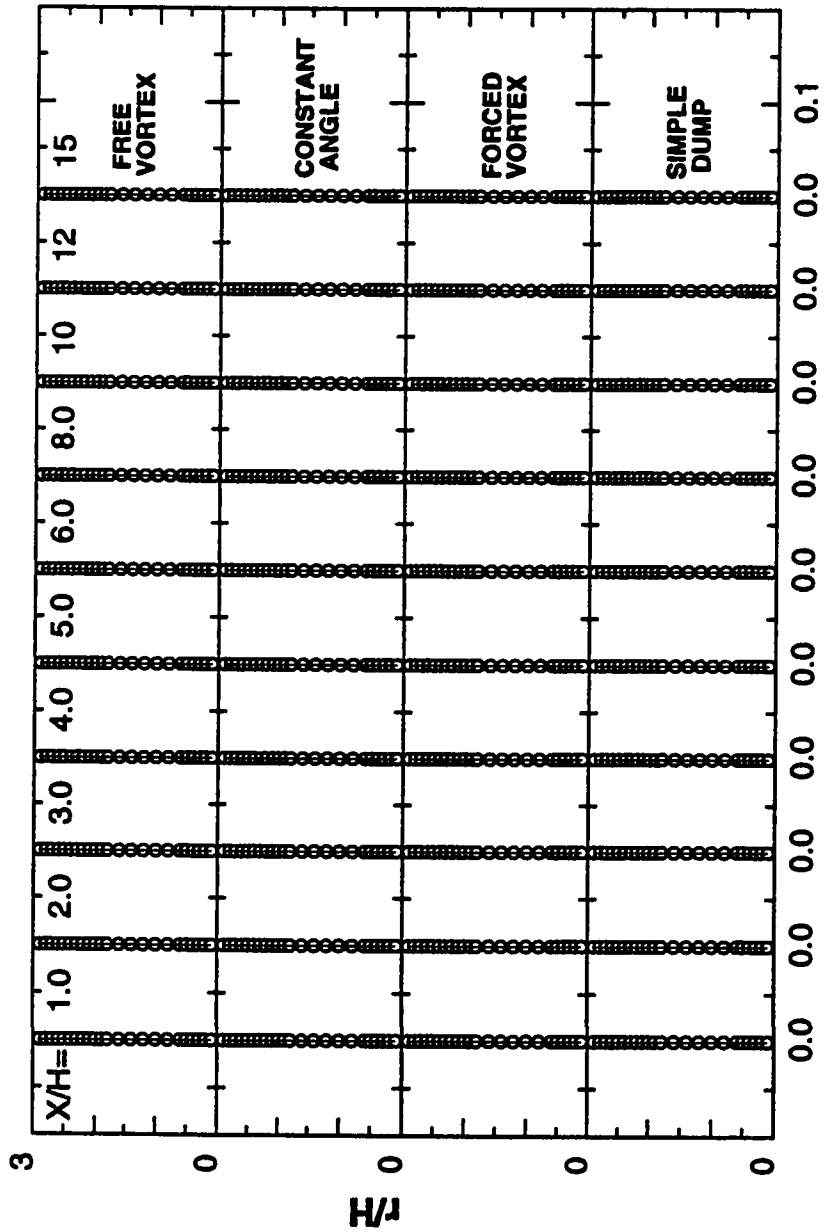

Figure D.19: Ninth Component Term of Diffusion, D9

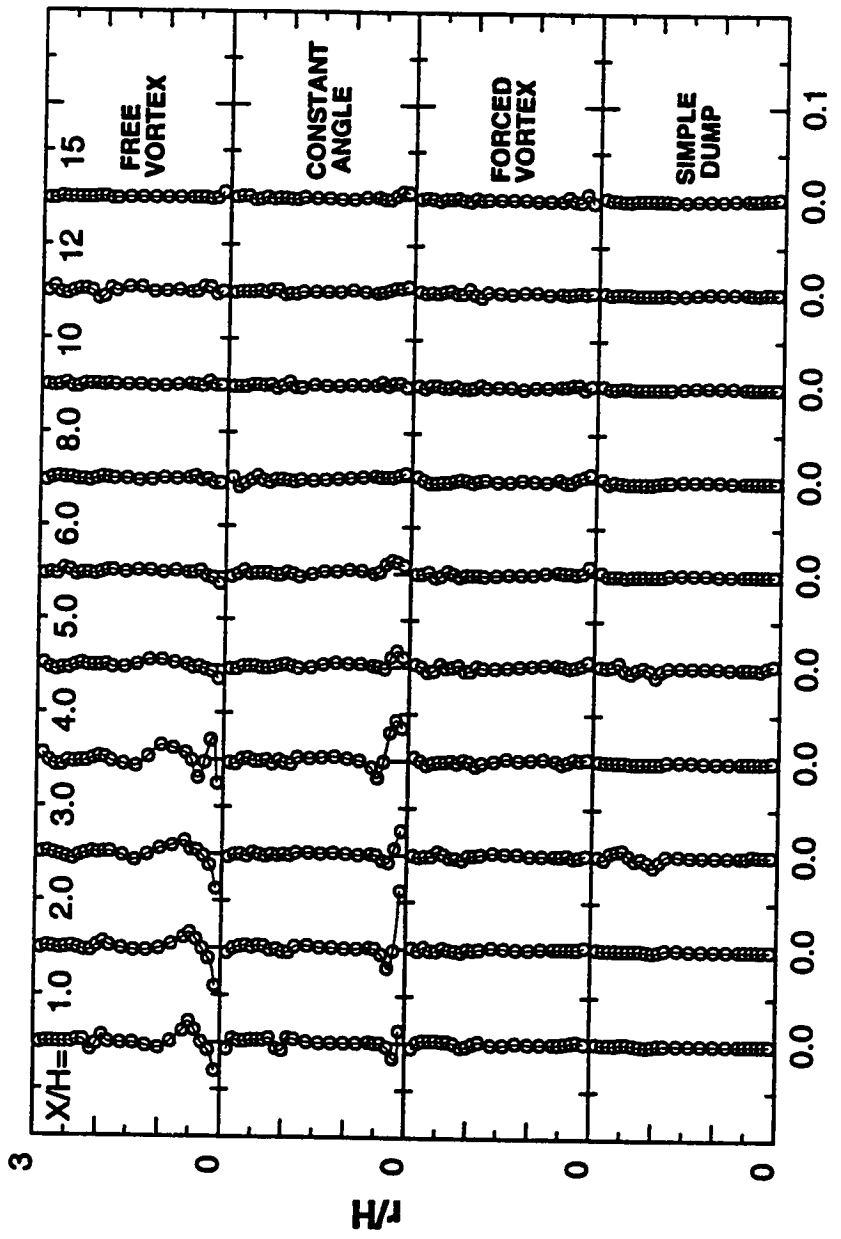

Figure D.20: Tenth Component Term of Diffusion, D10

Appendix E

Computer Program

```
********** Initialising arrays ****************

 REAL RHO(12,25),V(12,25),U(12,25),W(12,25),K(12,25),UP(12,25
&),VP(12,25),WP(12,25),UW(12,25),U3(12,25),V3(12,25),W3(12,25
&),U2V(12,25),SU(12,25),U2W(12,25),UW2(12,25),R(25),X(16),UV(
&12,25),UV2(12,25),SV(12,25),CR(12,25),CRA(12,25),CRG(12,25),
&CTG(12,25),CX(12,25),SW(12,25),D2(12,25),D3(12,25),D4(12,25)
&,D10(12,25),D1(12,25),D5(12,25),D6(12,25),D7(12,25),D8(12,25
&),D9(12,25),PR1(12,25),PR2(12,25),PR3(12,25),PR4(12,25),PR5(
&12,25),PR6(12,25),PR8(12,25),PR7(12,25),SF(12,25),CT(12,25),
&DT(12,25), PRT(12,25),DR(25),DX(16),DR2(25), DX2(25),DKDR(12
&,25),DUDR(12,25),DVDR(12,25),DWDR(12,25),DKDX(12,25),DUDX(12
&,25),DVDX(12,25),DWDX(12,25),DU3DX(12,25),NIF(12,25),VDT(12,
&25),DUV2DX(12,25),DUW2DX(12,25),D2KDX2(12,25),D2KDR2(12,25)



** Opening data files provided by user e.g.,******

      open(2,file='data1.dat',status='old')
      open(50,file='data2.dat',status='old')

** Opening files where results are to be written **

      open(3,file='c:\proplot\dn3\d1.dat',status='unknown')
      open(4,file='c:\proplot\dn3\d2.dat',status='unknown')

* Assigning the number of points in the X & Y axis for the
  source files
* M rep. no. of pts along the X-axis; N rep. no. of pts along
  the Y axis
* Y data points has to be uniform

      M=12
      N=25
      H=1.0
      PNEU=1.789E-5

***** Read data provided by user ***********

      DO 1 I=1,M
      DO 1 J=1,N
```

```
 READ(50,*) X(I),R(J),SF(I,J),U(I,J),V(I,J),W(I,J),K(I,J),
&UP(I,J),VP(I,J),WP(I,J),UV(I,J),UW(I,J)
 READ(2,*)DUM,DUM,DUM,DUM,SU(I,J),SV(I,J),SW(I,J),U2V(I,J),
&UV2(I,J),U2W(I,J),UW2(I,J)

       RHO(I,J)=1.225
       R(J)=R(J)/H
1      X(I)=X(I)/H

** CALL statements for the various subroutines ******

 CALL FNIP(M,N,UP,K,NIF)
 CALL TRIP(M,N,U3,V3,W3,SU,SV,SW,UP,VP,WP)
 CALL CHANGES1(M,N,DR,DX,R,X,DKDR,DUDR,DVDR,DWDR,DKDX,DUDX,
&DVDX,DWDX,DU3DX,DUV2DX,DUW2DX,K,U,V,W,U3,V3,W3,UV2,UW2,UV,UW
&)
 CALL CHANGES2(M,N,X,R,DR2,DX2,K,D2KDR2,D2KDX2)
 CALL CONVEC(M,N,DKDR,R,RHO,V,K,U,DKDX,CR,CRA,CRG,CTG,DR,
&CX,DX,CT)
 CALL DIFFUS(M,N,D1,D2,D3,D4,D5,D6,D7,D8,D9,D10,DT,UW2,DKDR,
D2KDX2,DU3DX,DUV2DX,DUW2DX,PNEU,R,RHO,V3,U2V,VP,WP)
 CALL PRODUC(M,N,PR1,PR2,PR3,PR4,PR5,PR6,PR7,PR8,PRT,RHO,UV,
&DVDR,DUDR,DVDX,DUDX,DWDX,DWDR,UW,UP,VP,WP,V,W,R)
 CALL DISSIP(M,N,VDT,CTG,DT,PRT)


********** WRITING THE RESULTS ************************
***** Print results in tecplot format ***

 WRITE(39,*)'TITLE= "flow in a dump combor, effect of swirl n
&umber" '
 WRITE(39,*)'VARIABLES ="X","Y","CX","CRG","CTG"      '
 WRITE(39,*)'ZONE T="data of 0.3 swirl 2",I=23,J=10,F=POINT '
 WRITE(40,*)'TITLE= "flow in a dump combor, effect of swirl n
&umber" '
 WRITE(40,*)'VARIABLES ="X","Y","PR1","PR2","PR3","PR4","PR5"
&,"PR6","PR7","PR8","PRT" '
 WRITE(40,*)'ZONE T="data of 0.3 swirl 2",I=23,J=10,F=POINT '
 WRITE(41,*)'TITLE= "flow in a dump combor, effect of swirl n
&umber" '
 WRITE(41,*)'VARIABLES ="X","Y","D1","D2","D3","D4","D5","D6"
&,"D7","D8","D9","D10","DT"      '
 WRITE(41,*)'ZONE T="data of 0.3 swirl 2",I=23,J=10,F=POINT '
```

```
 WRITE(42,*)'TITLE= "flow in a dump combor, effect of swirln
    &umber" '
       WRITE(42,*)'VARIABLES="X","Y","K","PRT","CTG",
      &"DT","VDT"," &NIF"'
       WRITE(42,*)'ZONE T="data of 0.3 swirl 2",I=23,J=10
      &,F=POINT '

       DO 4339 J=1,N
4339   R(J)=R(J)+3.0
       write(43,2000)
       do 1001 j=1,n
1001   write(43,2001)r(j),u(1,j),v(1,j),w(1,j)
2000   format('(R',9x,'U',9x,'V',9x,'W)')
2001   format(4f9.5)

       DO 4337 I=2,M-1
       DO 4337 J=2,N-1
       WRITE(39,207)X(I),R(J),CX(I,J),CRG(I,J),CTG(I,J)
       WRITE(40,204)X(I),R(J),PR1(I,J),PR2(I,J),PR3(I,J),
      &PR4(I,J ),PR5(I,J),PR6(I,J),PR7(I,J),PR8(I,J),PRT
      &(I,J), X(I),R(J),D1(I,&J),D2(I,J),D3(I,J),D4(I,J),
      &D5(I,J),D6(I,J),D7(I,J),D8(I,J),D&9(I,J),D10(I,J)
      &,DT(I,J)
4337   WRITE(42,206)X(I),R(J),K(I,J),PRT(I,J),CTG(I,J),
     &DT(I,J),VDT(I,J),NIF(I,J)

*** Print results in desired proplot format ************

       write(3,203)(X(I),I=2,11)
       write(4,203)(X(I),I=2,11)
       write(5,203)(X(I),I=2,11)
       write(7,203)(X(I),I=2,11)
       write(8,203)(X(I),I=2,11)
       write(9,203)(X(I),I=2,11)
       write(10,203)(X(I),I=2,11)
       write(11,203)(X(I),I=2,11)
       write(12,203)(X(I),I=2,11)
       write(13,203)(X(I),I=2,11)
       write(14,203)(X(I),I=2,11)
       write(15,203)(X(I),I=2,11)
       write(16,203)(X(I),I=2,11)
       write(17,203)(X(I),I=2,11)
       write(18,203)(X(I),I=2,11)
       write(19,203)(X(I),I=2,11)
```

```
      write(20,203)(X(I),I=2,11)
      write(21,203)(X(I),I=2,11)
      write(22,203)(X(I),I=2,11)
      write(29,203)(X(I),I=2,11)
      write(30,203)(X(I),I=2,11)
      write(31,203)(X(I),I=2,11)
      write(33,203)(X(I),I=2,11)
      write(34,203)(X(I),I=2,11)
      write(35,203)(X(I),I=2,11)
      write(36,203)(X(I),I=2,11)
      write(37,203)(X(I),I=2,11)



       AJ=0.025

       DO 488 I=2,11

       DO 477 J=2,24

         d1(I,J)=d1(I,J)+AJ

         d2(I,J)=d2(I,J)+AJ
         d3(I,J)=d3(I,J)+AJ
         cr(I,J)=cr(I,J)+AJ
         cra(I,J)=cra(I,J)+AJ
         crg(I,J)=crg(I,J)+AJ
         pr1(I,J)=pr1(I,J)+AJ
         pr2(I,J)=pr2(I,J)+AJ
         pr7(I,J)=pr7(I,J)+AJ
         d10(I,J)= d10(I,J)+AJ
477    CONTINUE
        AJ=AJ+0.025

488    CONTINUE

         AJ=0.025
       DO 4088 I=2,11
       DO 4077 J=2,24
         d4(I,J)=d4(I,J)+AJ
         d5(I,J)=d5(I,J)+AJ
         d6(I,J)=d6(I,J)+AJ
         d7(I,J)=d7(I,J)+AJ
         cx(I,J)=cx(I,J)+AJ
```

```
          pr3(I,J)=pr3(I,J)+AJ
          pr4(I,J)=pr4(I,J)+AJ
          pr6(I,J)=pr6(I,J)+AJ
4077      CONTINUE
          AJ=AJ+0.025

4088      CONTINUE
         AJ=0.025
         DO 4188 I=2,11
         DO 4177 J=2,24
           d8(I,J)=d8(I,J)+AJ
           d9(I,J)=d9(I,J)+AJ
           dt(I,J)=dt(I,J)+AJ
           ct(I,J)=ct(I,J)+AJ
           ctg(I,J)=ctg(I,J)+AJ
           pr5(I,J)=pr5(I,J)+AJ
           pr8(I,J)=pr8(I,J)+AJ
           prt(I,J)=prt(I,J)+AJ
           vdt(I,J)=vdt(I,J)+AJ
4177      CONTINUE
         AJ=AJ+0.025
4188      CONTINUE
         DO 499 J=2,24
          write(3,202) R(J),(d1(I,J),I=2,11)
          write(4,202) R(J),(d2(I,J),I=2,11)
          write(5,202) R(J),(d3(I,J),I=2,11)
          write(16,202) R(J),(cr(I,J),I=2,11)
          write(33,202) R(J),(cra(I,J),I=2,11)
          write(34,202) R(J),(crg(I,J),I=2,11)
          write(17,202) R(J),(pr1(I,J),I=2,11)
          write(18,202) R(J),(pr2(I,J),I=2,11)
          write(30,202) R(J),(pr7(I,J),I=2,11)
499       write(36,202) R(J),(d10(I,J),I=2,11)

          DO 4091 J=2,24
          write(7,202) R(J),(d4(I,J),I=2,11)
          write(8,202) R(J),(d5(I,J),I=2,11)
          write(9,202) R(J),(d6(I,J),I=2,11)
          write(10,202) R(J),(d7(I,J),I=2,11)
          write(15,202) R(J),(cx(I,J),I=2,11)
          write(19,202) R(J),(pr3(I,J),I=2,11)
          write(20,202) R(J),(pr4(I,J),I=2,11)
4091      write(29,202) R(J),(pr6(I,J),I=2,11)
```

```
          DO 4191 J=2,24
          write(11,202) R(J),(d8(I,J),I=2,11)
          write(12,202) R(J),(d9(I,J),I=2,11)
          write(13,202) R(J),(dt(I,J),I=2,11)
          write(14,202) R(J),(ct(I,J),I=2,11)
          write(35,202) R(J),(ctg(I,J),I=2,11)
          write(21,202) R(J),(pr5(I,J),I=2,11)
          write(31,202) R(J),(pr8(I,J),I=2,11)
          write(37,202) R(J),(vdt(I,J),I=2,11)
4191      write(22,202) R(J),(prt(I,J),I=2,11)

******* Formats used for the output files ********************

202     FORMAT(1F5.2,3X,10F7.3)

203     FORMAT(1X,'(X/H=',4X,1F3.1,4X,1F3.1,4X,1F3.1,4X,1F3.1,
     &4X,1F3.1,4X
     &,1F3.1,3X,1F4.1,3X,1F4.1,3X,1F4.1,3X,1F4.1,')',/'( R
     &)')
207     FORMAT(F5.2,1x,F5.2,1X,3F8.4)
204     FORMAT(F5.2,1x,F5.2,1X,9F8.4)
205     FORMAT(F5.2,1x,F5.2,1X,11F8.4)
206     FORMAT(F5.2,1x,F5.2,1X,6F8.4)
        STOP

        END


************************************************************
These Are The Subroutines CALLed By The CALLing Statements
Above
************************************************************

****** Calculate non-isotropy factors **************

        SUBROUTINE FNIP(M,N,UP,K,NIF)
        REAL UP(12,25),K(12,25),NIF(12,25)

        DO 191 I=2,M
        DO 191 J=2,N
191     NIF(I,J)=(3.*UP(I,J)**2-2.0*K(I,J))/(2.0*K(I,J))
        RETURN
        END
```

```
*** Calculate first derivatives ******************

      SUBROUTINE CHANGES1(M,N,DR,DX,R,X,DKDR,DUDR,DVDR,DWDR,
     &DKDX,DUDX,DVDX,DWDX,DU3DX,DUV2DX,DUW2DX,K,U,V,W,U3, V3,
     &W3,UV2,UW2,UV,UW)
      REAL  U(12,25),K(12,25),V(12,25),W(12,25),UV(12,25),
     &UW(12,25),U3(12,25),V3(12,25),W3(12,25),UV2(12,25),
     &UW2(12,25),R(25),X(16),DR(25),DX(16),DKDR(12,25),
     &DUDR(12,25),DVDR(12,25),DWDR(12,25),  DKDX(12,25),
     &DUDX(12,25),DVDX(12,25),DWDX(12,25),DU3DX(12,25),
     &DUV2DX(12,25),DUW2DX(12,25)

      DO 8 J=2,N-1
8     DR(J)=R(J+1)-R(J-1)
      DO 9 I=2,M-1
9     DX(I)=X(I+1)-X(I-1)


********* Derivatives w.r.t. R *******************************

      DO 10 I=1,M
      DO 10 J=2,N-1
      DKDR(I,J)=(K(I,J+1)-K(I,J-1))/DR(J)
      DUDR(I,J)=(U(I,J+1)-U(I,J-1))/DR(J)
      DVDR(I,J)=(V(I,J+1)-V(I,J-1))/DR(J)
10    DWDR(I,J)=(W(I,J+1)-W(I,J-1))/DR(J)


******** Derivatives w.r.t. X ********************************

      DO 11 J=1,N
      DO 11 I=2,M-1
      DKDX(I,J)=(K(I+1,J)-K(I-1,J))/DX(I)
      DUDX(I,J)=(U(I+1,J)-U(I-1,J))/DX(I)
      DVDX(I,J)=(V(I+1,J)-V(I-1,J))/DX(I)
      DWDX(I,J)=(W(I+1,J)-W(I-1,J))/DX(I)
      DU3DX(I,J)=(U3(I+1,J)-U3(I-1,J))/DX(I)
      DUV2DX(I,J)=(UV2(I+1,J)-UV2(I-1,J))/DX(I)
11    DUW2DX(I,J)=(UW2(I+1,J)-UW2(I-1,J))/DX(I)
      RETURN
      END
```

```
******* Calculating second derivatives of K *****************

       SUBROUTINE CHANGES2(M,N,X,R,DR2,DX2,K,D2KDR2,D2KDX2)
       REAL X(16),K(12,25),DR2(25),DX2(25),D2KDR2(12,25),
      &D2KDX2(12,25),R(25)

***** Second derivatives of K w.r.t. R ******

       DO 12 I=1,M
       DO 12 J=2,N-1
       H1=R(J)-R(J-1)
       H2=R(J+1)-R(J)
       ALPHA1=1./(H1**2/2+H2*H1/2)
       ALPHA2=1./(H2*H1/2+H2**2/2)
       ALPHA0=-1.*(ALPHA1+ALPHA2)
12     D2KDR2(I,J)=ALPHA2*K(I+1,J)+ALPHA0*K(I,J)+ALPHA1*
      &K(I-1,J)

****  Second derivatives of K w.r.t. X Using the Method of
*Undetermined Coefficient Since X-Values Are Not Uniformly
*Spaced Within Some Range This equations Are Also Valid For
*Uniform Spacing i.e when H1=H2

       DO 13 J=1,N
       DO 13 I=2,M-1

       H1=X(I)-X(I-1)
       H2=X(I+1)-X(I)
       ALPHA1=1./(H1**2/2+H2*H1/2)
       ALPHA2=1./(H2*H1/2+H2**2/2)
       ALPHA0=-1.*(ALPHA1+ALPHA2)
13     D2KDX2(I,J)=ALPHA2*K(I+1,J)+ALPHA0*K(I,J)+ALPHA1
      &*K(I-1,J)
       RETURN
       END

** Calculate triple products ( u'u'u',v'v'v',w'w'w') from
*** skewness

       SUBROUTINE TRIP(M,N,U3,V3,W3,SU,SV,SW,UP,VP,WP)
       REAL U3(12,25),V3(12,25),W3(12,25),SU(12,25),
      &SV(12,25),SW(12,25),UP(12,25),VP(12,25), WP(12,25)
```

```
      DO 2 I=1,M
      DO 2 J=1,N
      U3(I,J)=SU(I,J)*(UP(I,J)**3)
      V3(I,J)=SV(I,J)*(VP(I,J)**3)
2     W3(I,J)=SW(I,J)*(WP(I,J)**3)
      RETURN
      END

*** Calculating convection terms  ***************

      SUBROUTINE CONVEC(M,N,DKDR,R,RHO,V,K,U,DKDX,CR,CRA,
     &CRG,CTG,DR,CX,DX,CT)
      REAL R(25),RHO(12,25),V(12,25),U(12,25),CRA(12,25),
     &CRG(12,25),CR(12,25),DR(25),CX(12,25),DX(16),CTG
     &(12,25), CT(12,25),K(12,25),DKDR(12,25),DKDX(12,25)



      DO 15 I=1,M
      DO 15 J=1,N
      CR(I,J)=RHO(I,J)*V(I,J)*DKDR(I,J)+RHO(I,J)*V(I,J)*
     &K(I,J)/R(J)
15    CRG(I,J)=RHO(I,J)*V(I,J)*DKDR(I,J)
      DO 105 I=1,M
      DO 105 J=2,N-1
105   CRA(I,J)=RHO(I,J)*V(I,J)*K(I,J)/R(J)
      DO 16 J=1,N
      DO 16 I=2,M-1
16    CX(I,J)=RHO(I,J)*U(I,J)*DKDX(I,J)
      DO 17 J=1,N
      DO 17 I=1,M
      CTG(I,J)=CRG(I,J)+CX(I,J)
17    CT(I,J)=CR(I,J)+CX(I,J)
      RETURN
      END


*** Calculate diffusion terms ***************************

      SUBROUTINE DIFFUS(M,N,D1,D2,D3,D4,D5,D6,D7,D8,D9,
     &D10,DT,UW2, DKDR,D2KDX2,DU3DX,DUV2DX,DUW2DX,PNEU,R
     &,RHO,V3,U2V,VP,WP)
```

```
      REAL D1(12,25),D2(12,25),D3(12,25),D4(12,25),D5
     &(12,25), D6(12,25),D7(12,25),D8(12,25),D9(12,25),
     &DT(12,25), D10(12,25),DKDR(12,25),D2KDX2(12,25),
    &DU3DX(12,25),DUV2DX(12,25),VP(12,25),DUW2DX(12,25),
    &PNEU,R(25),RHO(12,25),V3(12,25),U2V(12,25),
      &UW2(12,25),WP(12,25)



       DO 18 I=1,M
       DO 18 J=2,N-1

         D1(I,J)=PNEU/R(J)*(R(J+1)*DKDR(I,J+1)-R(J-1)*
          DKDR(I,J-1))/(R(J+1)-R(J-1))
         D2(I,J)=-.005*RHO(I,J)/R(J)*(R(J+1)*V3(I,J+1)-
      &R(J-1)*V3(I,J-1))/(R(J+1)-R(J-1))
      &D10(I,J)=-.005*RHO(I,J)/R(J)*(R(J+1)*UW2(I,J+1)
      &-R(J-1)*UW2(I,J-1)/(R(J+1)-R(J-1))
18     D3(I,J)=-.005*RHO(I,J)/R(J)*(R(J+1)*U2V(I,J+1)-
        R(J-1)*U2V(I,J-1))/(R(J+1)-R(J-1))

       DO 1018 J=1,N
       DO 1018 I=2,M-1
       D4(I,J)=PNEU*D2KDX2(I,J)
       D5(I,J)=-.005*RHO(I,J)*DU3DX(I,J)
       D6(I,J)=-.005*RHO(I,J)*DUV2DX(I,J)
1018   D7(I,J)=-.005*RHO(I,J)*DUW2DX(I,J)
       DO 1028 J=2,N-1
       DO 1028 I=1,M
       D8(I,J)=-1.*PNEU*((VP(I,J)/R(J))**2)
1028   D9(I,J)=-1.*PNEU*((WP(I,J)/R(J))**2)
       DO 19 J=1,N
       DO 19 I=1,M
19     DT(I,J)=D1(I,J)+D2(I,J)+D3(I,J)+D4(I,J)+
       D5(I,J)+D6(I,J)+D7(I,J)
     & +D8(I,J)+D9(I,J)+D10(I,J)
       RETURN
       END


***** Calculate production terms ****************************

       SUBROUTINE PRODUC(M,N,PR1,PR2,PR3,PR4,PR5,PR6,PR7,PR8,
     & PRT,RHO,UV,DVDR,DUDR,DVDX,DUDX,DWDX,DWDR,UW,UP,VP,WP,
```

```
      V,W,R)
      REAL PR1(12,25),PR2(12,25),PR3(12,25),PR4(12,25),
     & PR5(12,25),PR6(12,25),PR7(12,25),PR8(12,25),      &
DWDX(12,25),DWDR(12,25),UW(12,25),PRT(12,25),RHO
& (12,25),UP(12,25),VP(12,25),W(12,25),
& WP(12,25),UV(12,25) ,DVDR(12,25),DUDR(12,25),DVDX
& (12,25),DUDX(12,25),V(12,25),R(25)

      DO 20 J=2,N-1
      DO 20 I=1,M
      PR1(I,J)=-1.*RHO(I,J)*(VP(I,J)**2)*DVDR(I,J)
      PR2(I,J)=-.01*RHO(I,J)*UV(I,J)*DUDR(I,J)
20    PR7(I,J)=-.01*RHO(I,J)*UW(I,J)*DWDR(I,J)
      DO 2201 J=1,N
      DO 2201 I=2,M-1
      PR3(I,J)=-.01*RHO(I,J)*UV(I,J)*DVDX(I,J)
      PR4(I,J)=-1.*RHO(I,J)*(UP(I,J)**2)*DUDX(I,J)
2201  PR6(I,J)=-.01*RHO(I,J)*UW(I,J)*DWDX(I,J)
      DO 2101 J=1,N-1
      DO 2101 I=1,M
      PR5(I,J)=-1.*RHO(I,J)*(WP(I,J)**2)*V(I,J)/R(J)
2101  PR8(I,J)=.01*RHO(I,J)*UW(I,J)*W(I,J)/R(J)
      DO 21 J=1,N
      DO 21 I=1,M
21    PRT(I,J)=PR1(I,J)+PR2(I,J)+PR3(I,J)+PR4(I,J)+PR5(I,J)
     & +PR6(I,J)+PR7(I,J)+PR8(I,J)
      RETURN
      END

********* Calculate VDT by balancing the turbulent kinetic **
** equ.

      SUBROUTINE DISSIP(M,N,VDT,CTG,DT,PRT)
      REAL VDT(12,25),CTG(12,25),DT(12,25),PRT(12,25)
      DO 23 J=1,N
      DO 23 I=1,M
23    VDT(I,J)=CTG(I,J)-PRT(I,J)-DT(I,J)
      RETURN
      END

***** This is the end of the program **********************
```

NOMENCLATURE

CT	:	normalized total convection terms
$Ci,\ i = 1..2$	:	component parts of convection terms (see Table 5.1)
d	:	swirler hub diameter
D	:	combustor diameter
$Di,\ i = 1..10$	:	component parts of diffusion terms (see Table 5.1)
G_x	:	axial flux of axial momentum, see equation 2.1
G_θ	:	axial flux of angular momentum, see equation 2.2
H	:	step height
ID	:	inner diameter
$k = \frac{1}{2}\left(\overline{u'^2} + \overline{v'^2} + \overline{w'^2}\right)$	:	turbulent kinetic energy
L	:	characteristic length scale
N	:	sample size
$\overline{p}$	:	mean pressure value
PT	:	normalized total production terms
$\Delta\overline{U}$	:	uncertainty in velocity $\overline{U}$
σ_u	:	true standard deviation
$\delta_{i,j}$	:	kronecker delta

R_c	:	combustor radius
S	:	swirl number, see equation 2.3
u', v', w'	:	fluctuating velocity components
$\rho\overline{u'v'}, \rho\overline{u'w'}, \rho\overline{v'w'}$	:	Reynolds shear stresses
$\rho\overline{u'^2}, \rho\overline{v'^2}, \rho\overline{w'^2}$	:	Reynolds normal stresses
$\overline{U}, \overline{V}, \overline{W}$	:	mean velocity components
$\overline{U}_o$	:	mean axial velocity, immediately upstream of swirler
x, r, θ	:	axial, radial, and azimuthal coordinates

Greek Letters

γ	:	swirler vane angle
θ	:	azimuthal coordinates
μ	:	dynamic viscousity
$\overline{\rho}$	:	mean flow density

Subscripts

i	:	inlet pipe
o	:	zero swirl results

Superscripts

-	:	time mean value
$'$	:	fluctuating component

REFERENCES

[1] Ahmed, S. A., Rose, A., and Nejad, A. S., (1992) "Three Component LDV Velocity Measurements in a Can Type Research Combustor for CFD Validation Part 1. Isothermal Flow," ASME 92-GT-138.

[2] Ahmed, S.A., and Nejad, A.S.,"Swirl Effects on Confined Flows in Axisymmetric Geometries", *Journal of Propulsion and Power*, 8; March - April 1992: 339-345

[3] Buckley et al.,'The Design and combustion Performance of Practical Swirlers for Integral Rocket/Ramjets', *AIAA Journal*, 21; May 1983: 733-740, .

[4] Chigier, N.A., and Beér, J.M.,'Velocity and Static Pressure Distribution in Swirling Air Jets Issuing from Annular and Divergent Nozzles',em Journal of Basic Engineering, Vol. 4, pp 788-796, 1964.

[5] Chigier, N.A., and Chervinsky, A.,"Experimental Investigation of Swirling Vortex Motions in Jets", *Journal of Applied Mechanics*, 89;Series E, 1967:443

[6] Craig et al.,'A General Approach for Obtaining Unbiased LDV Data in Highly Turbulent Non-reacting and Reacting Flows', AIAA Paper No. 84-0366, 1984.

[7] Craya, A., and Karrigol, M.,"Turbulent Swirling Jet", *Physics of Fluids Supl., Boundary Layers and Turbulence*, 1967:197

[8] Driver. D. M. and Seegmiller, H L., (1985) "Features of a Reattaching Turbulent Shear Layer in Divergent Channel Flow," *AIAA Journal*, Vol . 23, pp. 163-171.

[9] ElBanhawy et al.,"Premixed Turbulent Combustion of a Sudden Expansion Flow" *Combustion and Flame*, 1983; 50:153-165

[10] Fornoff, M.,"Experimentalle und Theoretische Untersuchung von Drallstrahlen",*Diplomarbeit*, Univ. of Karlsruhe, Germany, 1978.

[11] Fujii, S. , Eguchi, K., and Gomi, M.,'Swirling Jets With and Without Combustion', AIAA Journal, Vol 19, No 11, pp 1483-1442, 1981.

[12] Gore, R.W. and Ranz, W.E.,'Backflows in Rotating Fluids Moving Axially Through Expanding Cross Sections', *AIChE Journal*, Vol. 10, pp 83-88, 1964.

[13] Gould, R.D, Stevenson, W.H. and Thompson, H.D.(1990)"Investigation of Turbulent Transport in an Axisymmetric Sudden Expansion," AIAA Journal, vol. 28, pp. 276-283.

[14] Hosel, W.,"Drallstrahlenuntersuchungen mit Einen Weiterentwicketten Laser Doppler-Messverfahren",*Dept. SFB 80/E/120*, Univ. of Karlsruhe, Germany, 1979.

[15] Keer, N.M, and Fraser, D.,"Swirl, Part I: Effects on Axisymmetric Turbulent Jets", *Journal of Institute Fuel*, 1965:519

[16] *Kilik*^{a}, E.,'Better Swirl Generation by Using Curved Vane Swirlers', *AIAA-85-1103*, 1985.

[17] *Kilik*^{b}, E.,'Influence on the Blockage Ratio on the Efficiency of Swirl Generation with Vane Swirlers', *AIAA-85-1103*, 1985.

[18] Lapidus, L., and Pinder, G.F.,(1982)"Numerical Solution of Partial Differential Equations in Science and Engineering", John Wiley and Sons, New York.

[19] Lefebvre, A.H., 'Gas Turbine Combustion', Hemisphere, Washington DC, 1983.

[20] Maier, P.,"Untersuchung Isothermer Turbulenter Drallfreistrahlen und Turbulenter Drallflammen", *Dissertation Thesis*, University of Karlsruhe, Germany.

[21] Martin, C.A.,'Aspects of the Design of Swirlers as Used in Fuel Injectors for Gas Turbine Combustors', ASME, NY, Paper 87-GT-139, June 1987.

[22] Mathur, M.L., and MacCallum, N.R.L.,"Swirl Air Jets Issuing from Vane Swirlers. Part I: Free Jets", *Journal of Institute Fuel*, 1967:214

[23] Nejad et al.,'Application of Laser Velocimetry for Characterization of Confined Swirling Flow,' *Journal of Engineering for Gas Turbines and Power*, Vol. 111, pp 36-45, 1984.

[24] Pitz, R.W. and Daily, J.W.,"Combustion in a Turbulent Mixing Layer Formed at a Rearward-facing Step",*AIAA Journal*, 1983, 21:1565-1570

[25] Prandtl, L., (1925) "Uber die Ausgebildete Turbulenz," ZAMM, Vol. 5, pp. 36.

[26] Pratte, E.D., and Keffer, J.F.,"The Swirling Turbulent Jet",*Journal of Basic Engineering*, Series D, 94(1972):739

[27] Riberio, M.M., and Whitelaw, J.H.,"Co-axial Jets with and Without Swirl",*Journal of Fluid Mechanics*, 96(1980):769

[28] Rouse, H., Yih, C. S. and Humphreys, H.W., (1952) "Gravitational Convection from a boundary Source," Tellus, 4, pp. 201-210.

[29] Snyder, P.K., Orloff, K.L., and Reinath, M.S.,'Reduction of Flow Measurement Uncertainties in Laser Velocimeters With Nonorthogonal Channels', *AIAA Journal*, Vol. 22, No. 8, pp. 1115-1123, 1984.

[30] Squire, H.B.,'Analysis of the *Vortex Breakdown* Phenomenon', *Miszellanen der Angerwandten Mechanik, Akademic, Berlin*, pp. 306-312, 1962.

[31] Stevenson et al.,"Laser Velocity Measurements and Analysis in Turbulent Flows with Combustion", *Parts I and II, AFWAL-TR-82-2076*, 1983

[32] Syred, N., Chigier, N.A., and Beér, J.M,"Turbulence Measurements in Swirling Recirculating Flow", *Symposium on Internal Flows*, Univ. of Salford, Paper 13, 1971, B27

[33] Wilhelmi, J., 'Axisymmetric Swirl Stabilized Combustion', PhD Thesis, imperial College London ENGLAND, June 1984.

Vitae

- Kamorudeen Babatunde ABIDOGUN
- Born in 1968 at Ibadan, Nigeria.
- Received Bachelor of Science (**B.Sc.**) degree in Mechanical Engineering from Obafemi Awolowo University, Ile Ife, Nigeria in 1991.
- Joined Mechanical Engineering department of King Fahd University of Petroleum and Minerals (**KFUPM**), Dhahran, Saudi Arabia as a Research Assistant in August 1993